Modelling features of the biological pump and its impact on marine oxygen distribution

Dissertation

ZUR ERLANGUNG DES DOKTORGRADES
DER MATHEMATISCH - NATURWISSENSCHAFTLICHEN FAKULTÄT
DER CHRISTIAN-ALBRECHTS-UNIVERSITÄT ZU KIEL

VORGELEGT VON
DANIELA NIEMEYER
KIEL, JUNI 2020

Referent:	Dr. habil. Iris Kriest
Koreferent:	Prof. Dr. Birgit Schneider

Tag der mündlichen Prüfung: 17.08.2020

gez. Prof. Dr. Frank Kempken, Dekan

Für Henning

Summary

The marine biological pump not just impacts the uptake of atmospheric CO_2 but also contributes to the regulation of ocean dissolved oxygen concentrations. The degree of ocean oxygenation has varied strongly throughout earth's history. After several periods of oxygen depletion, the ocean currently exhibits relatively high oxygen concentrations. However, in the past 50 years, a decrease in oxygen concentrations of 2% in the global ocean has been observed and it is expected that the oxygen concentration will decrease even further with global change conditions, reducing the habitat volume of hypoxia-sensitive pelagic species. Although the interplay between supply of oxygen by ventilation and its consumption by biogeochemical processes is generally known, it is still unclear to which degree both processes influence the global marine oxygen distribution even under today's climate conditions. Thus, this thesis focuses on features of the biological pump that might impact the marine oxygen distribution. Moreover, a comprehensive understanding of processes that influence the oxygen distribution is important to be able to estimate potential changes under future global change scenarios.
Global models are an important tool to get a deeper insight into determinative processes for the marine oxygen distribution. In this thesis, three approaches regarding the biological pump are tested to advance the understanding of processes that determine the oxygen distribution under current climate conditions, which, in turn, potentially enable understanding of the expansion of oxygen minimum zones (OMZs) under future global change conditions:

In the second chapter of this thesis, I test two competing feedbacks, which impact future oxygen concentrations, in the University of Victoria Earth System Climate Model (UVic ESCM) of intermediate complexity. This study shows, that the warming-induced phosphorus-oxygen feedback at the sediment-water interface and the resulting potential increase of released phosphorus does not constitute a major feedback in our model. It thus seems that other processes control the strength of future deoxygenation.
In the third chapter of this thesis, a global biogeochemical ocean model is coupled to a

particle aggregation model, which, using an appropriate parameterisation, improves the vertical and lateral representation of OMZs compared to the original model without aggregation. As there are still uncertainties in the parameterisation of the particle aggregation, a model calibration against an observed particle dataset seems necessary.
In the fourth chapter two new processes influencing particle dynamics, namely particle breakup (disaggregation of large particles into smaller ones) and mesozooplankton migration are included in the biogeochemical model, which is optimised against observed particles, dissolved inorganic tracers and the overlap between modelled and observed OMZs. This study further improves the representation of OMZs. However, it also shows that the model is not able to represent shallow and deep particles realistically at the same time, which indicates that important processes that enhance particle export flux are still unknown and thus not considered in the model parameterisation.

Zusammenfassung

Die marine biologische Pumpe beeinflusst nicht nur die Aufnahme von atmosphärischem CO_2 sondern trägt auch zu der Regulierung von gelösten Sauerstoffkonzentrationen im Ozean bei. Der Grad der Sauerstoffzufuhr unterlag in der Erdgeschichte starken Schwankungen. Nach einigen Phasen in der Erdgeschichte, in denen geringe Sauerstoffkonzentrationen nachgewiesen wurden, weist der Ozean aktuell vergleichsweise hohe Konzentrationen auf. Dennoch zeigen aktuelle Messungen, dass der Ozean in den letzten 50 Jahren Sauerstoffverluste von 2% zu verzeichnen hatte. Es wird angenommen, dass dieser Trend unter zukünftigen Bedingungen des globalen Wandels weiter anhält, was das Habitatvolumen von pelagischen Spezies, welche empfindlich gegenüber Sauerstoffmangel sind, reduziert. Auch wenn der Zusammenhang zwischen Sauerstoffzufuhr durch Ozeanzirkulation und dessen Verbrauch durch biogeochemische Prozesse grundsätzlich bekannt ist, ist weiterhin unklar, in welcher Größenordnung beide Prozesse die globale marine Sauerstoffverteilung unter aktuellen Bedingungen beeinflussen. Daher legt diese Arbeit einen Schwerpunkt auf Komponenten der biologischen Pumpe, welche die marine Sauerstoffverteilung beeinflussen können. Darüber hinaus ist ein korrektes Verständnis der Prozesse, welche die Sauerstoffverteilung aktuell beeinflussen, wichtig, um Abschätzungen für mögliche zukünftige Veränderungen treffen zu können.
Globale Modelle sind ein wichtiges Werkzeug, um einen tieferen Einblick in bestimmende Prozesse für die Sauerstoffverteilung zu erhalten. In der vorliegenden Arbeit werden drei verschiedene Ansätze bezüglich der biologischen Pumpe getestet, um das Verständnis von Prozessen, welche die Sauerstoffverteilung bestimmen, zu verbessern. Dies wiederum bewirkt möglicherweise ein Verständnis von sich ausdehnenden Sauerstoffminiumzonen unter Szenarien des globalen Wandels:

In dem zweiten Kapitel dieser Arbeit werden zwei gegensätzliche Rückkopplungen, welche zukünftige Sauerstoffkonzentrationen beeinflussen, in dem Erdsystemmodell mittlerer Komplexität der Universität von Victoria (UVic ESCM) getestet. Diese Studie zeigt, dass die durch Wärme hervorgerufene Phosphor-Sauerstoff Rückkopplung an der

Sediment-Wasser-Grenzschicht und der dadurch mögliche Anstieg von freigesetztem Phosphor in dem Modell keine vorrangige Rückkopplung darstellt. Es ist anzunehmen, dass andere Prozesse die Stärke des zukünftigen Sauerstoffverlustes bestimmen.
Für das dritte Kapitel dieser Arbeit wird ein globales biogeochemisches Modell mit einem Partikel-Aggregationsmodul gekoppelt. Dieses führt unter Verwendung einer passenden Parametrisierung zu einer verbesserten vertikalen und lateralen Darstellung von Sauerstoffminimumzonen im Vergleich zu einem Modell ohne Aggregation. Da weiterhin Unsicherheiten bezüglich der Parametrisierung der Partikelaggregation vorherrschen, scheint eine Modellkalibrierung gegen einen beobachteten Partikeldatensatz notwendig zu sein.
In dem vierten Kapitel werden mit dem Partikelzerfall von großen Partikeln in kleinere Partikel und der Vertikalwanderung von Mesozooplankton zwei weitere Prozesse, welche die Partikeldynamiken beeinflussen, in das biogeochemische Modell integriert. Das Modell wird darüber hinaus gegen beobachtete Partikeldaten, gelöste inorganische Marker und die Überlappung von modellierten und beobachteten Sauerstoffminimumzonen optimiert. Diese Studie zeigt, dass hierdurch eine weitere Verbesserung der Darstellung von Sauerstoffminimumzonen ermöglicht wird, weist jedoch darauf hin, dass eine realistische Repräsentation von Partikeln in flachen und tiefen Wasserschichten zur selben Zeit nicht möglich ist. Dies führt zu der Annahme, dass weitere wichtige Prozesse, welche den Export von Partikeln verstärken, noch unbekannt sind und daher in der Modellparametrisierung nicht enthalten sind.

Contents

1 Introduction

1.1 Motivation

The marine biological pump not only buffers atmospheric CO_2 but also helps to regulate marine biogeochemical cycles as well as marine oxygenation. A substantial fraction of the atmospheric CO_2 is taken up into the euphotic zone of the ocean. Carbon dioxide in combination with nutrients is transformed into organic matter, which is transported into the deep ocean and sequestered on long timescales [Sarmiento and Orr, 1991]. This, in turn, impacts the global carbon cycle and thus the climate.
Both, physical and biological, processes play a substantial role in regulating marine oxygen conditions. In general, marine oxygen concentrations are determined by the balance of ocean circulation (as an oxygen source) and oxygen-consuming biogeochemical processes [Karstensen et al., 2008]. The particle flux profile, which depends on the relative rates of particle sinking and remineralisation, which consumes oxygen [Jokulsdottir, 2011], has an increasingly dominant role in regulating oxygen concentration with increasing depth. Therefore, oxygen is a sensitive tracer for physical and biological changes in the ocean [Solomon et al., 2007].
In regions where oxygen concentration is lowest, the productivity and thus the fishing rate is highest [Chavez and Messié, 2009]. As those oxygen-depleted regions are expected to expand [Schmidtko et al., 2017] in the future and in combination with other stressors like acidification [Miller et al., 2016], this could lead to a potential habitat loss and thus a decrease in fish harvests in terms of number [Hughes et al., 2015] and size [Breitburg, 2002]. Fish provides 15% of the average animal protein uptake per capita for 4.5 billion people. Fishing-based revenues also indirectly provide food security for 10% of the human population [Béné et al., 2015]. This underlines the vulnerability of human well-being to declines in ocean oxygen and the expansion of OMZs. Ocean productivity, marine diversity and biogeochemical cycling are strongly affected by reduced oxygen concentrations [Stramma et al., 2011; Cooley, 2012]. Thus, understanding processes that determine low oxygen concentrations in the ocean and identifying feedbacks that are responsible for the expansion of regions with low oxygen conditions are important in the anthropocene.
Biogeochemical models serve as a necessary tool to understand potential processes and feedbacks leading to low oxygen conditions. However, global models exhibit different parameterisations regarding the biogeochemistry as well as physics [Cabré et al., 2015] leading to large disagreements in the representation of oxygen depleted regions [Cocco et al., 2013; Bopp et al., 2013]. Bopp et al. [2013] showed in their study that, depending on the model, the volume of low-oxygen-waters varies over a wide range (see their Table 2). Even for a quite high criterion of 80 mmol m^{-3} the water volume with concentrations

lower than the given criterion ranges between 24.1x10^{15} m^3 and 363x10^{15} m^3, while the observed volume is 126x10^{15} m^3 [Bopp et al., 2013]. Global models therefore exhibit high uncertainties in estimating the lateral and vertical extent of low-oxygen waters under current and future conditions [Cabré et al., 2015]. Kriest and Oschlies [2015] show that the suboxic volume is strongly linked to particle flux, i.e. an increasing sinking speed reduces water column particle remineralisation, decreases the suboxic volume and enhances the burial in the sediment on long time-scales and vice versa. The challenge thus consists in improving our understanding of essential processes such as particle dynamics, which can than enhance the representation of marine biogeochemical interactions under steady state conditions. This, in turn, potentially allows us to predict more reliably the expansion of oxygen depleted waters and to identify driving factors and responsible feedbacks for the future.
This thesis targets understanding biological processes that affect the oxygen distribution under current conditions and feedbacks that potentially lead to an expansion of oxygen-depleted regions under global change conditions using global models.

1.2 Marine oxygen distribution

Sediment records of black shales suggest that several periods of large-scale anoxia prevailed throughout earth's history [Schlanger and Jenkyns, 1976]. Holland [2006] finds that 3.85 billion years ago the ocean was mostly anoxic, followed by a mild oxygenation 0.54 billion years ago and relatively high oxygen levels in the present.
In the past 50 years, the global mean oxygen content decreased by 2% (i. e. 96 Tmol yr^{-1}) and oxygen-deficient layers in the water column, called oxygen minimum zones (OMZs) [Paulmier and Ruiz-Pino, 2009], quadrupled [Schmidtko et al., 2017]. However, the oxygen trend in a depth level of 300 dbar over the past 50 years strongly depends on the considered region: In the tropics between 20°N and 20°S, the oxygen concentration has decreased by 0.83 µmol kg^{-1} yr^{-1}, whereas in the subtropics and some subpolar regions the distribution is balanced, i.e. there are regions with decreasing and increasing oxygen concentrations. Contrary to the negative global trend, the extratropics even exhibit an increase in the oxygen concentration from 1960 to 2010 of 0.68 mol kg^{-1} yr^{-1} (see Fig. 1.1 b) [Stramma et al., 2012].
As shown in Fig. 1.1 a, global recent oxygen concentrations exhibit a decreasing trend at the western continental boundaries spreading from the equator polewards mostly in a depth between 100 m and 900 m [Karstensen et al., 2008]. This pattern is depicted very clearly by the Pacific but also by the Atlantic basin and the Arabian Sea [Stramma et al., 2012].
Water masses are roughly grouped into three categories depending on oxygen concentration: anoxic, suboxic and oxic. Anoxic waters exhibit no measurable dissolved oxygen and a high amount of sulfide is released into the water [Karstensen et al., 2008], as e.g. the Black Sea [Murray et al., 2005]. Suboxic waters are widely defined by oxygen levels ranging between 2 to 10 mmol m^{-3} [Bianchi et al., 2012] up to 50 mmol m^{-3} [Cabré

et al., 2015], whereas oxic describes water masses with higher oxygen concentrations. As there is no common definition of OMZs existent in the literature, the choice of the OMZ-criterion depends on two factors: As different species need different oxygen levels to survive [Seibel, 2011], the OMZ-citerion depends on the selected species. Moreover, the Atlantic basin, for example, has a considerably higher oxygen threshold than the Pacific basin, which, in turn, implies that using one criterion for both basins under- or overestimates one of both OMZ-volumes. Thus, the estimated global OMZ-volume also strongly depends on the defined threshold [Paulmier and Ruiz-Pino, 2009].

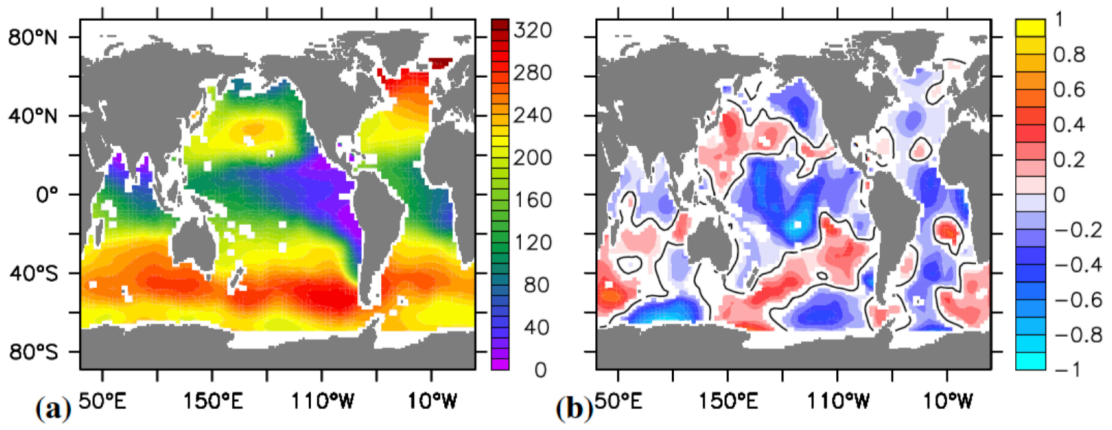

Fig. 1.1: *Global mean oxygen concentration in µmol kg^{-1} (a) and changes in the oxygen concentration in µmol kg^{-1} yr^{-1} between 1960 and 2010 (b) both at 300 dbar. Figure is taken from Stramma et al. [2012].*

The marine oxygen concentration is generally based on the interplay of circulation, which provides the ocean interior with oxygen, and oxygen-consuming biogeochemical processes [Karstensen et al., 2008]. For example in the tropics, the circulation in the 'shadow zones' [Karstensen et al., 2008] is reduced and the productivity is very high, which in combination leads to very low oxygen concentrations in this area (see Fig. 1.1 a). The importance of both processes is still not completely understood and quantified.

1.3 Ocean deoxygenation

Likely reasons for the decreasing trend of oxygen concentrations over the past 50 years consist in eutrophication in coastal areas [Rabalais et al., 2014], which, in turn, consumes oxygen, and moreover on global scale changing climate conditions since the preindustrial due to increasing anthropogenic carbon emissions [Limburg et al., 2020]. It is expected that the emissions will increase even further in the future, which, in turn, potentially leads to a further decrease in the marine oxygen concentrations.

This trend is confirmed by global models, which consistently show a decrease in the marine oxygen inventory of 2% to 4% between 1990 to 2090 - depending on the chosen global change scenario [Matear and Hirst, 2003; Bopp et al., 2002; Oschlies et al., 2008; Cocco et al., 2013; Bopp et al., 2013]. Although the global mean oxygen concentration and the size of OMZs are not necessarily correlated, it is expected that the volume of OMZs will expand even further in the future.
Previous studies show that under global change conditions three main drivers for ocean deoxygenation can be identified: (1) Changes in circulation, convective mixing and stratification [Sarmiento et al., 1998], (2) decreased oxygen solubility due to higher ocean surface temperature [Bopp et al., 2002] and (3) the effect of warming on biological production, respiration and remineralisation [Bopp et al., 2002; Oschlies et al., 2008; Hofmann and Schellnhuber, 2010].
It is still unclear, which processes govern marine oxygen concentrations under current conditions and deoxygenation under potential future global change conditions. This thesis focusses in the following on two aspects regarding the biological pump: The particulate flux determining remineralisation under current conditions as well as potential benthic feedbacks from the sediment under future global warming conditions.

1.4 Biological pump

The biological pump [Volk and Hoffert, 1985] describes the uptake of dissolved and photosynthetically produced particulate matter in the euphotic zone (0 down to ~100 m depth), its vertical transport through the mesopelagic (~100 down to ~1000 m depth) and potential remineralisation in the water column, and its deposition in the deep ocean or at the sediment. The interaction between vertical flux of organic matter as well as biological and physical processes leads to a gradient of marine nutrients, oxygen and carbon in the water column [Meyer et al., 2016] as described below. The biological pump can be divided into three steps: (1) The production of organic matter in the euphotic zone, (2) its flux divergence and remineralisation in the water column, and finally (3) its deposition in the deep ocean and on the sea floor [Le Moigne et al., 2013] (see Fig. 1.2).

1.4.1 Production

The ocean absorbs CO_2 from the atmosphere via air-sea gas exchange and receives inorganic nutrients via river runoff and atmospheric deposition. Moreover, the primary production in the epipelagic open ocean is fuelled by upwelled recycled nutrients. The uptake of inorganic carbon and nutrients enables phytoplankton to produce organic matter through photosynthesis in the euphotic zone. The produced organic matter is either remineralized under oxygen consumption by microbes or metazoan consumers, or sinks out of the euphotic zone through the mesopelagic into the deep ocean.

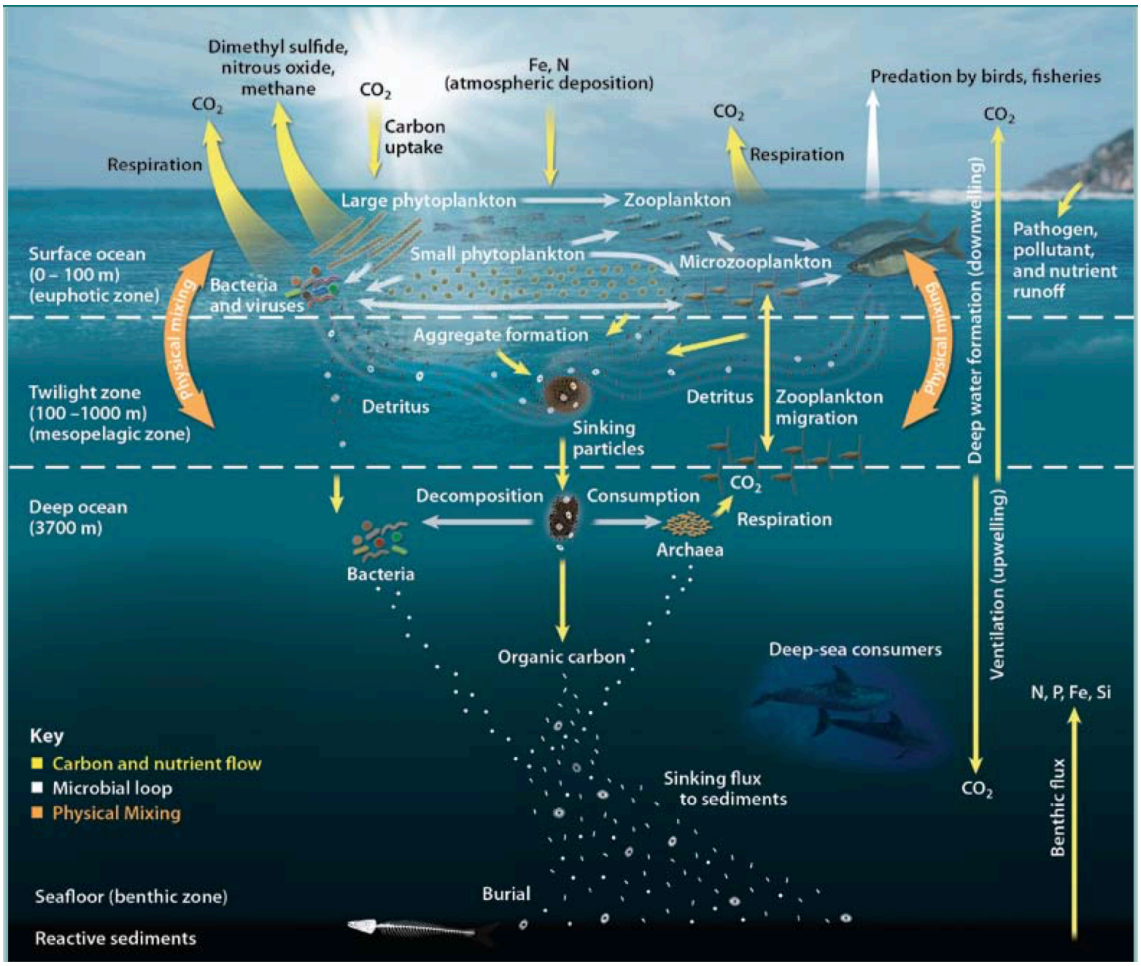

Fig. 1.2: *Oceanic Food Web [U.S. Department of Energy Office of Science, 2008].*

1.4.2 Flux divergence and remineralisation in the water column

The transport from the euphotic zone through the mesopelagic takes place through physical transport of dissolved organic matter and particulate organic matter as well as migrating zooplankton and gravitational sinking of particulate organic matter [Passow and Carlson, 2012]. The particulate organic matter sinking into the ocean interior is not only a food source for deep organisms [Stukel et al., 2019], but is also important for regulating air-sea gas exchange [Sarmiento and Toggweiler, 1984; Kwon et al., 2009] and the volume of OMZs through remineralisation [Kriest and Oschlies, 2015]. The dual processes that regulate export, the rate of particle sinking and the rate of particle remineralisation [Jokulsdottir, 2011], are both strongly linked to environmental conditions, ecosystem structure and particle characteristics [Stemmann et al., 2004].
Marine aggregates consist of living organisms, organic matter, zooplankton and nekton fecal pellets, transparent exopolymer particles (TEP) as well as minerals of biogenic and terrestrial origin [McDonnell, 2011]. Their size ranges from submicron (colloidal) to macroscopic size (marine snow) [Wells and Goldberg, 1992; Burd and Jackson, 2009], i.e.

a size of millimetres to centimetres [Alldredge and Gotschalk, 1988; Burd and Jackson, 2009]. Aggregates are formed by particles sticking together, which increases the likelihood they reach the deep ocean. [Alldredge et al., 1990]. Previous studies describe relationships between aggregate size and mass [Stemmann et al., 2004; McDonnell, 2011], carbon and nitrogen content [Alldredge, 1998], settling speed [Alldredge and Gotschalk, 1988], coagulation rate [Jackson and Lochmann, 1992] and the extent of colonization of microbes and zooplankton [Kiørboe, 2003]. However, many of those relationships are limited to the euphotic zone and it is still unclear if these relationships can be extrapolated to the mesopelagic [McDonnell, 2011].

The described size spectrum is linked via processes that affect the size, i.e. particle aggregation and its breakup [Burd and Jackson, 2009]. Large aggregates are formed by smaller particles sticking together [Alldredge et al., 1990; Burd and Jackson, 2009]. This process is characterised by physical interactions, namely the diffusion of particles towards each other (Brownian motion), movement of particles through turbulent shear and differential settling [McCave, 1984; Jackson and Burd, 2015]. Particle size, mass and concentration, in turn, determine the collision rate and thus also the aggregation rate. Although some studies do not consider aggregation to be an important process determining the entire flux from the euphotic zone through the mesopelagic to the deep ocean interior [Burd and Jackson, 2009], several studies show that aggregation and thus its transformation from small particles into larger and faster aggregates is a necessary process to prevent them from remineralisation and to carry them into the deep ocean [McCave, 1975; Fowler and Knauer, 1986; Alldredge and McGillivary, 1991]. However, the presence of small particles in the deep ocean [Kiko et al., 2017] suggests that the breakup of particles can introduce smaller particle size fractions to the deep ocean [Ruiz and Izquierdo, 1997; Dilling and Alldredge, 2000; Burd and Jackson, 2009]. The breakup of aggregates into their primary components, without losing mass, and can be caused, for example, by physically induced particle shear [Stemmann et al., 2004; Turner, 2015].

However, aggregates are not only passively affected by gravitational sinking [Volk and Hoffert, 1985] and breakup/shedding, but also by active biological processes [Stemmann et al., 2004; Steinberg et al., 2002]. Sloppy feeding by zooplankton and microbial degradation are responsible for a loss of mass and number of aggregates [Dilling and Alldredge, 2000; Stemmann et al., 2004] and for changing aggregate characteristics over the full water column. Particle attached bacteria degrade aggregates through the release of exoenzymes [Biddanda and Pomeroy, 1988]. Based on their observations, Ploug and Grossart [2000] estimated the microbial degradation on aggregates at a rate of 0.083 d^{-1}.

For a realistic representation of the particulate flux, a closer look at zooplankton diurnal vertical migration (DVM) is necessary [Aumont et al., 2018; Archibald et al., 2019]. Zooplankton graze aggregates and phytoplankton in the euphotic zone during the night. To hide from predators during daytime, several zooplankton species migrate into the deeper ocean, i.e. 300 to 600 m depth [Kiko et al., 2017], where they egest their gut content as dense and fast sinking faecal pellets [Longhurst et al., 1990; Steinberg et al., 2002; Archibald et al., 2019]. The contribution of active flux by migrating zooplankton to total particulate flux is not well constrained and ranges in literature between 18% and 84% [Kiko et al., 2020; Kelly et al., 2019; Hernández-León et al., 2019]. Zooplankton thus

serves as an aggregate shuttle from the surface to the deeper ocean and has an important impact on the overall particle flux [Kiko et al., 2020].
Remineralisation of organic matter depends on four factors: The first is temperature, which increases remineralisation [Segschneider and Bendtsen, 2013; Marsay et al., 2015]. Moreover, oxygen, as the final electron acceptor, directly determines respiration rate of microbes [Ploug, 2001; Iversen and Ploug, 2013] and metazoans [Seibel, 2011; Kiko and Hauss, 2019]. An increasing aggregate age during settling through the water column increases the density and thus the sinking speed [Guidi et al., 2008]. Ballast, which describes the amount of biominerals in the aggregates, enhances the sinking speed and thus reduces remineralisation [Ploug et al., 2008; Bach et al., 2016].
In conclusion, food web dynamics [Boyd et al., 1999; Wilson et al., 2008], aggregation and shedding processes [Burd and Jackson, 2009] oxygen availability [Devol and Hartnett, 2001; Guidi et al., 2015] and temperature [Marsay et al., 2015] thus directly determine sinking and remineralisation, and finally the overall particulate export and flux from the euphotic through the mesopelagic into the deep ocean.

1.4.3 Benthic processes

For a correct representation of biogeochemical tracers as well as OMZs in the global ocean it is necessary to include benthic processes [Maier-Reimer, 1993; DeVries et al., 2014; Kriest and Oschlies, 2013].
After particle sinking through the water column, a fraction of the exported organic matter is buried in sediments on long timescales. Another fraction is released by remineralisation processes back into the water column. Thus, nutrients are released and again bioavailable for marine organisms. Both processes, burial and release, are highly dependent on the availability of electron acceptors in the sediments, such as oxygen. Under suboxic conditions, the increased benthic release of phosphate and iron from the sediments stimulates biological production in the sunlit surface layer, further intensifying the oxygen depletion in the underlying water column [Ingall and Jahnke, 1994; Wallmann, 2010], while oxic conditions increase the phosphate burial in the sediment on long timescales.
It can be concluded that changing conditions from the surface ocean layer through the water column down to the sediment can have an important impact on particles and thus marine nutrient and oxygen concentrations, as well as on features such as OMZs.

1.4.4 Potential feedbacks of the biological pump on long timescales

The biological pump exhibits potential feedback loops on long timescales. This section focusses on the description of a potential negative feedback loop of the biological pump to atmospheric CO_2 as well as a positive feedback loop to marine OMZs (see Fig. 1.3).

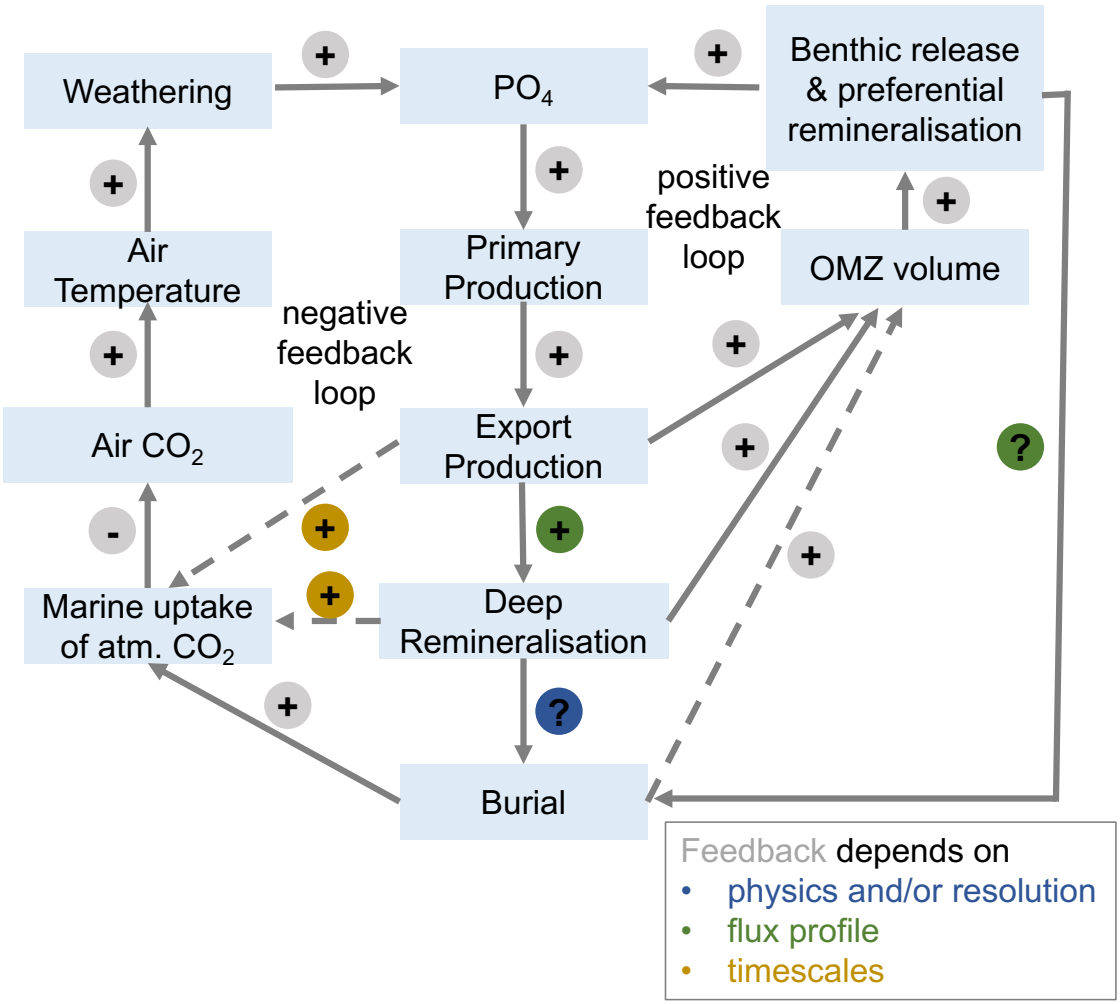

Fig. 1.3: *Potential feedback loops of the biological pump on long timescales. Illustration is based on the references cited in the text.*

The negative feedback on long timescales, i.e. timescales of 10000 to 100000 years, arises through the assumption of increasing air temperature under global change conditions due to enhanced anthropogenic carbon dioxide emissions. Higher temperatures are assumed to be linked to enhanced weathering rates on land [Berner, 1992], e.g. apatite, which increases the phosphorus flux into the marine environment by river input. This, in turn, strengthens primary production in the euphotic zone and the export in the mesopelagic as described by Tsandev and Slomp [2009]. Export production, deep remineralisation as well as burial potentially enhance the marine uptake of atmospheric CO_2 [Sarmiento and Orr, 1991], on short up to millennial timescales. Although it is assumed that the link between export and deep remineralisation strongly depends on the flux profile, the link between deep remineralisation and benthic burial still remains unclear. The carbon sequestration, in turn, potentially reduces CO_2 concentration in the atmosphere and the air temperature, limits the weathering on land and thus constitutes a negative feedback loop on long timescales (see Fig. 1.3).

The positive feedback is generally induced by increasing export into the mesopelagic and deep remineralisation, which is strongly linked to enhanced oxygen consumption [Wallmann, 2010] and increasing OMZ volume. This, in turn, is assumed to fuel benthic release and preferential reminalisation, which constitutes a positive feedback to the marine P inventory (see Fig. 1.3).

1.5 Particle dynamics in models

As shown above, particle characteristics and dynamics are complex and controlling factors are not yet completely understood. As the high number of model parameters moreover impedes the model parametrisation, an appropriate model assessment is necessary [Arhonditsis et al., 2004]. In the following, two different approaches of modelling particle dynamics will be described in detail and afterwards it will be focussed on how such models can be assessed against observations.

1.5.1 Approaches of modelling particle dynamics

Three approaches are suggested in the literature when modelling particle dynamics: (1) suggesting a ballast effect on the remineralisation length (2) describing the particle flux implicitly with depth, called the implicit approach, (3) or using explicit assumptions about the sinking speed for each individual particle size class, called the explicit approach hereafter.
The ballast approach suggests that minerals of biogenic and lithogenic origin increase the density and thus the sinking speed of particles [Armstrong et al., 2009]. As the relationship between particle sinking speed and the mineral component of particles is not yet understood [Lee et al., 2009], this study does not go into detail regarding models that include the ballast effect, which are described e.g. in Bach et al. [2016] for a 1D-model and in Gehlen et al. [2006] for a global biogeochemical model.

The simplest method is to prescribe the particle flux implicitly. As it describes the particle flux directly, it is a rather distinct and pragmatic approach. This section focusses on three attempts with varying complexity within the implicit approach to describe the particle flux profile.
The simplest approach assumes a number of particles at the surface with equal particle mass. The sinking speed and decay rate of every single particle is assumed to be uniform [Kriest and Oschlies, 2008], leading to the following equation:

$$F(z) = F(0) \cdot e^{-r/w \cdot (z - z_0)} \tag{1.1}$$

In this equation, *F(z)* describes the particle flux at a specific depth, z, r is the constant decay rate of particles and w the constant sinking speed. The particle flux decreases with depth (see also in Fig. 1.4, left panel, green line). For example Bacastow et al. [1991] use

this approach in a carbon cycle model and find that including only particulate organic carbon (POC) leads to a strong oxygen depletion of deep water, which is caused by nutrients that are trapped in the deep ocean. However, including POC and DOM, dissolved organic matter, in the model solves the problem of nutrients trapped in the deep ocean and thus reduces the model-data misfit [Bacastow et al., 1991].

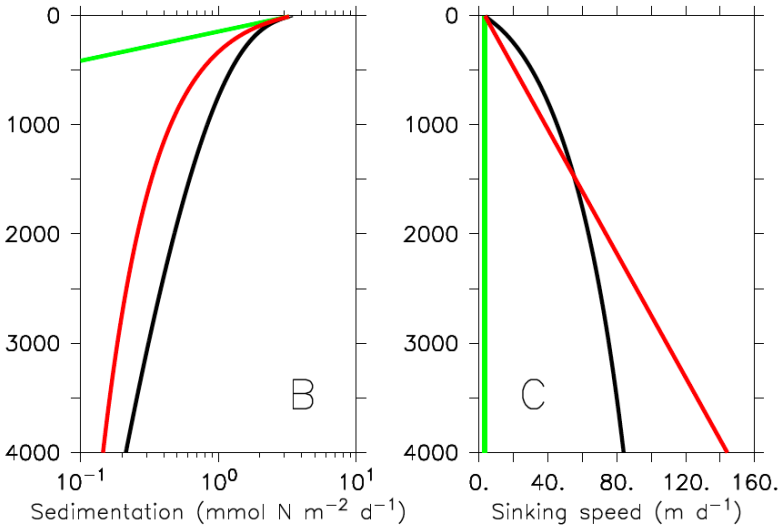

Fig. 1.4: *Modelled particle dynamics using the implicit approach focussing on the particle flux (left panel, green line: remineralisation and sinking speed are constant, red line: power-law function, black line: ensemble of particles with specific sinking speed) and the explicit approach with a focus on the average sinking speed of the particles (right panel, green line: vertically constant sinking speed, red line: depth-dependent sinking speed, black line: depth-dependent sinking speed and detritus concentration). Figure is taken from Kriest and Oschlies [2008].*

More frequently, the particle flux from the surface to the ocean interior is described by an empirically parametrised power-law function [Martin et al., 1987] (see also in Fig. 1.4, left panel, red line):

$$F(z) = F(0) \cdot (z/z_0)^{-b} \tag{1.2}$$

The so called 'Martin curve' is a simplified representation of the particle flux, where F is the particle flux, z defines the depth in metres and b is the exponent that describes the particle flux attenuation. This equation is based on in situ deep-moored and free-floating sediment traps off Peru and California [Martin et al., 1987] and exhibits a decreasing particle flux with depth, which is either linked to depth-dependent remineralisation or sinking speed [Kriest and Oschlies, 2008]. Based on these observations, the power b is set to a value of 0.858 [Martin et al., 1987]. Najjar et al. [2007] implement this power-law-function-approach in a global model utilising a b-value of 0.9 and find, as in the previous approach using constant remineralisation and sinking speed [Bacastow et al., 1991], an accumulation of nutrients in the ocean interior, namely nutrient trapping, although depth-

dependent remineralisation is included [Najjar et al., 2007]. Due to global variations in physical and biological factors several recent studies figure out that b-values range between 0.36 and 1.6 - a broad range which is applied and examined for small-scale observations [Martin et al., 1987; Berelson, 2002; Buesseler et al., 2007] and modelling studies with globally constant b-values [Kwon and Primeau, 2006; Kriest and Oschlies, 2008; Kriest et al., 2012; Kwon et al., 2009]. It is thus suggested that the empirically parametrised power law function neglects changes and variability in this highly complex system.
A more complex approach assumes a particle ensemble at the surface. In this particle ensemble each particle has its characteristic sinking speed depending on size. The decay rate is constant. As it is moreover assumed that the sinking speed of the particles increases with the particle size, this would result in a high remineralisation of small particles in the upper ocean and large particles reaching the deeper ocean. This, in turn, implies that the particle size and thus the sinking speed is increasing with depth [Kriest and Oschlies, 2008] (see also in Fig. 1.4, left panel, black line). To describe the particle flux from an ensemble of particles the following equation is used:

$$F \propto f(z, \varepsilon) \tag{1.3}$$

In this equation, z is again the depth and ε is the log-log slope of a particle size distribution, i.e. between particle size and particle number. A high ε thus corresponds with a high amount of small particles, while an decreasing ε is linked to an increasing amount of larger particles. DeVries et al. [2014] implement this approach into a global model and find that the model is not able to fit to both observed datasets, nutrient distributions and sediment traps. However, integrating benthic processes including a burial component, which removes organic matter on long timescales in the sediment, combined with a low decay rate of particles solve this problem.

While the previous implicit approach describes the overall particle flux directly, the explicit approach prescribes sinking speed and remineralisation for groups of particles. Taking into consideration the number of particles and their specific sinking speed enables the calculation of the particle flux. Under the umbrella of the explicit approach, again three methods of different complexity can be distinguished to determine the particle flux, which will be described in the following.

The simplest approach to describe the particle flux explicitly consists in assuming a constant sinking speed for each particle over the full water column

$$F(z) = w \cdot C(z), \tag{1.4}$$

where F is again the overall particle flux, w the constant sinking speed and C describes the detritus concentration, which is dependent on depth (see also in Fig. 1.4, right panel, green line). In this approach the sinking speed is assumed to be vertically constant. This approach is used in Schmittner et al. [2005] in a global model. They show that a high sinking speed reduces the probability that nutrients are trapped in the deep ocean. More-

over, they find that particles at the surface layer in the eastern tropical Pacific exhibit a high sensitivity to particle sinking speed. Although a sinking speed of 5 m d^{-1} exhibits the best fit between model and observations, a constant sinking speed and remineralisation rate over the water column results in an underestimation of the POC-flux in the deep ocean interior [Schmittner et al., 2005].
Thus, a more complex approach is developed assuming an increasing sinking speed with depth calculated by:

$$F(z) = a \cdot z \cdot C(z). \tag{1.5}$$

In this equation, a is the rate of increase of sinking speed with depth, z, and C describes again the detritus concentration, which is depth-dependent. In fact, the sinking speed in this approach is linearly increasing with depth, which is based on the assumption that the mean particle size is increasing with depth, which, in turn, affects the sinking speed (see also in Fig. 1.4, right panel, red line). Keller et al. [2012] modify the approach by Schmittner et al. [2008] of using a constant detritus sinking below 1000 m depth in the University of Victoria Earth System Climate Model (UVic). However, Keller et al. [2012] assume a sinking speed of 14 m d^{-1} at the surface, which increases linearly with depth over the full water column, and find that the model tends to underestimate the particle flux compared to the observed dataset by Honjo et al. [2008] based on sediment traps. Finally, different model parameterisations induce a broad range of model dynamics and thus also exhibit different representations of the particle flux.
The most complex approach of the three described approaches assumes particles of different size at the surface. Each particle has its characteristic sinking speed, which increases with particle size. Together with a constant (size-independent) remineralisation rate, this approach implies an enhanced sinking speed with depth, as only large particles sink to the deeper ocean before being remineralised. To calculate the particle flux for discrete size classes, the following equation is defined:

$$F(z) = \sum w_i(z) \cdot C_i(z) \tag{1.6}$$

The depth-dependent particle flux *F(z)* is calculated by the product of the sinking speed, w, and the detritus concentration C, both dependent on depth, z, which are summed up over all particle size classes, i. Within this approach a distinction can be drawn between models using one small and one large particle size class [Aumont and Bopp, 2006; Aumont et al., 2015, 2017; Yool et al., 2011] and models that include an infinite number of particle size classes [Oschlies and Kähler, 2004; Maier-Reimer et al., 2005; Gehlen et al., 2006] within a given particle size spectrum.
Gehlen et al. [2006] find in their study that including a parameterisation of an infinite number of particle size classes improves the ratio of particle export to primary production compared to observations. Although the model is not able to reproduce the strong decrease of the particle flux with depth, the authors assume that the formation of aggregates is important to increase the turnover of the biological pump [Gehlen et al., 2006].
Finally, as in a model, which includes discrete particle size classes, a definition of the size spectrum is not necessary, this approach is more flexible compared to an infinte number

of particle size classes. However, this approach also requires higher computing time leading to the assumption that implementing a particle size spectrum is more convenient using global or large-scale models. Thus, in the global biogeochemical model MOPS (Model of Oceanic Pelagic Stoichiometry), which is used in two of the following studies, the particle size distribution is described by the spectral slope between number and mass of particles [Kriest and Evans, 2000]. Size-dependent aggregation, sinking and particle breakup enable a changing slope of the particle size distribution. The described approach using a similar parameterisation has already been applied by Gehlen et al. [2006], Oschlies and Kähler [2004] and Schwinger et al. [2016].

1.5.2 Model assessment and calibration

As described above, a large number of model parameters have a decisive impact on model dynamics. For a good fit between model and observations an appropriate model choice is necessary. A highly complex system in combination with limited computing power as well as a limited number of observations thus impedes model calibration and makes model assessment against observed datasets necessary. In the optimal case, an appropriate parametrisation leads to model results that fit observed datasets and thus exhibit the lowest possible misfit between model results and observations [Schartau et al., 2017]. To find the best possible model fit, 'conventional modelling procedures' are developed [Arhonditsis et al., 2004]. This thesis focusses on a sensitivity study, a subjective, unsystematic parameter adjustment and an objective parameter optimisation.
The first step, the sensitivity analysis, explores the model's sensitivity towards circulation and forcing as well as selected biogeochemical model parameters. It is essential to select an appropriate model complexity and structure as well as to estimate parameters as good as possible [Arhonditsis et al., 2004]. As a higher model complexity does not necessarily improve the model fit to observations, an appropriate parameterisation is equally important. This, in turn, implies that a poor model performance can also be induced by an inappropriate parameter choice [Kriest et al., 2010].
In the model calibration, most of the models are adjusted following the range of observed or literature findings. However, this step does not necessarily ensure the best possible model fit as the parameter choice or model structure could be inappropriate [Arhonditsis et al., 2004]. Thus, finding the optimal parameter set is only possible after a very detailed investigation of the full parameter space for multiple parameters [Kriest et al., 2012; Arhonditsis et al., 2004]. Model optimisation thus reduces the defined cost function aiming at minimising the misfit between model and observations [Arhonditsis et al., 2004]. Most of the modelling studies neglect this step [Arhonditsis et al., 2004] possibly due to high computational demand. Moreover, Kriest et al. [2017] show in their study, that a single-objective optimisation against observed climatological nitrate, phosphate and oxygen concentrations can enhance the model fit in terms of dissolved inorganic tracers but also of independent diagnostics. But even when the model exhibits the best fit to a given variable, this does not necessarily ensure the best fit to another variable due to potential contrary processes included in the variables [Moore and Doney, 2007; Kriest and

Oschlies, 2013; Sauerland et al., 2019].
A multi-objective optimisation is potentially able to overcome this problem by finding a compromise solution for both objectives, i.e. an ensemble of parameter sets, which constitutes an approximation of the Pareto Front (see Fig. 1.5) [Sauerland et al., 2019]. In this case, one objective function, i.e. the model-data misfit with respect to certain target observations, ranges between zero and one, where zero represents the best possible fit. The squared minimum distance between coordinate origin and possible solutions represents the minimum misfit for the equally weighted combination of both objectives (called the 'knee' of the Pareto Front). Depending on the research question, it is possible to choose a solution with varying weightings between both objectives, e.g. the downright corner of the Pareto Front represents an overweighting regarding the second objective, f_2, and the top left an overweighting of the first objective, f_1 (see Fig. 1.5).

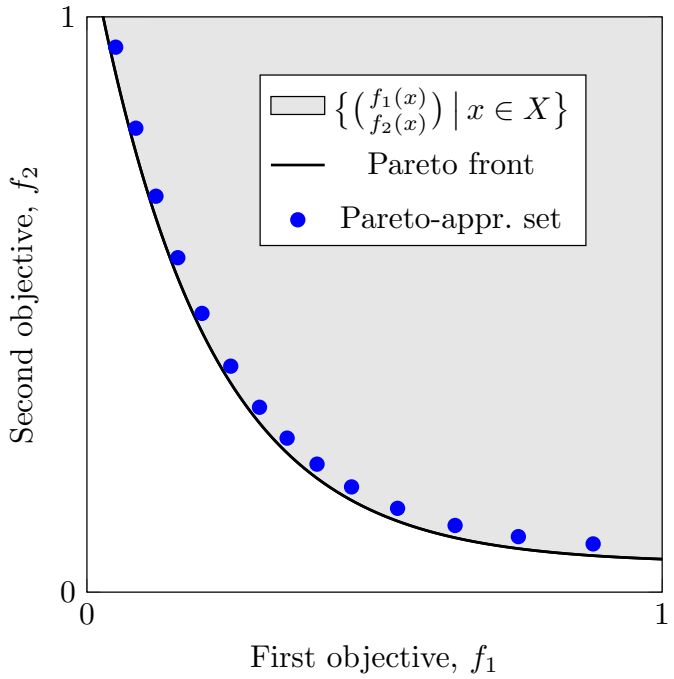

Fig. 1.5: *The Pareto Front shows potential best solutions of the weighted deviation normalised by global mean observations between two objectives (f_1 and f_2) for a given parameter space. The squared minimum distance between coordinate origin and possible solutions represents the best solution for the equally weighted combination of both objectives. Figure is taken from Sauerland et al. [2019].*

In conclusion, model optimisation provides a very systematic approach to calibrate models targeting observed datasets. Moreover, the approach of multi-objective optimisation offers a broad range of solutions, which enables to answer several questions with different foci combined in one optimisation.
For this thesis, the multi-objective optimisation offers an opportunity of finding a parameterisation that constitutes the best possible representation of the vertical and horizontal

extent of OMZs, the number and size of marine particles and dissolved inorganic tracers compared to observations.

1.6 Thesis overview

As emphasised in section 1.1, representing current OMZs and estimating their future expansion is highly uncertain - under steady state conditions as well as under future global change conditions. This thesis therefore aims at understanding processes and interactions regarding the biological pump that are of relevance for an improved representation of OMZs over space and time. The first study focusses on feedback loops between benthic processes and the marine oxygen inventory under future climate change conditions (RCP8.5 scenario), while the second and third studies both investigate export processes with a global model that includes detailed particle dynamics such as aggregation, thereby potentially improving the representation of OMZs under steady state conditions.

This thesis therefore addresses the following questions:

1. Under a business as usual global change scenario, which is the dominant feedback determining the expansion of OMZs - the positive feedback between benthic release of phosphorus and marine biological production or the negative one between marine uptake of CO_2 and air temperature (Chapter 2)?

2. Does a global biogeochemical model that includes particle dynamics improve the representation of OMZs under steady state conditions (Chapter 3)?

3. Does calibration against observed particle abundance and size help to improve simulated oxygen distribution, and are additional model processes besides aggregation necessary to improve the model fit? (Chapter 4)?

In the following, the chapters are summarised.

Chapter 2 studies two different feedback loops based on increasing phosphorus weathering under a RCP 8.5 scenario. On the one hand, a positive feedback loop involving increased remineralisation may extend OMZs, which, in turn, enhances the release of benthic phosphorus and therefore the global phosphorus inventory. On the other hand a negative feedback arises by an increased marine uptake of atmospheric CO_2 leading to

decreasing air temperature and therefore to a decline of phosphorus weathering, which reduces the marine phosphorus inventory. This study shows that the benthic release from the sediment is not a main factor for the expansion of OMZs. Instead, the study turned out that the negative feedback involving enhanced weathering, an increased marine uptake of CO_2 and thus a limited warming of the surface air temperature, which, in turn, potentially counteract the expansion of OMZs, is the more significant effect.

This chapter is based on the publication: Niemeyer D., Kemena T. P., Meissner K. J., Oschlies A. (2017), *A model study of warming-induced phosphorus–oxygen feedbacks in open-ocean oxygen minimum zones on millennial timescales*, Earth Syst. Dyn., 8, 357–367. doi: 10.5194/esd-8-357-2017.

AO, KJM and TPK initiated, conceived and designed the experiments. TPK performed the experiments. DN analysed the data and wrote the manuscript with contributions from AO, KJM and TPK.

Chapter 3 presents a parameter sensitivity study of a global biogeochemical model including a particle aggregation module and its impact on simulated dissolved inorganic tracers and OMZs under steady state conditions. This study shows that including an aggregation module improves the representation of OMZs. Moreover, a good model fit is tightly linked to a high model resolution, porous particles, an intermediate-to-high sinking speed and a moderate-to-high stickiness. Calibrating against nutrients and oxygen seems to be not sufficient for global model calibration and optimisation against an observed particle dataset is necessary to improve the representation of OMZs.

This chapter is based on the publication: Niemeyer D., Kriest I., Oschlies A. (2019), *The effect of marine aggregate parameterisations on nutrients and oxygen minimum zones in a global biogeochemical model*, Biogeosciences, 16, 3095-3111, doi: 10.5194/bg-16-3095-2019.

DN, IK and AO conceived the study. DN performed and analysed the simulations. DN wrote the manuscript with contributions from all co-authors.

In **Chapter 4**, a global biogeochemical model is optimised and compared towards a global observed dataset of marine particles, dissolved inorganic tracers and the vertical and horizontal extent of OMZs. Moreover, two new processes are added in the model, namely particle breakup, which reduces the size of the particles, and zooplankton migration, which transports the particles into the ocean interior. The simulations show that an increasing number of processes influencing the particle dynamics improves the representation of OMZs. Despite this improvement, some processes seem to be not captured yet as there is a trade-off between modelled and observed particles. Integrating more processes that

enhance particle flux could further improve the representation of OMZs.

This chapter is a manuscript in preparation by Niemeyer, D., Kriest, I., Kiko, R., and Oschlies, A. and with potential contributions by Guidi, L., Hauss, H., McDonnell, A., Picheral, M., Rogge, A., Sauerland, V., Stemmann, L. and Waite, A.

DN, IK and AO initiated and conceived the study. DN performed the experiments, analysed the data and wrote the manuscript with contributions from all co-authors. The observed UVP 5 dataset has been compiled by DN and RK.

2 A model study of warming-induced phosphorus-oxygen feedbacks in open-ocean oxygen minimum zones on millennial timescales

This chapter is based on the paper 'A model study of warming-induced phosphorus-oxygen feedbacks in open-ocean oxygen minimum zones on millennial timescales' published in Earth System Dynamics.
Citation: Niemeyer, D., Kemena, T. P., Meissner, K. J., and Oschlies, A.: A model study of warming-induced phosphorus–oxygen feedbacks in open-ocean oxygen minimum zones on millennial timescales, Earth Syst. Dynam., 8, 357-367, https://doi.org/10.5194/esd-8-357-2017, 2017.

Earth Syst. Dynam., 8, 357–367, 2017
www.earth-syst-dynam.net/8/357/2017/
doi:10.5194/esd-8-357-2017

Earth System Dynamics
Open Access
EGU

A model study of warming-induced phosphorus–oxygen feedbacks in open-ocean oxygen minimum zones on millennial timescales

Daniela Niemeyer[1], **Tronje P. Kemena**[1], **Katrin J. Meissner**[2], **and Andreas Oschlies**[1]

[1]Helmholtz-Zentrum für Ozeanforschung Kiel (GEOMAR), Düsternbrooker Weg 20, 24105 Kiel, Germany
[2]Climate Change Research Centre and ARC Centre of Excellence for Climate System Science, University of New South Wales, Level 4 Mathews Building, Sydney, New South Wales, 2052, Australia

Correspondence to: Daniela Niemeyer (dniemeyer@geomar.de)

Received: 20 October 2016 – Discussion started: 31 October 2016
Revised: 20 March 2017 – Accepted: 12 April 2017 – Published: 19 May 2017

Abstract. Observations indicate an expansion of oxygen minimum zones (OMZs) over the past 50 years, likely related to ongoing deoxygenation caused by reduced oxygen solubility, changes in stratification and circulation, and a potential acceleration of organic matter turnover in a warming climate. The overall area of ocean sediments that are in direct contact with low-oxygen bottom waters also increases with expanding OMZs. This leads to a release of phosphorus from ocean sediments. If anthropogenic carbon dioxide emissions continue unabated, higher temperatures will cause enhanced weathering on land, which, in turn, will increase the phosphorus and alkalinity fluxes into the ocean and therefore raise the ocean's phosphorus inventory even further. A higher availability of phosphorus enhances biological production, remineralisation and oxygen consumption, and might therefore lead to further expansions of OMZs, representing a positive feedback. A negative feedback arises from the enhanced productivity-induced drawdown of carbon and also increased uptake of CO_2 due to weathering-induced alkalinity input. This feedback leads to a decrease in atmospheric CO_2 and weathering rates. Here, we quantify these two competing feedbacks on millennial timescales for a high CO_2 emission scenario. Using the University of Victoria (UVic) Earth System Climate Model of intermediate complexity, our model results suggest that the positive benthic phosphorus release feedback has only a minor impact on the size of OMZs in the next 1000 years. The increase in the marine phosphorus inventory under assumed business-as-usual global warming conditions originates, on millennial timescales, almost exclusively (> 80 %) from the input via terrestrial weathering and causes a 4- to 5-fold expansion of the suboxic water volume in the model.

1 Introduction

Oxygen minimum zones (OMZs) have more than quadrupled over the past 50 years and it has been suggested that this expansion is related to recent climate change (Stramma et al., 2008; Schmidtko et al., 2017). However, current CO_2 emission-forced models are challenged to reproduce this expansion in detail (Stramma et al., 2012; Cabré et al., 2015). There are at least three different processes that can have an impact on the size of OMZs in a warming climate: ocean warming and its impact on solubility of O_2 in the ocean (Bopp et al., 2002), changes in ocean dynamics, e.g. stratification, convective mixing and circulation (Manabe and Stouffer, 1993; Sarmiento et al., 1998), biological production effects (Bopp et al., 2002) including possible CO_2-driven changes in stoichiometry (Oschlies et al., 2008) and CO_2-induced changes in ballasting particle export (Hofmann and Schellnhuber, 2010). Here, we investigate how changes in biological production and subsequent remineralisation can affect OMZs in addition to the above-mentioned thermal and dynamic effects. We focus on changes in the phosphorus (P) cycle. P is the main limiting nutrient on long timescales (Tyrell, 1999; Palastanga et al., 2011) and we examine possible effects of changes in the P cycle on millennial timescales.

The major source of P for the ocean is river input (Filippelli, 2008; Payton and McLoughlin, 2007; Föllmi, 1996; Palastanga et al., 2011; Froelich et al., 1982), which is determined by terrestrial weathering of apatite (Filippelli, 2002; Föllmi, 1996). The main factors controlling terrestrial weathering are temperature, precipitation and vegetation. Higher temperatures are generally associated with enhanced precipitation and occur in many places with higher terrestrial net primary productivity (Monteiro et al., 2012), which all tend to increase weathering rates (Berner, 1991).

It is difficult to determine how much of the globally weathered P enters the ocean in a bioavailable form. Today, about 0.09–0.15 Tmol a^{-1} of prehuman, potentially bioavailable P is transported globally by rivers including dissolved organic and inorganic P, particulate organic P and iron-bound P (Compton et al., 2000). About 25 % of this potentially bioavailable P is trapped in coastal estuaries and will not enter the open ocean (Compton et al., 2000). Ruttenberg (2004) estimated a bioavailable P flux under pre-industrial conditions including dissolved P and bioavailable particulate P (35 % of total particulate P) of 0.24–0.29 Tmol P a^{-1} excluding the atmospheric input (Ruttenberg, 2004). Marine organisms take up P most easily as dissolved inorganic P (DIP). Riverine measurements suggest that only a small fraction of the total P (0.012 to 0.032 Tmol a^{-1}) enters the ocean as DIP (Filippelli, 2002; Harrison et al., 2005; Compton et al., 2000; Wallmann, 2010; Palastanga et al., 2011; Ruttenberg, 2004). However, passing through estuaries can increase the fraction of DIP by 50 % (Froelich, 1984) to 80 % (Berner and Rao, 1994).

After taking up the bioavailable P for photosynthetic production of biomass, a large fraction of the newly produced organic matter is exported out of the euphotic zone as detritus (6.42 Tmol P a^{-1}, according to the model study by Palastanga et al., 2011) and the vast majority of this exported organic matter is remineralised in the deeper ocean by bacteria (6.26 Tmol P a^{-1}; Palastanga et al., 2011), which is an oxygen consuming process. A small fraction of the exported organic matter is deposited at the sediment surface (0.16 Tmol P a^{-1}; Palastanga et al., 2011), about 20 % of the deposited P is buried in the sediments on long timescales (0.032 Tmol P a^{-1}; Palastanga et al., 2011) and the remaining 80 % (0.13 Tmol P a^{-1}; Palastanga et al., 2011) is released back into the water column as DIP, where it is again available for the uptake of marine primary producers (Palastanga et al., 2011; Wallmann, 2010).

The processes of burial and release of P are redox dependent. Under oxic conditions the burial rate is high, while under suboxic conditions the benthic release of P is elevated (Ingall and Jahnke, 1994; Kraal et al., 2012; Wallmann, 2010; Slomp and Van Cappellen, 2007; Floegel et al., 2011; Lenton and Watson, 2000; Tsandev and Slomp, 2009). The redox-dependent release of P into the water column and the decrease in marine oxygen due to remineralisation therefore represent a positive feedback loop on marine biological production (see Fig. 1). Although the feedbacks between ocean and atmosphere are complex (Sabine et al., 2004), we assume that an enhanced detritus export into the ocean interior results in an increased marine uptake of atmospheric CO_2 (Sarmiento and Orr, 1991). Consequently, surface air temperatures decrease with decreasing atmospheric CO_2 concentrations, which, in turn, leads to lower weathering rates (see Fig. 1).

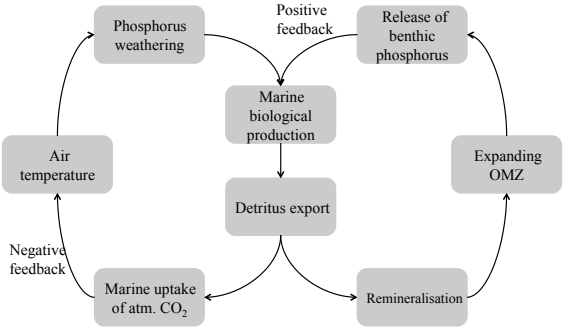

Figure 1. Possible feedbacks in the global phosphorus cycle under climate warming conditions.

These redox-dependent benthic P fluxes have been investigated in a previous study with the HAMOCC global ocean biogeochemistry model by Palastanga et al. (2011). Palastanga et al. (2011) show that doubling the input of dissolved P from rivers results in an increased benthic release of P. This leads to a rise in primary production as well as in oxygen consumption, which in turn affects the oxygen availability in sediments. The benthic release of P acts therefore as a positive feedback on expanding oxygen minimum zones on timescales of 10 000 to 100 000 years (Palastanga et al., 2011).

Other studies on marine oxygen deficiency focused on the geological past, especially the mid-Cretaceous warm period (120–80 Ma) (Tsandev and Slomp, 2009; Handoh and Lenton, 2003; Bjerrum et al., 2006; Föllmi et al., 1996). Several periods of oceanic oxygen depletion have been inferred from sediment data of black shales (Schlanger and Jenkyns, 1976), for example, for the Cretaceous oceanic anoxic event 2 (OAE) at the Cenomanian–Turonian boundary (93.5 Myr). Whether processes such as surface warming, sea-level rise (Handoh and Lenton, 2003), and possibly a slow-down of the ocean overturning circulation and vertical mixing (Monteiro et al., 2012; Tsandev and Slomp, 2009; Ruvalcaba Baroni et al., 2014) – as assumed for the Cretaceous – will lead to widespread oxygen depletion in the future is a reason of concern. Consequently, a better understanding of biogeochemical processes associated with Cretaceous OAE might help assess the risk of possible future events of low marine oxygen concentrations (Tsandev and Slomp, 2009).

In contrast to previous studies that focus on the geological past, we investigate possible future changes over the next 1000 years using an Earth System Climate Model of intermediate complexity to investigate the feedbacks between the P cycle and OMZs under the extended Representative Concentration Pathways Scenario 8.5 (RCP8.5) of the Intergovernmental Panel on Climate Change (IPCC) AR5 report. The RCP8.5 scenario is characterised by an increase in atmospheric CO_2 concentrations and associated with an increase in radiative forcing of up to 8.5 W m^{-2} by year 2100 (in comparison to pre-industrial conditions) and is also known as the "business as usual" scenario (Riahi et al., 2011).

2 Methods

2.1 UVic model

The University of Victoria Earth System Climate model (UVic ESCM) version 2.9 (Weaver et al., 2001; Eby et al., 2009) is a model of intermediate complexity and consists of a terrestrial model based on TRIFFID and MOSES (Meissner et al., 2003) including weathering (Meissner et al., 2012), an atmospheric energy–moisture balance model (Fanning and Weaver, 1996), a $CaCO_3$-sediment model (Archer, 1996), a sea-ice model (Semtner, 1976; Hibler, 1979; Hunke and Dukowicz, 1997) and a three-dimensional ocean circulation model (MOM2) (Pacanowski, 1995). The ocean model includes a marine ecosystem model based on a nutrient–phytoplankton–zooplankton–detritus model (Keller et al., 2012). The horizontal resolution of all model components is 1.8° latitude × 3.6° longitude. The ocean model has 19 layers with layer thicknesses ranging from 50 m at the sea surface to 500 m in the deep ocean. We use a sub-grid-scale bathymetry as described in Somes et al. (2013) to simulate benthic fluxes of phosphorus. The sub-grid bathymetry is inferred from the ETOPO2v2[1] and represents global spatial distributions of continental shelves, slopes and other topographical features (1/5°). For the topography used here, the shelf (0–200 m) covers 6.5 %, the slope (200–2000 m) 11.7 % and the deep sea (> 2000 m) 81.9 % of the global ocean. Downward fluxes of organic matter are intercepted by the sub-grid bathymetry related to the fractional sediment cover for each ocean grid box, and benthic fluxes of phosphorus are calculated based on the transfer functions described in the following section.

2.2 Phosphorus cycle in UVic model

Earlier applications of the UVic ESCM assumed a fixed marine P inventory. We included a representation of the dynamic P cycle for this study. It consists of a modified terrestrial weathering module (Meissner et al., 2012) and a redox-sensitive transfer function for burial and benthic release of P (Floegel et al., 2011; Wallmann, 2010).

[1] https://www.ngdc.noaa.gov/mgg/global/etopo2.html

The continental weathering module developed earlier for fluxes of dissolved inorganic carbon (DIC) and alkalinity (Meissner et al., 2012; Lenton and Britton, 2006) is based on the following equations:

$$F_{\mathrm{DIC,w}} = F_{\mathrm{DIC,w,0}} \cdot \left\lfloor f_{\mathrm{Si}} + f_{\mathrm{Ca}} \cdot \left(\frac{\mathrm{NPP}}{\mathrm{NPP}_0}\right) \cdot (1 + 0.087 \cdot (\mathrm{SAT} - \mathrm{SAT}_0)) \right\rfloor = F_{\mathrm{DIC,w,0}} \cdot f(\mathrm{NPP}, \mathrm{SAT}) \quad (1)$$

$$F_{\mathrm{Alk,w}} = F_{\mathrm{Alk,w,0}} \cdot \left(\frac{\mathrm{NPP}}{\mathrm{NPP}_0}\right) \cdot \left\lfloor f_{\mathrm{Si}} \cdot (1 + 0.038) \cdot (\mathrm{SAT} - \mathrm{SAT}_0) \cdot 0.65^{0.09 \cdot (\mathrm{SAT} - \mathrm{SAT}_0)} \right\rfloor + f_{\mathrm{Ca}} \cdot (1 + 0.087 \cdot (\mathrm{SAT} - \mathrm{SAT}_0)), \quad (2)$$

where $F_{\mathrm{DIC,w}}$ and $F_{\mathrm{Alk,w}}$ represent the globally integrated flux of DIC and alkalinity via river runoff; f_{Si} and f_{Ca} stand for the fraction of silicate (0.25) and carbonate (0.75) weathering; and NPP and SAT are the global mean net primary production on land and global mean surface air temperature over land (in degrees Celsius). The index 0 stands for pre-industrial values.

We added the following flux to account for P weathering ($F_{\mathrm{DP,w}}$) with the same dependencies on globally and annually averaged net primary production (NPP) and surface air temperature (SAT) as those for DIC:

$$F_{\mathrm{DP,w}} = F_{\mathrm{DP,0}} \cdot f(\mathrm{NPP}, \mathrm{SAT}). \quad (3)$$

The global river input of DIP is the only continental source for P in the model. The global DIP input is distributed over all coastal points of discharge scaled according to their individual volume discharge. The pre-industrial DIP input to the ocean ($F_{\mathrm{DP,0}}$) is assumed to be in steady state and in equilibrium with the total globally integrated pre-industrial net burial of P ($\mathrm{BUR_P}$):

$$F_{\mathrm{DP,0}} = \mathrm{BUR}_{\mathrm{P,0}}. \quad (4)$$

We use an empirical transfer function for $\mathrm{BUR_P}$ and for the benthic release of DIP ($\mathrm{BEN_{DIP}}$) derived from observations across bottom-water oxygen gradients (Wallmann, 2010; Flögel et al., 2011). The release of dissolved inorganic P ($\mathrm{BEN_{DIP}}$) is calculated as follows:

$$\mathrm{BEN_{DIP}} = \frac{\mathrm{BEN_{DIC}}}{r_{\mathrm{reg}}}. \quad (5)$$

Benthic release of dissolved inorganic carbon ($\mathrm{BEN_{DIC}}$) is calculated from an empirical transfer function (Fig. 2 in Flögel et al., 2011) to determine $\mathrm{BEN_{DIP}}$ fluxes at the bottom of the ocean. In our model configuration, particulate organic carbon (POC) is remineralised completely at the ocean bottom and no ocean-to-sediment fluxes of POCs occur, i.e. $\mathrm{BEN_{DIC}}$ is equivalent to $\mathrm{RR_{POC}}$, where $\mathrm{RR_{POC}}$ denotes the

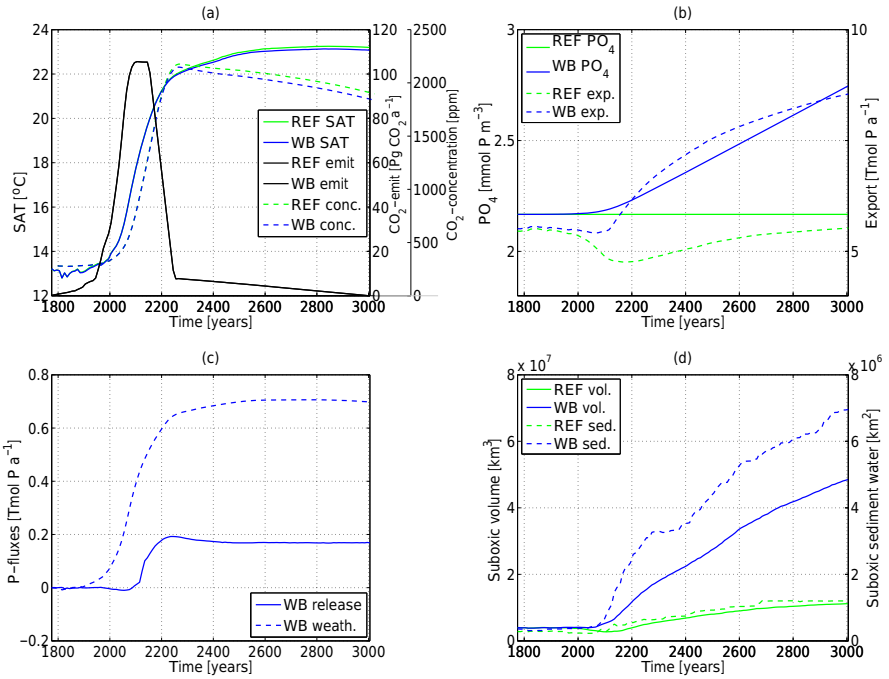

Figure 2. Global and annual mean time series of **(a)** surface air temperature in degree Celsius (solid lines), CO_2 emissions in Pg CO_2 a^{-1} (black solid line – for both simulations) and CO_2 concentration in ppm (dashed lines); **(b)** global mean phosphorus concentration in mmol P m^{-3} (solid lines) and export rate in Tmol P a^{-1} at 130 m depth (dashed lines); **(c)** anomalies of phosphorus input via sediment in Tmol P a^{-1} (solid line) and anomalies of phosphorus weathering input in Tmol P a^{-1} (dashed line); **(d)** suboxic volume (< 0.005 mol m^{-3}) of the ocean in km^3 (solid lines) and surface of ocean bottom layer with O_2 concentrations below 0.005 mol m^{-3} in km^2 (dashed lines). The control simulation (REF) is shown in green; the second simulation (WB) is in blue.

rain rate of particulate organic carbon to the sediment. Wallmann (2010) calculated r_{reg} by a regression of observational data to bottom-water oxygen concentrations:

$$r_{reg} = \frac{RR_{POC}}{BEN_{DIP}} = Y_F + A \cdot \exp\left(\frac{-[O_2]}{r}\right). \quad (6)$$

The regeneration ratio is calculated by dividing the depth-integrated rate of organic matter degradation in surface sediments (RR_{POC}) by the benthic flux of dissolved inorganic P into the bottom water (BEN_{DIP}). Parameters are defined as $Y_F = 123 \pm 24$, $A = -112 \pm 24$ and $r = 32 \pm 19$, and O_2 is in µmol L^{-1} (Wallmann, 2010). Under oxic conditions r_{reg} is higher than the Redfield ratio (106; Redfield et al., 1963) and under oxygen-depleted conditions r_{reg} reduces to 10 (Wallmann, 2010).

The rain rate of POP (RR_{POP}) is calculated by the rain rate of POC (RR_{POC}) divided by the Redfield ratio. As a result BUR_P can be calculated as follows:

$$BUR_P = RR_{POP} - BEN_{DIP}. \quad (7)$$

The burial of P (BUR_P) in the sediment is equal to the rain rate of particulate organic P (RR_{POP}) minus BEN_{DIP} (Floegel et al., 2011). If the benthic release overcomes the rain rate of POP at depths below 1000 m, the burial is set to zero. Following Floegel et al. (2011), this condition is not applied to shallower sediments because these deposits receive both marine particles and high fluxes of riverine particulate phosphorus.

2.3 Model simulations

Two model simulations were performed. Our control simulation, called simulation REF hereafter, includes neither weathering, benthic release nor burial of P. The global amount of P in the ocean is therefore conserved in this simulation over time. The second simulation, called WB, includes P weathering as well as benthic burial and release of P but excludes additional anthropogenic input. The spin-up was performed by computing the burial and benthic release according to Eq. (6). The weathering fluxes were set to a value to compensate the burial rate (Eq. 4) during the spin-up but not thereafter.

After a spin-up of 20 000 years under pre-industrial boundary conditions, we forced the model with anthropogenic CO_2 concentrations following the RCP8.5 scenario of the IPCC AR5 assessment (Meinshausen et al., 2011; Riahi et al., 2011). The CO_2 emissions in the UVic ESCM reach

105.6 Pg CO_2 a^{-1} in year 2100. Between years 2100 and 2150, the models are forced with constant CO_2 emissions (105 Pg CO_2 a^{-1}), followed by a linear decline until year 2250 to a level of 11.5 Pg CO_2 a^{-1} and then linearly to zero emissions in year 3005 (see Fig. 2a). Simulated atmospheric CO_2 concentrations peak in year 2250 with 2148.6 ppmv and equal 1835.8 ppmv in year 3005 (see Fig. 2a).

2.4 Simulated pre-industrial equilibrium

The UVic ESCM has been validated under present-day and pre-industrial conditions in numerous studies (Eby et al., 2009; Weaver et al., 2001). In particular, Keller et al. (2012) recently compared results of its ocean biogeochemical component to observations and previous model formulations. We therefore concentrate our validation on the new model component in this study, the P cycle.

Estimates of pre-industrial burial rates vary over a wide range in the literature. The comprehensive review by Slomp (2011) reported a burial rate of 0.032–0.35 Tmol P a^{-1} for the total ocean, while Baturin (2007) suggests a burial rate of 0.419 Tmol P a^{-1} based on observational data described in detail by Wallmann (2010). The burial rate diagnosed by the UVic ESCM in simulation WB for the total ocean under pre-industrial boundary conditions (0.38 Tmol P a^{-1}) is within range of these earlier estimates. The burial at the continental margin (0–200 m) accounts for 50–84 % of total burial corresponding to 0.016–0.175 Tmol P a^{-1} calculated in Slomp (2011). Ruttenberg (2004) estimated a burial rate at continental margins of 0.15–0.22 Tmol P a^{-1}, while the UVic ESCM calculated a burial rate of 0.33 Tmol P a^{-1} for the continental margins in year 1775. The open-ocean burial contributes only a minor part to total burial (0.04–0.13 Tmol P a^{-1}; Ruttenberg, 2004; in the UVic it is 0.046 Tmol P a^{-1}).

To conserve marine P during long model spin-ups, the dissolved weathering flux of P under pre-industrial conditions is set equal to the diagnosed total burial rate during the spin-up: 0.38 Tmol P a^{-1}. Following the method of calculating the reactive P flux (defined in Ruttenberg, 2004 as the sum of > 50 % of total dissolved P (i.e. dissolved organic P) plus 25–40 % of particulate P flux), our result fits well with estimates summarised by Slomp (2011) ranging from 0.13 Tmol P a^{-1} (natural P flux) to 0.36 Tmol P a^{-1} (modern P flux) and Ruttenberg (2004) (0.16–0.32 Tmol P a^{-1}).

Global values for benthic release under pre-industrial conditions equal 0.78 Tmol P a^{-1} in the UVic ESCM (simulation WB), while Ruttenberg (2004) described a range from 0.51 to 0.84 Tmol P a^{-1} based on pore water measurements (Colmann and Holland, 2000) for coastal regions. For the deep sea, Colmann and Holland (2000) specified the benthic release value with 0.41 Tmol P a^{-1}. In the UVic ESCM, the benthic release for continental margins was calculated as 0.4816 Tmol P a^{-1} and for the open ocean as 0.2951 Tmol P a^{-1}.

3 Results

3.1 Simulated climate

The global mean atmospheric surface temperature, as simulated by the WB run, increases until year 2835 and peaks at 23.1 °C, i.e. 9.9 °C above pre-industrial levels. Simulation REF shows similar changes in temperature with an increase until year 2855 and a peak at 23.3 °C (see Fig. 2a). Both simulations show a slight recovery in temperatures after the peak (REF: 23.2 °C; WB: 23.1 °C; year 3005). Atmospheric temperatures in the WB simulation are slightly lower than in the reference simulation, due to slightly lower carbon dioxide concentrations in the atmosphere, caused by increased global ocean alkalinity (REF: 2.498 mol m^{-3}; WB: 2.481 mol m^{-3}; both for year 3005), the enhanced biological pump and a rise in detritus export rate (see Sect. 3.2) and therefore increased marine uptake of atmospheric CO_2. The impact of the negative feedback via enhanced biotically and chemically induced marine uptake of atmospheric CO_2 on surface air temperatures is thus small compared to the CO_2-induced warming in a high-emission scenario.

Given that the response in temperature is similar for both simulations compared to considerable differences in biological productivity (see below), differences in oxygen concentration mainly originate from biogeochemical changes, which will be discussed in Sect. 3.3.

3.2 Phosphorus dynamics

The weathering rate (see Fig. 3b) and associated flux of P into the ocean via river discharge more than doubles relative to the pre-industrial situation in our WB simulation and leads to an enhancement in global mean oceanic P concentrations by 27 % over 1000 years (see Fig. 2b). At the same time, benthic burial acts as the only P sink in our model (see the Supplement, Fig. S1), mitigating the total increase in marine P. The P concentration remains constant in the control run REF.

The weathering input in the WB simulation is largest north of 30° N (0.338 Tmol P a^{-1} in year 3005; see Fig. 3a), while south of 30° S (0.138 Tmol P a^{-1}) and in the low-latitude Pacific Ocean the input is lowest (0.117 Tmol P a^{-1}). Weathering fluxes into the low-latitude Indian and Atlantic oceans equal 0.187 and 0.267 Tmol P a^{-1}, respectively.

Increasing P concentrations as well as climate warming result in an increase in net primary production in the ocean (ONPP). Globally integrated ONPP ranges between 43.8 Tmol P a^{-1} (REF) and 44.1 Tmol P a^{-1} (WB) under pre-industrial conditions and 65 Tmol P a^{-1} (REF) and 116.4 Tmol P a^{-1} (WB) in year 3005 (see Fig. S1). The main areas of ONPP increase are located in the tropical ocean, where higher temperatures favour net primary production in the model (results not shown).

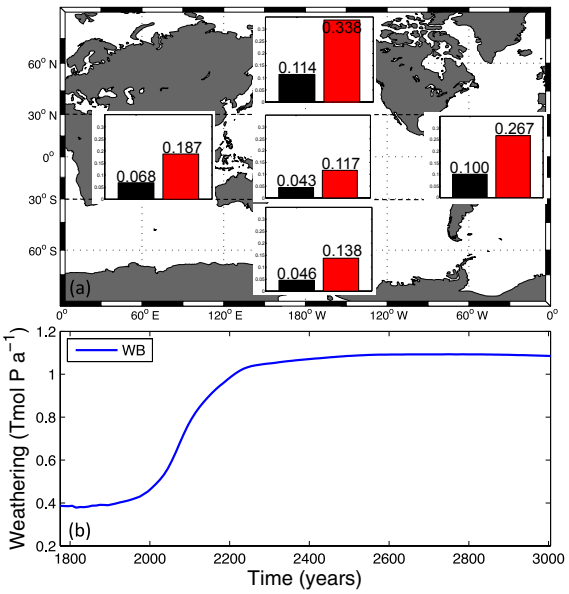

Figure 3. **(a)** Phosphorus weathering input (in Tmol a^{-1}) into the tropical Pacific Ocean (middle), tropical Atlantic Ocean (right, middle), tropical Indian Ocean (left, middle), northern oceans (oceans north of 30° N; upper middle) and Southern Ocean (ocean south of 30° S; lower middle) in 1775 (black bars) and 3005 (red bars). **(b)** Annual mean averaged phosphorus weathering input (global sum) of 1775 until year 3005.

Due to enhanced P inventory and enhanced ONPP, the WB simulation also has a higher export rate (8.6 Tmol P a^{-1}, computed at 130 m depth; see Fig. 2b) when compared to the reference run (5.5 Tmol P a^{-1}) in year 3005. In the REF simulation, the export rate declines until year 2175 (4.8 Tmol P a^{-1}) in response to enhanced stratification, associated declining nutrient supply and stronger nutrient recycling in the upper layers (Schmittner et al., 2008; Steinacher et al., 2010; Bopp et al., 2013; Moore et al., 2013; Yool et al., 2013; Kvale et al., 2015). The export rate recovers to reach 5.5 Tmol P a^{-1} at the end of the simulation in experiment REF.

The globally integrated remineralisation rate in the aphotic zone (results not shown) ranges between 5.1 Tmol P a^{-1} (WB) and 5.2 Tmol P a^{-1} (REF) in year 1775. Simulation WB is characterised by a strong increase in remineralisation until 3005 with a maximum of 8.1 Tmol P a^{-1} (in year 3005), while in the reference run the remineralisation rate first decreases, followed by a moderate increase to 5.3 Tmol P a^{-1}. Regions with highest remineralisation are located on the continental margins, especially in the Indian Ocean.

The P burial in the WB simulation equals 0.38 Tmol P a^{-1} in year 1775 and decreases by 44.3 % to 0.2 Tmol P a^{-1} in year 3005 (see Fig. S1). One reason for this decrease is the redox state of the bottom water. The strong expansion of the area of ocean bottom waters with O_2 concentrations below 0.005 mol m^{-3} (see Fig. 2d) in the WB simulation leads to a decrease in benthic burial of P despite an increase in the rain rate of particulate organic P, RR_{POP}. In general, burial rates are largest along the coastal margins, where 87.9 % of the total flux is buried in 1775. Highest increases in burial rates between years 1775 and 3005 are located in the Arctic Ocean (see Fig. 4a), whereas burial rates decrease in the Bay of Bengal and the Gulf of Mexico where low-oxygen bottom waters expand (see Fig. 5).

The benthic P release in the WB simulation increases by 119 % until year 3005 to 1.7 Tmol P a^{-1} (see Fig. S1). As mentioned above, the benthic release is a redox-dependent process, which commonly takes place at the coastal margins (Wallmann, 2010; in our model, under pre-industrial conditions, 62 % of total release is from coastal margins). This means that an increase in suboxic bottom water area (see Fig. 2d) leads to an enhanced release of benthic P in WB. A rapid increase between years 1775 and 3005 can be found in the Bay of Bengal, the Gulf of Mexico and in the Arctic Ocean (see Fig. 4b).

In our model simulations, both the weathering-induced P flux into the ocean (see Fig. 2c) as well as the net P released from the sediments (see Fig. 2c) show a strong increase under continued global warming, which explains the increase in the marine P inventory in the WB simulation (see Fig. 2b). However, the simulated increase in the weathering input has a much stronger (about 4 times larger) impact on the P budget and therefore on the expansion of OMZs than the benthic release feedback (see Fig. 2c). We note that even at the end of the 1000-year simulation, the P cycle has not yet reached a new steady state in experiment WB. Weathering rates are high in the warm climate and burial of P has not increased to counteract the supply by weathering (see Figs. 3b and S1). The release of P from sediments also adds to this imbalance. As a result, the marine P inventory is still increasing almost linearly at the end of our simulation. Extending the simulation until year 10 000 reveals that the ocean – as well as the coastal regions – does not become anoxic despite a more than 3-fold increase in oceanic P inventory (see Sect. 3.3 and Fig. S2) while the P cycle still exhibits a strong imbalance between sources and sinks.

3.3 Oxygen response

The black contours in Fig. 5 indicate the lateral extent of OMZs for a depth of 300 m (see Fig. S3 for a depth of 900 m). In year 1775, the suboxic volume, defined here as waters with oxygen concentrations of less than 5 mmol m^{-3}, equals 3.9×10^6 km^3 in both simulations (see Fig. 2d). An observational estimate of today's suboxic water volume equals $102 \times 10^6 \pm 15 \times 10^6$ km^3 for oxygen concentrations less than 20 mmol m^{-3} (Paulmier and Ruiz-Pino, 2009), which is considerably larger than the volume of O_2 concentrations less than 20 mmol m^{-3} in our WB simula-

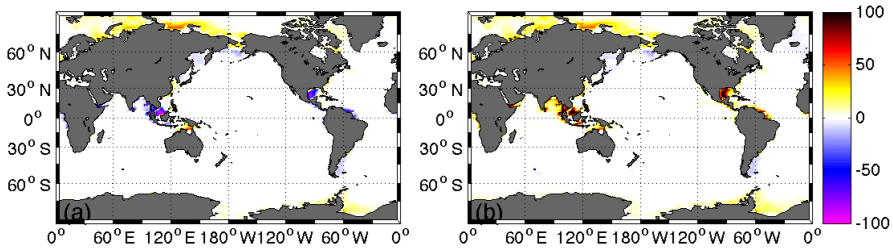

Figure 4. Difference (year 3005 minus year 1775) in **(a)** burial and **(b)** benthic release flux in mmol P m^{-2} a^{-1} for simulation WB.

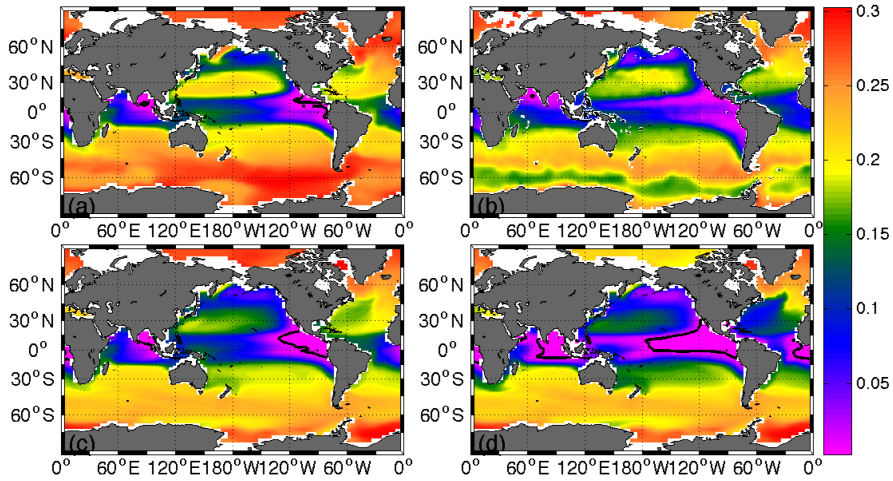

Figure 5. Oxygen concentration in mol O_2 m^{-3} at 300 m depth simulated by the **(a)** control simulation in year 1775 (representative for both REF and WB model runs in year 1775), **(b)** the World Ocean Atlas in 2009, **(c)** the control simulation in year 3005 and **(d)** simulation WB in year 3005. The black contour lines at 0.005 mol m^{-3} highlight the oxygen minimum zones (OMZs).

tion ($WB_{2005} = 15.8 \times 10^6$ km^3). However, in consideration of the studies of Bianchi et al. (2012) and their calculated OMZ volume of 2.28–2.78 $\times 10^6$ km^3, as well as the World Ocean Atlas ($WOA_{2005} = 4.12 \times 10^5$ km^3), it can be concluded that estimations of the volume of OMZs vary over a wide range and that our results are within this range. Comparing our results with observational data from the WOA, a generally good agreement can be found with regard to the spatial distribution of low-oxygen waters (see Fig. 5). The suboxic areas are located in the upwelling regions of the tropical eastern Pacific and eastern Atlantic as well as in the Indian Ocean (see Fig. 5; representative for both simulations in 1775).

During our transient simulations, we find a considerable expansion of OMZs until year 3005 in both simulations (see Figs. 2d and 5). The expansion of the suboxic volume between 300 and 900 m is particularly pronounced in the WB simulation where the OMZs account for 4.85 $\times 10^7$ km^3 in year 3005, i.e. an increase by a factor of 12.4. The control simulation (REF) shows a much smaller increase in the volume of OMZs (1.12 $\times 10^7$ km^3 between 300 and 900 m depth). As both simulations display similar climates (see Fig. 2a), the difference in the oxygen fields is largely due to the differences in the simulated P cycle.

The sea-floor area in contact with suboxic bottom waters, which directly impacts the redox-sensitive benthic burial and P release, shows an increase by more than a factor of 19 ($WB_{1775} = 3.59 \times 10^5$ km^2; $WB_{3005} = 6.95 \times 10^6$ km^2) in the WB simulation (see Fig. 2d) compared to a factor of 4 increase in the REF simulation ($REF_{1775} = 2.79 \times 10^5$ km^2; $REF_{3005} = 1.2 \times 10^6$ km^2). Our present-day results ($WB_{2005} = 3.8 \times 10^5$ km^2) compare well with data of the WOA ($WOA_{2005} = 2.48 \times 10^5$ km^2).

Somewhat unexpectedly, in our study, an increase in continental weathering does not result in an anoxic ocean under current topography and seawater chemistry – at least not until year 10 000. At the pre-industrial state (year 1775), 0.12 % of all coastal margins are characterised by oxygen concentrations below 0.005 mol m^{-3}. While this portion increases by about a factor of 50 to 5.57 % by year 3005, this is too low for the generation of widespread coastal anoxia. Conversely, the global mean oxygen concentration starts to increase again in year 3415 when it has reached a minimum of about two-

thirds of the pre-industrial oxygen inventory in the WB simulation (see Fig. S1). This suggests that the positive feedback between the release of benthic P and marine net primary production is – in this study, for present-day bathymetry and geography – not the decisive factor for a rapid transition into an anoxic ocean.

4 Uncertainties

Although the model's subcomponents for weathering, burial and benthic release rates are highly simplified in this study, the simulated global P fluxes fall within the range suggested by earlier studies and observational estimates (Palastanga et al., 2011; Filippelli, 2002; Baturin, 2007; Wallmann, 2010). The weathering fluxes are calibrated against global mean burial rates under an implicit steady-state assumption, although it is unclear whether the pre-industrial P cycle in the ocean was in equilibrium (Wallmann, 2010). The relatively high P weathering fluxes as well as the assumed indefinite P reservoir in the shelf sediments in our simulations might lead to an overestimation of the effects on the P cycle and OMZs.

In our model, the increase in the P inventory results in a strong increase in ONPP. Contrary to other studies, e.g. Gregg et al. (2005) or Boyce et al. (2010), in our study the temperature effect overcompensates the stratification effect as described by Sarmiento et al. (2004), Taucher and Oschlies (2011) and Kvale et al. (2015), and thus leads to an increase in ONPP also in the reference run. While the net effect of warming on ONPP is not well constrained and differs considerably among models, the impact of changing environmental conditions on export production appears to be better constrained (Taucher and Oschlies, 2011). In agreement with simulations by other models, experiment REF shows a stratification-induced decline in export production, while the increase in P induces an increase in export production in WB. Although we use a coarse-resolution model, the applied sub-grid-scale bathymetry allows the calculation of more accurate benthic burial and release fluxes than otherwise possible with such a model. It should also be noted that the benthic release feedback on OMZs might have been more efficient under Cretaceous boundary conditions because the shelf area was considerably larger due to higher sea levels (late Cretaceous shelf area: 46×10^6 km^2; present-day shelf area: 26×10^6 km^2; Bjerrum et al., 2006). Cretaceous topography might therefore have induced a stronger benthic release feedback, as shown in Tsandev and Slomp (2009).

Filippelli (2002) showed in his study that due to the anthropogenic activities the global, total present-day river input of P has doubled in the last 150 years. In our study, the direct anthropogenic influence, such as agricultural input of P into the system, is excluded and should be considered in future studies even though the human impact is projected to decrease until year 3500 (Filippelli, 2008). Filippelli (2008) and Harrison et al. (2005) estimated a rate of 0.03 Tmol P a^{-1} and 0.7 Tg P a^{-1} (0.023 Tmol P a^{-1}), respectively, for anthropogenic P delivered to the ocean as a result of fertilisation, deforestation and soil loss as well as sewage in year 3000. In comparison to our simulated maximum weathering value of 1.09 Tmol P a^{-1} until year 3005, the direct anthropogenic impact seems to be small.

5 Conclusions

This study constitutes a first approach to estimate the potential impact of changes in the marine P cycle on the expansion of global ocean OMZs under global warming on millennial timescales. Model simulations show that the warming-induced increase in terrestrial weathering (see Fig. 3b) leads to an increase in marine P inventory (see Fig. 2b) resulting in an intensification of the biological pump, corroborating the findings by Tsandev and Slomp (2009). As a consequence, oxygen consumption as well as the volume of OMZs increase in our simulations by a factor of 12 over the next millennium (see Figs. 2d and 5).

The positive feedback involving redox-sensitive benthic P fluxes – where the expansion of OMZs leads to an increase in benthic release of P (see Figs. 2c and S1), which in turn enhances biological production and subsequent oxygen consumption (Wallmann, 2010) – has only limited relevance for the expansion of OMZs in this study. Instead, a negative feedback dominates, which involves enhanced weathering and P supply to the ocean, an intensification of the biological carbon pump and associated marine uptake of atmospheric CO_2. The atmospheric CO_2 impacts the surface air temperature through a negative feedback loop, which limits the warming and weathering and, eventually, the expansion of the OMZs. We can therefore conclude that, based on the parameterisations used in this study, the P weathering and biological pump feedback outcompetes the redox-sensitive benthic P-release feedback on millennial timescales. Although the ocean does not become anoxic in our simulations, the benthic P-release feedback may have played a role in past oceanic anoxic events. An increase in shelf areas due to higher sea levels, such as during the Cretaceous, would have led to a more powerful benthic P-release feedback as a much larger sediment area could have been in contact with low-oxygen bottom waters. Whether this different bathymetry alone could result in a more dominant benthic P-release feedback needs to be investigated in future studies.

Code availability. The model data and model code are available at http://data.geomar.de/thredds/catalog/open_access/niemeyer-et-al_2016/catalog.html.

The Supplement related to this article is available online at doi:10.5194/esd-8-357-2017-supplement.

Competing interests. The authors declare that they have no conflict of interest.

Acknowledgements. This work is a contribution to the Sonderforschungsbereich (SFB) 754 "Climate-Biogeochemical Interactions in the Tropical Ocean" and the BMBF project PalMod. We thank M. Eby for his excellent help with the UVic ESCM and K. F. Kvale and J. Getzlaff for proofreading. Katrin J. Meissner is thankful for UNSW Science Silver- and Goldstar Awards.

The article processing charges for this open-access publication were covered by a Research Centre of the Helmholtz Association.

Edited by: A. Levermann
Reviewed by: two anonymous referees

References

Archer, D.: A data-driven model of the global calcite lysocline, Global Biogeochem. Cy., 10, 511–526, doi:10.1029/96GB01521, 1996.

Baturin, G. N.: Issue of the Relationship between Primary Productivity of Organic Carbon in Ocean and Phosphate Accumulation (Holocene-Late Jurassic), Lith. Mineral Res., 42, 318–348, doi:10.1134/S0024490207040025, 2007.

Berner, R. A.: Weathering, plants and the long-term carbon cycle, Geochim. Cosmochim. Ac., 56, 3225–3231, 1991.

Berner, R. A. and Rao, J.-L.: Phosphorus in sediments of the Amazon River and estuary: Implications for the global flux of phosphorus to the sea, Geochim. Cosmochim. Ac., 58, 2333–2339, 1994.

Bianchi, D., Dunne, J. P., Sarmiento, J. L., and Galbraith, E. D.: Data-based estimates of suboxia, denitrification, and N_2O production in the ocean and their sensitivities to dissolved O_2, Global Biogeochem. Cy., 26, GB2009, doi:10.1029/2011GB004209, 2012.

Bjerrum, C. J., Bendtsen, J., and Legarth, J. I. F.: Modelling organic carbon burial during sea level rise with reference to the Cretaceous, Geochem. Geophy. Geosy., 7, Q05008, doi:10.1029/2005GC001032, 2006.

Bopp, L., Le Quere, C., Heimann, M., and Manning, A.: Climate-induced oceanic oxygen fluxes: Implications for the contemporary carbon budget, Global Biogeochem. Cy., 16, 6-1–6-13, doi:10.1029/2001GB001445, 2002.

Bopp, L., Resplandy, L., Orr, J. C., Doney, S. C., Dunne, J. P., Gehlen, M., Halloran, P., Heinze, C., Ilyina, T., Séférian, R., Tjiputra, J., and Vichi, M.: Multiple stressors of ocean ecosystems in the 21st century: projections with CMIP5 models, Biogeosciences, 10, 6225–6245, doi:10.5194/bg-10-6225-2013, 2013.

Boyce, D. G., Lewis, M. R., and Worm, B.: Global phytoplankton decline over the past century, Nature, 466, 591–596, 2010.

Cabré, A., Marinov, I., Bernardello, R., and Bianchi, D.: Oxygen minimum zones in the tropical Pacific across CMIP5 models: mean state differences and climate change trends, Biogeosciences, 12, 5429–5454, doi:10.5194/bg-12-5429-2015, 2015.

Colmann, A. S. and Holland, H. D.: The global diagenetic flux of phosphorus from marine sediments to the oceans: Redox sensitivity and the control of atmospheric oxygen levels, Marine Authigenesis: From Global to Microbial, Spec. Publ. SEPM Soc. Sediment. Geol., 66, 21–33, 2000.

Compton, J., Mallinson, D., Glenn, C. R., Filippelli, G., Föllmi, K., Shields, G., and Zanin, Y.: Variations in the global phosphorus cycle, Marine Authigenesis: From Global to Microbial, edited by: Glenn, C. R., Prévôt, L., and Lucas, J., SEPM Spec. Publ., 66, 53–75, 2000.

Eby, M., Zickfeld, K., Montenegro, A., Archer, D., Meissner, K. J., Weaver, A. J.: Lifetime of Anthropogenic Climate Change: Millennial Time Scales of Potential CO_2 and Surface Temperature Perturbations, J. Climate, 22, 2501–2511, doi:10.1175/2008JCLI2554.1, 2009.

Fanning, A. G. and Weaver, A. J.: An atmospheric energy-moisture model: Climatology, interpentadal climate change and coupling to an ocean general circulation model, J. Geophys. Res., 101, 15111–15128, doi:10.1029/96JD01017, 1996.

Filippelli, G. M.: The Global Phosphorus Cycle, Rev. Mineral. Geochem., 48, 391–425, doi:10.2138/rmg.2002.48.1, 2002.

Filippelli, G. M.: The Global Phosphorus Cycle: Past, Present, and Future, Elements, 4, 89–95, doi:10.2113/GSELEMENTS.4.2.89, 2008.

Floegel, S., Wallmann, K., Poulson, C. J., Zhou, J., Oschlies, A., Voigt, S., and Kuhnt, W.: Simulating the biogeochemical effects of volcanic CO_2 degassing on the oxygen-state of the deep ocean during the Cenomanian/Turonian Anoxic Event (OAE2), Earth. Planet. Sc. Lett., 305, 371–384, doi:10.1016/j.epsl.2011.03.018, 2011.

Föllmi, K. B.: The phosphorus cycle, phosphogenesis and marine phosphate-rich deposits, Earth-Sci. Rev., 40, 55–124, doi:10.1016/0012-8252(95)00049-6, 1996.

Froelich P. N.: Interactions of the marine phosphorus and carbon cycles, in: The Interaction of Global Biogeochemical Cycles, edited by: Moore, B. and Dastoor, M. N., California Institute of Technology, Pasadena, NASA – JPL Publication 84–21, 141–176, 1984.

Froelich, P. N., Bender, M. L., and Luedtke, N. A.: The marine phosphorus cycle, Am. J. Sci., 282, 474–511, doi:10.2475/ajs.282.4.474, 1982.

Gregg, W. G., Casey, N. W., and McClain, C. R.: Recent trends in global ocean chlorophyll, Geophys. Res. Lett., 32, L03606, doi:10.1029/2004GL021808, 2005.

Handoh, I. and Lenton, T. M.: Periodic mid-Cretaceous oceanic anoxic events linked by oscillations of the phosphorus and oxygen biogeochemical cycles, Global Biogeochem. Cy., 17, 1092, doi:10.1029/2003GB002039, 2003.

Harrison, J., Seitzinger, S. P., Bouwman, F., Caraco, N. F., Beusen, A. H. W., and Vörösmarty, C. J.: Dissolved inorganic phosphorus export to the coastal zone: Results from a spatially explicit, global model, Global Biogeochem. Cy., 19, GB4S03, doi:10.1029/2004GB002357, 2005.

Hibler, W. D.: A dynamic thermodynamic sea ice model, J. Phys. Oceanogr., 9, 815–846, 1979.

Hofmann, M. and Schellnhuber, H. J.: Ocean acidification: a millennial challenge, Energy Environ. Sci., 3, 1883–1896, doi:10.1039/C000820F, 2010.

Hunke, E. C. and Dukowicz, J. K.: An Elastic-Viscous-Plastic Model for Sea Ice Dynamics, J. Phys. Oceanogr., 27, 1849–1867, 1997.

Ingall, E. and Jahnke, R.: Evidence for enhanced phosphorus regeneration from marine sediments overlain by oxygen depleted waters, Geochim. Cosmochim. Ac., 58, 2571–2575, doi:10.1016/0016-7037(94)90033-7, 1994.

Keller, D. P., Oschlies, A., and Eby, M.: A new marine ecosystem model for the University of Victoria Earth System Climate Model, Geosci. Model Dev., 5, 1195–1220, doi:10.5194/gmd-5-1195-2012, 2012.

Kraal, P., Slomp, C. P., Reed, D. C., Reichart, G.-J., and Poulton, S. W.: Sedimentary phosphorus and iron cycling in and below the oxygen minimum zone of the northern Arabian Sea, Biogeosciences, 9, 2603–2624, doi:10.5194/bg-9-2603-2012, 2012.

Kvale, K. F., Meissner, K. J., and Keller, D. P.: Potential increasing dominance of heterotrophy in the global ocean, Environ. Res. Lett., 10, 074009, doi:10.1088/1748-9326/10/7/074009, 2015.

Lenton, T. M. and Britton, C.: Enhanced carbonate and silicate weathering accelerates recovery from fossil fuel CO_2 perturbations, Global Biogeochem. Cy., 20, B3009, doi:10.1029/2005GB002678, 2006.

Lenton, T. M. and Watson, A. J.: Redfield revisited. 1. Regulation of nitrate, phosphate, and oxygen in the ocean, Global Biogeochem. Cy., 14, 225–248, doi:10.1029/1999GB900065, 2000.

Manabe, S. and Stouffer, R. J.: Multiple-Century Response of a Coupled Ocean-Atmosphere Model to an increase of Atmospheric Carbon Dioxide, J. Climate, 7, 5–23, 1993.

Meinshausen, M., Smith, S. J., Calvin, K., Daniel, J. S., Kainuma, M. L. T., Lamarque, J.-F., Matsumoto, K., Montzka, S. A., Raper, S. C. B., Riahi, K., Thomson, A., Velders, G. J. M., and van Vuuren, D. P. P.: The RCP greenhouse gas concentrations and their extensions from 1765 to 2300, Climatic Change, 109, 213–241, doi:10.1007/s10584-011-0156-z, 2011.

Meissner, K. J., Weaver, A. J., Matthews, H. D., and Cox, P. M.: The role of land surface dynamics in glacial inception: a study with the UVic Earth System Model, Clim. Dynam., 21, 515–537, doi:10.1007/s00382-003-0352-2, 2003.

Meissner, K. J., McNeil, B., Eby, M., and Wiebe, E. C.: The importance of the terrestrial weathering feedback for multimillenial coral reef habitat recovery, Global Biogeochem. Cy., 26, GB3017, doi:10.1029/2011GB004098, 2012.

Monteiro, F. M., Pancost, R. D., Ridgwell, A., and Donnadieu, Y.: Nutrients as the dominant control on the spread of anoxia and euxinia across the Cenomanian-Turonian oceanic anoxic event (OAE2): Model-data comparison, Paleoceanography, 27, PA4209, doi:10.1029/2012PA002351, 2012.

Moore, J. K., Lindsay, K., Doney, S. C., Long, M. C., and Misumi, K.: Marine Ecosystem Dynamics and Biogeochemical Cycling in the Community Earth System Model [CESM1(BGC)]: Comparison of the 1990s with the 2090s under the RCP4.5 and RCP8.5 Scenarios, J. Climate, 26, 9291–9312, doi:10.1175/JCLI-D-12-00566.1, 2013.

Oschlies, A., Schulz, K. G., Riebesell, U., and Schmittner, A.: Simulated 21^{st} century's increase in oceanic suboxia by CO_2-enhanced biological carbon export, Global Biogeochem. Cy., 22, GB4008, doi:10.1029/2007GB003147, 2008.

Pacanowski, R. C.: MOM 2 Documentation User's Guide and Reference Manual, Version 1.0. GFDL Technical Report, 1995.

Palastanga, V., Slomp, C. P., and Heinze, C.: Long-term controls on ocean phosphorus and oxygen in a global biogeochemical model, Global Biogeochem. Cy., 25, GB3024, doi:10.1029/2010GB003827, 2011.

Paulmier, A. and Ruiz-Pino, D.: Oxygen minimum zones (OMZs) in the modern ocean, Prog. Oceanogr., 80, 113–128, doi:10.1016/j.pocean.2008.08.001, 2009.

Payton, A. and McLoughlin, K.: The Oceanic Phosphorus Cycle, Chem. Rev., 107, 563–576, doi:10.1021/cr0503613, 2007.

Redfield, A. C., Ketchum, B. H., and Richards, F. A.: The influence of organisms on the composition of seawater, The Sea, edited by: Hill, M. N., 2, 26–77, 1963.

Riahi, K., Rao, S., Krey, V., Cho, C., Chirkov, V., Fischer, G., Kindermann, G., Nakicenovic, N., and Rafaj, P.: RCP 8.5 – A scenario of comparatively high greenhouse gas emissions, Climatic Change, 109, 33–57, doi:10.1007/s10584-011-0149-y, 2011.

Ruttenberg, K. C.: The global phosphorus cycle. The Global Phosphorus Cycle. Treatise on Geochemistry, edited by: Schlesinger, W., 585–643, Elsevier, Amsterdam, 2004.

Ruvalcaba Baroni, I., Topper, R. P. M., van Helmond, N. A. G. M., Brinkhuis, H., and Slomp, C. P.: Biogeochemistry of the North Atlantic during oceanic anoxic event 2: role of changes in ocean circulation and phosphorus input, Biogeosciences, 11, 977–993, doi:10.5194/bg-11-977-2014, 2014.

Sabine, C. L., Feely, R. A., Gruber, N., Key, R. M., Lee, K., Bullister, J. L., Wanninkhof, R., Wong, C. S., Wallace, D. W. R., Tilbrook, B., Millero, F. J., Peng, T.-H., Kozyr, A., Ono, T., and Rios, A. F.: The Oceanic Sink for Anthropogenic CO_2, Science, 305, 367–371, doi:10.1126/science.1097403, 2004.

Sarmiento, J. L. and Orr, J. C.: Three-dimensional simulations of the impact of Southern Ocean nutrient depletion on atmospheric CO_2 and ocean chemistry, Limnol. Oceanogr., 36, 1928–1950, 1991.

Sarmiento, J. L., Hughes, T. M. C., Stouffer, R. J., and Manabe, S.: Simulated response of the ocean carbon cycle to anthropogenic climate warming, Letters to Nature, 393, 245–249, doi:10.1038/30455, 1998.

Sarmiento, J. L., Slater, R., Barber, R., Bopp, L., Doney, S. C., Hirst, A. C., Kleypas, J., Mataer, R., Mikolajewicz, U., Monfray, P., Soldatov, V., Spall, S. A., and Stouffer, R.: Response of ocean ecosystems to climate warming, Global Biogeochem. Cy., 18, GB3003, doi:10.1029/2003GB002134, 2004.

Schlanger, S. O. and Jenkyns, H. C.: Cretaceous oceanic anoxic events: causes and consequences, Geologie Mijnbouw, 55, 179–184, 1976.

Schmidtko, S., Stramma, L., and Visbeck, M.: Decline in global oceanic oxygen content during the past five decades, Nature, 542, 335–339, doi:10.1038/nature21399, 2017.

Schmittner, A., Oschlies, A., Matthews, H. D., and Galbraith, E. D.: Future changes in climate, ocean circulation, ecosystems, and biogeochemical cycling simulated for a business-as-usual CO_2 emission scenario until year 4000 AD, Global Biogeochem. Cy., 22, GB1013, doi:10.1029/2007GB002953, 2008.

Semtner, A. J.: A Model for the Thermodynamic Growth of Sea Ice in Numerical Investigations of Climate, J. Phys. Oceanogr., 6, 379–389, 1976.

Slomp, C. P.: Phosphorus cycling in the estuarine and coastal zones: Sources, sinks, and transformations. Treatise on Estuarine and

Coastal Science, edited by: Wolanski, E. and McLusky, D., 201–230, 2011.

Slomp, C. P. and Van Cappellen, P.: The global marine phosphorus cycle: sensitivity to oceanic circulation, Biogeosciences, 4, 155–171, doi:10.5194/bg-4-155-2007, 2007.

Somes, C. J., Oschlies, A., and Schmittner, A.: Isotopic constraints on the pre-industrial oceanic nitrogen budget, Biogeosciences, 10, 5889–5910, doi:10.5194/bg-10-5889-2013, 2013.

Steinacher, M., Joos, F., Frölicher, T. L., Bopp, L., Cadule, P., Cocco, V., Doney, S. C., Gehlen, M., Lindsay, K., Moore, J. K., Schneider, B., and Segschneider, J.: Projected 21st century decrease in marine productivity: a multi-model analysis, Biogeosciences, 7, 979–1005, doi:10.5194/bg-7-979-2010, 2010.

Stramma, L., Johnson, G. C., Sprintall, J., and Mohrholz, V.: Expanding Oxygen-Minimum Zones in the Tropical Ocean, Science, 320, 655–658, doi:10.1126/science.1153847, 2008.

Stramma, L., Oschlies, A., and Schmidtko, S.: Mismatch between observed and modeled trends in dissolved upper-ocean oxygen over the last 50 yr, Biogeosciences, 9, 4045–4057, doi:10.5194/bg-9-4045-2012, 2012.

Taucher, J. and Oschlies, A.: Can we predict the direction of marine primary production change under global warming?, Geophys. Res. Lett, 38, L02603, doi:10.1029/2010GL045934, 2011.

Tsandev, I. V. and Slomp, C. P.: Modelling phosphorus cycling and carbon burial during Cretaceous Oceanic Anoxic Events, Earth Planet. Sc. Lett., 286, 71–79, doi:10.1016/j.epsl.2009.06.016, 2009.

Tyrell, T.: The relative influences of nitrogen and phosphorus on oceanic primary production, Nature, 400, 525–531, doi:10.1038/22941, 1999.

Wallmann, K.: Phosphorus imbalance in the global ocean?, Global Biogeochem. Cy., 24, GB4030, doi:10.1029/2009GB003643, 2010.

Weaver, A. J., Eby, M., Wiebe, E. C., Bitz, C. M., Duffy, P. B., Ewen, T. L., Fanning, A. F., Holland, M. M., MacFadyen, A., Matthews, H. D., Meissner, K. J., Saenko, O., Schmittner, A., Wang, H., and Yoshimori, M.: The UVic Earth System Climate Model: Model Description, Climatology and Applications to Past, Present and Future Climates, Atmos. Ocean, 39, 361–428, doi:10.1080/07055900.2001.9649686, 2001.

Yool, A., Popova, E. E., Coward, A. C., Bernie, D., and Anderson, T. R.: Climate change and ocean acidification impacts on lower trophic levels and the export of organic carbon to the deep ocean, Biogeosciences, 10, 5831–5854, doi:10.5194/bg-10-5831-2013, 2013.

Supplement of Earth Syst. Dynam., 8, 357–367, 2017
http://www.earth-syst-dynam.net/8/357/2017/
doi:10.5194/esd-8-357-2017-supplement

Earth System Dynamics
Open Access
EGU

Supplement of

A model study of warming-induced phosphorus–oxygen feedbacks in open-ocean oxygen minimum zones on millennial timescales

Daniela Niemeyer et al.

Correspondence to: Daniela Niemeyer (dniemeyer@geomar.de)

Contents of this file

Benthic burial, benthic release, O_2 concentration & ONPP

O_2 map in year 10,000

O_2 map in a depth of 900 m

Introduction

The supplement provides one figure showing the global and annual mean phosphorus fluxes (benthic burial & benthic release), the oxygen concentration and the ocean net primary production. Figure S2 illustrates the oxygen concentration in year 10,000 for a depth of 300 m and 900 m, while the last figure shows the oxygen concentration in a depth of 900 m.

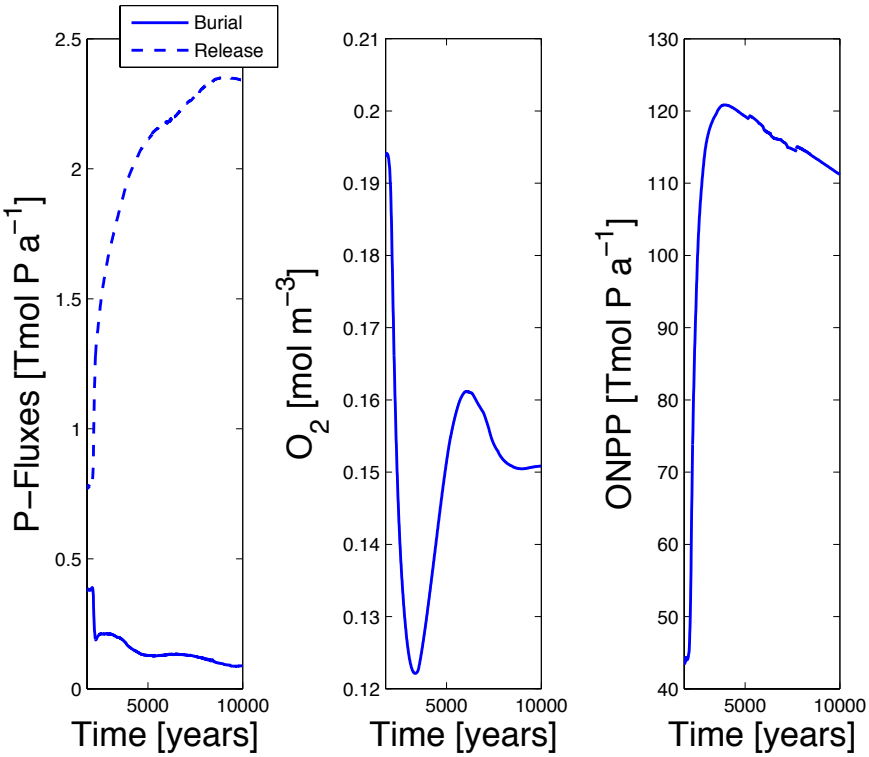

Figure S1: Global mean and annual mean time series of phosphorus burial (blue solid line; left), phosphorus release (blue dashed line; left), oxygen (blue solid line; middle) and ONPP (blue solid line; right) for simulation WB until year 10,000.

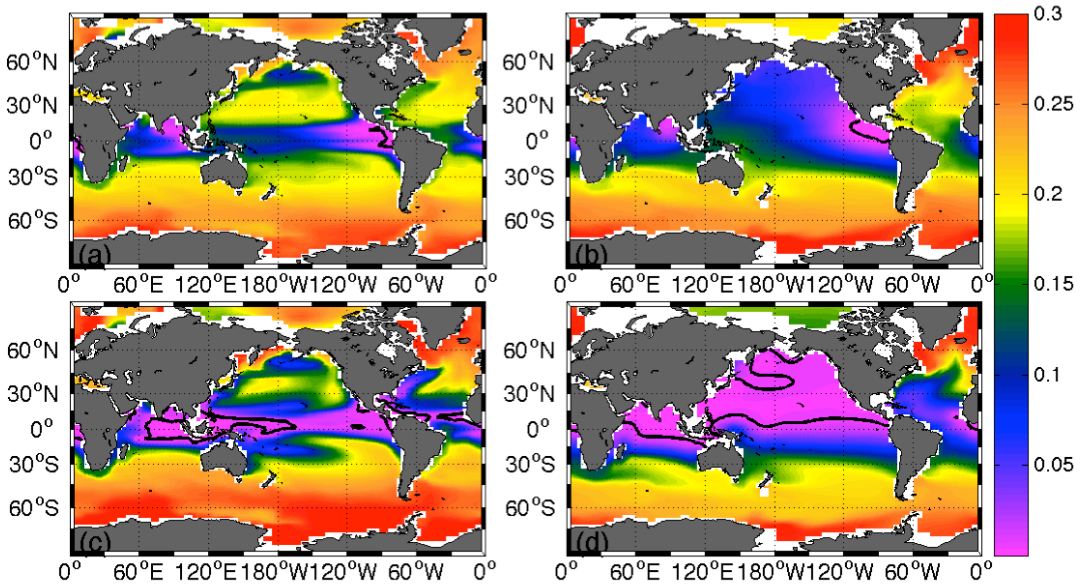

Figure S2: Oxygen concentration in mol O_2 m^{-3} at year 10,000 simulated by the (a) control simulation at 300m depth, (b) and 900m depth, (c) simulation WB at 300m depth and (d) simulation WB at 900 m depth. The black contour lines at 0.005 mol m^{-3} highlight the oxygen minimum zones (OMZs).

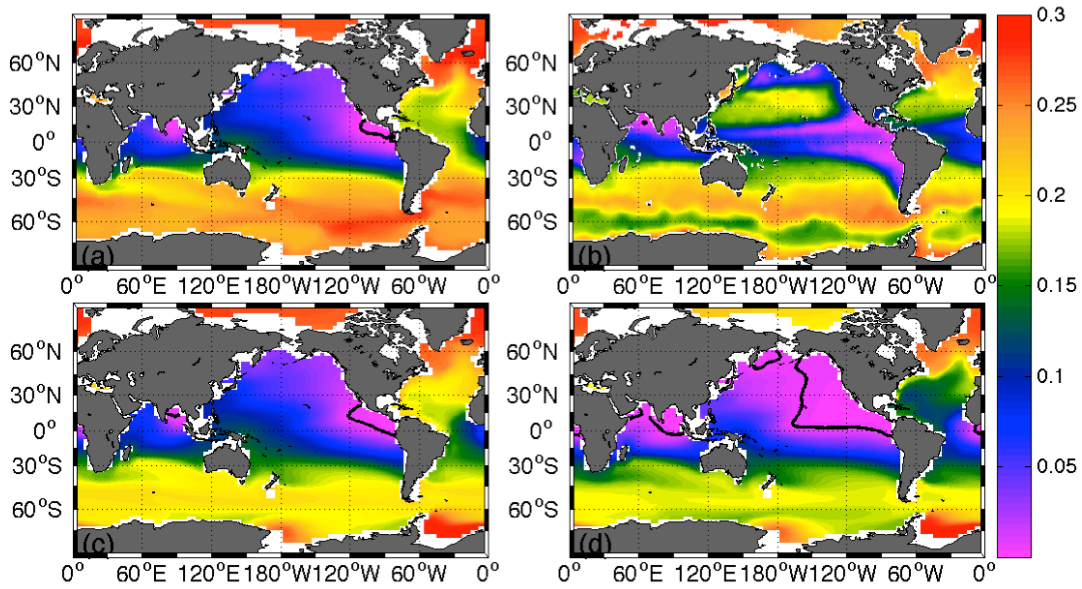

Figure S3: Oxygen concentration in mol O_2 m^{-3} at 900m depth simulated by the (a) control simulation at year 1775 (representative for both REF and WB model runs in year 1775), (b) the World Ocean Atlas in 2009, (c) the control simulation at year 3005 and (d) simulation WB at year 3005. The black contour lines at 0.005 mol m^{-3} highlight the oxygen minimum zones (OMZs).

5

Corrigendum to Earth Syst. Dynam., 8, 357–367, 2017
https://doi.org/10.5194/esd-8-357-2017-corrigendum

Earth System Dynamics
Open Access
EGU

Corrigendum to "A model study of warming-induced phosphorus–oxygen feedbacks in open-ocean oxygen minimum zones on millennial timescales" published in Earth Syst. Dynam., 8, 357–367, 2017

Daniela Niemeyer[1], **Tronje P. Kemena**[1], **Katrin J. Meissner**[2], **and Andreas Oschlies**[1]

[1]Helmholtz-Zentrum für Ozeanforschung Kiel (GEOMAR), Düsternbrooker Weg 20, 24105 Kiel, Germany
[2]Climate Change Research Centre and ARC Centre of Excellence for Climate System Science, University of New South Wales, Level 4 Mathews Building, Sydney, New South Wales, 2052, Australia

Correspondence: Daniela Niemeyer (dniemeyer@geomar.de)

Published: 12 November 2019

In the paper "A model study of warming-induced phosphorus-oxygen feedbacks in open-ocean oxygen minimum zones (OMZs) on millennial timescales" in Sect. 3.3 "Oxygen response", the authors draw a comparison between their model results and the observational estimate of Paulmier and Ruiz-Pino (2009) regarding the global OMZ volume for a 20 mmol m^{-3} criterion. Unfortunately, an incorrect value was taken from the Paulmier and Ruiz-Pino (2009) study in our original study. The correct comparison results in a much improved agreement between the observed OMZ core volume of 10.3×10^6 km^3 (instead of the previously used OMZ volume of 102×10^6 km^3; Paulmier and Ruiz-Pino, 2009) and our modelled OMZ core volume of 15.8×10^6 km^3, further strengthening the results of our study.

References

Paulmier, A. and Ruiz-Pino, D.: Oxygen minimum zones (OMZs) in the modern ocean, Prog. Oceanogr., 80, 113–128, https://doi.org/10.1016/j.pocean.2008.08.001, 2009.

Published by Copernicus Publications on behalf of the European Geosciences Union.

3 The effect of marine aggregate parameterisations on nutrients and oxygen minimum zones in a global biogeochemical model

This chapter is based on the paper 'The effect of marine aggregate parameterisation on nutrients and oxygen minimum zones in a global biogeochemical model' published in Biogeosciences.
Citation: Niemeyer, D., Kriest, I., and Oschlies, A.: The effect of marine aggregate parameterisation on nutrients and oxygen minimum zones in a global biogeochemical model, Biogeosciences, 16, 3095–3111, https://doi.org/10.5194/bg-16-3095-2019, 2019.

Biogeosciences, 16, 3095–3111, 2019
https://doi.org/10.5194/bg-16-3095-2019

Biogeosciences Open Access EGU

The effect of marine aggregate parameterisations on nutrients and oxygen minimum zones in a global biogeochemical model

Daniela Niemeyer, Iris Kriest, and Andreas Oschlies

GEOMAR Helmholtz-Zentrum für Ozeanforschung, Düsternbrooker Weg 20, 24105 Kiel, Germany

Correspondence: Daniela Niemeyer (dniemeyer@geomar.de)

Received: 2 April 2019 – Discussion started: 10 April 2019
Revised: 17 July 2019 – Accepted: 25 July 2019 – Published: 15 August 2019

Abstract. Particle aggregation determines the particle flux length scale and affects the marine oxygen concentration and thus the volume of oxygen minimum zones (OMZs) that are of special relevance for ocean nutrient cycles and marine ecosystems and that have been found to expand faster than can be explained by current state-of-the-art models. To investigate the impact of particle aggregation on global model performance, we carried out a sensitivity study with different parameterisations of marine aggregates and two different model resolutions. Model performance was investigated with respect to global nutrient and oxygen concentrations, as well as extent and location of OMZs. Results show that including an aggregation model improves the representation of OMZs. Moreover, we found that besides a fine spatial resolution of the model grid, the consideration of porous particles, an intermediate-to-high particle sinking speed and a moderate-to-high stickiness improve the model fit to both global distributions of dissolved inorganic tracers and regional patterns of OMZs, compared to a model without aggregation. Our model results therefore suggest that improvements not only in the model physics but also in the description of particle aggregation processes can play a substantial role in improving the representation of dissolved inorganic tracers and OMZs on a global scale. However, dissolved inorganic tracers are apparently not sufficient for a global model calibration, which could necessitate global model calibration against a global observational dataset of marine organic particles.

1 Introduction

Oxygen is – beside light and nutrients – fundamental for marine organisms, such as bacteria, zooplankton, and fish. Only few specialised groups can tolerate regions of low oxygen, commonly referred to as oxygen minimum zones (OMZs). These regions are located in the tropical upwelling regions, where nutrient-rich water enhances primary production and subsequent transport of organic matter to deeper waters, which triggers respiration and consumes oxygen. Together with weak ventilation (which supplies oxygen), this results in oxygen concentrations well below 100 mmol m^{-3}. Global models that are used to reproduce OMZ's volume and location, and their evolution under climate change, differ with respect to the biogeochemical parameterisations as well as with respect to physics (Cabré et al., 2015), resulting in disagreements between projected OMZ extent (Cocco et al., 2013). To date, it is not clear whether these differences can be attributed to the differences in the model's biogeochemistry or the physical models.

One potential parameter affecting distributions of dissolved oxygen and thereby the volume and location of OMZs is the biological carbon pump (Volk and Hoffert, 1985). Global ocean model studies show that the biological pump is important for the distribution of dissolved inorganic tracers in the ocean (Kwon and Primeau, 2006, 2008) as well as atmospheric pCO_2 (Kwon et al., 2009; Roth et al., 2014). It further affects the feeding of deep sea organisms (Kiko et al., 2017) as well as the OMZ volume (Kriest and Oschlies, 2015). The biological carbon pump can be subdivided into three components: production of organic matter and biominerals in the euphotic surface layer, particle export into the ocean interior, and finally their decomposition in the water column and on the sea floor (Le Moigne et al., 2013). Esti-

mates of the export of organic carbon out of the surface layer range from 5 to 20 Gt C yr^{-1}, with the large uncertainty illustrating the gap in our understanding of this process (Henson et al., 2011; Honjo et al., 2008; Keller et al., 2012; Laws et al., 2000; Oschlies, 2001). Further uncertainties are associated with the exact shape of the particle flux profile (e.g. exponential function vs. power law; Banse, 1990; Berelson, 2002; Boyd and Trull, 2007; Buesseler et al., 2007; Lutz et al., 2002; Martin et al., 1987) and its possible variations in space and time. Recent studies suggest conflicting evidence with regard to the spatial variation of the particle flux length scale (Guidi et al., 2015; Marsay et al., 2015), which may again be influenced by the methodology of estimating the particle flux profile and thus the potential sensitivity to the considered depth (Marsay et al., 2015). Also, the underlying mechanisms for a potential spatio-temporal variation remain unclear: some studies attribute this to variations in temperature and associated temperature-dependent variation in remineralisation (Marsay et al., 2015), while other studies derive this from variations in particle size distributions (Guidi et al., 2015).

One mechanism that leads to a variation in particle size distribution consists in the formation of marine aggregates, which exhibit variable sinking speeds. For example, Alldredge and Gotschalk (1988) and Nowald et al. (2009) found sinking rates for aggregates ranging between 10 and 386 m d^{-1}. Particle sinking speed, and thus the particle flux profile, depends on mineral ballast (Armstrong et al., 2002; Ploug et al., 2008), porosity and particle size (Alldredge and Gotschalk, 1988; Kriest, 2002; Smayda, 1970). Large particles are associated with high sinking speed and fast passage through the water column, resulting in low remineralisation and thus a small OMZ volume and vice versa. It can therefore be expected that particle aggregation favouring fast sinking speeds can alter the volume of OMZs compared to small particles with low sinking speeds (Kriest and Oschlies, 2015).

However, there are still some gaps in our understanding of the parameters that control the aggregation rate as well as the particle's sinking behaviour. For example, in situ measurements show almost no dependency between diameter and sinking speed (Alldredge and Gotschalk, 1988), whereas aggregates produced on a roller table show a noticeable relationship (Engel and Schartau, 1999). Furthermore, values for stickiness, which defines the probability that after collision two particles stick together, vary over a wide range. Stickiness depends on the chemistry of the particle's surface (Metcalfe et al., 2006) and the particle type (e.g. Hansen and Kiørboe, 1997) and ranges between almost 0 and 1 (e.g. Alldredge and McGillivary, 1991; Kiørboe et al., 1990). Thus, aggregation as one process that induces variations in particle size, and thus sinking speed, is only loosely constrained through its parameters.

To explore these relationships further and to examine whether a spatially variable sinking speed improves the fit of a global biogeochemical model to global distributions of dissolved inorganic tracers and regional patterns of OMZs, this study uses the three-dimensional Model of Oceanic Pelagic Stoichiometry (Kriest and Oschlies, 2015), coupled with a module for particle aggregation and size-dependent sinking (Kriest, 2002). Given the large uncertainty associated with parameterisations of marine aggregates, we carried out 36 sensitivity experiments in which we varied parameters relevant for particle aggregation and sinking. As in previous studies, the model's fitness is evaluated by the root mean square error (RMSE) against observational data of dissolved inorganic tracers, namely PO_4, NO_3 and O_2 (Kriest et al., 2017). This study additionally determines the model fitness with respect to extent and location of OMZs, following the approach by Cabré et al. (2015).

To examine the above-mentioned questions, and explore the effects and uncertainties of a model that simulates particle dynamics on a global scale for a seasonally cycling stationary ocean circulation, our main questions are as follows:

1. Does a model that includes explicit particle dynamics improve the representation of observed PO_4, NO_3 and O_2?

2. Does a model that includes explicit particle dynamics improve the representation of observed OMZs, and do the "best" parameters with respect to this metric agree with those constrained by dissolved inorganic tracers?

3. What are the effects of uncertainties in the parameterisation of organic aggregates on model results?

4. Can the assumptions inherent in the model confirm either of the spatial particle flux length scale maps proposed by Marsay et al. (2015) or Henson et al. (2015) and Guidi et al. (2015)?

This paper is organised as follows: we first describe the model and its assessment with regard to dissolved inorganic tracers and OMZs, including the sensitivity experiments carried out with the model. We then present the outcome of the sensitivity experiments, with special focus on the metrics defined above. We finally examine and discuss derived maps of particle flux length scales against the background of maps derived from observed quantities (Henson et al., 2015; Marsay et al., 2015; Guidi et al., 2015).

2 Model description and methods

2.1 Oceanic transport

In this study, we used the "transport matrix method" (TMM) (Khatiwala et al., 2005; Khatiwala, 2007, 2018), as an efficient offline method to simulate biogeochemical tracer transport with monthly mean transport matrices (TMs). Additional fields of monthly mean wind, temperature and salinity extracted from the underlying circulation model are used to

simulate air–sea gas exchange of oxygen and to parameterise temperature-dependent growth of phytoplankton. For our experiments, we used two different types of TMs and forcing fields: one set derived from a coarser-resolution (hereafter called MIT2.8) and one from a finer-resolution version, based on a data-assimilated circulation (ECCO1.0) (Stammer et al., 2004). The MIT2.8 forcing and transport represent a resolution of $2.8^\circ \times 2.8^\circ$ and 15 depth layers with a thickness ranging between 50 and 690 m. ECCO1.0 TMs and forcing are based on a resolution of $1^\circ \times 1^\circ$ and 23 depth layers, with a thickness ranging between 10 and 500 m. Further details about the two setups can be found in Kriest and Oschlies (2013).

In general, we used a time step length of $1/2$ d for physical transport and a time step length of $1/16$ d for biogeochemical interactions in the coarse resolution, MIT2.8. Because some parameter configurations allow a very large particle sinking speed, which may exceed more than one box per time step, in MIT2.8 we used a biogeochemical time step length of $1/70$ d for all simulations with $\eta = 1.17$ (see Table 1), in the finer resolution, ECCO1.0, we used in all experiments a time step of $1/80$ d (see Table 1) but with the exception of three experiments, where we used a length of $1/160$ d (these are the experiments for a strong increase of sinking speed with particle size, given by parameter $\eta = 1.17$; see Table 1). Each model was integrated for 3000 years until tracers approached steady state. The last year is used for analysis as well as misfit calculations.

2.2 The biogeochemical model

2.2.1 Model of Oceanic Pelagic Stoichiometry

The Model of Oceanic Pelagic Stoichiometry, called MOPS (Kriest and Oschlies, 2015), is based on phosphorus and simulates phosphate, phytoplankton, zooplankton, dissolved organic phosphorus (DOP) and detritus. The unit of each tracer is given in millimoles of phosphate per cubic metre (mmol P m^{-3}). In addition, MOPS simulates oxygen and nitrate. The P cycle is coupled to oxygen by using a fixed stoichiometry of $R_{-O_2:P} = 171.739$ and to nitrogen by $R_{P:N} = 16$.

The stoichiometry of anaerobic and aerobic remineralisation is parameterised following Paulmier et al. (2009). Remineralisation of detritus and dissolved organic matter is fixed to a constant nominal remineralisation rate r and is dependent on oxygen but independent of temperature. If oxygen concentrations decrease, denitrification replaces aerobic respiration, consuming nitrate. If neither oxygen nor nitrate is sufficiently available, remineralisation stops as the model does not account for other electron acceptors such as sulfate. As both forms of remineralisation follow a saturation curve (Monod type), the realised remineralisation rate may diverge from the constant nominal remineralisation rate.

On long timescales, the loss of fixed nitrogen through denitrification is balanced by temperature-dependent nitrogen fixation. Therefore, it should be noted that while phosphorus is conserved, the inventory of fixed nitrogen as well as oxygen is variable and dependent on ocean circulation and biogeochemistry (Kriest and Oschlies, 2015).

In the basic model without aggregation the sinking speed of detritus increases linearly with depth. With constant remineralisation rate r, the particle flux can thus be described by $F(z) \propto z^{-b}$ with $b = \frac{r}{a}$ (Kriest and Oschlies, 2008) and is therefore (for constant r, e.g. in a fully oxic water column) comparable to the common power-law description of observed particle fluxes (Martin et al., 1987). The fraction of detritus reaching the seafloor follows two pathways: one fraction is re-suspended back into the deepest box of the water column, and the other one is buried into the sediment and therefore responsible for P removal. However, the P budget remains annually unchanged by the resupply of buried P via river runoff.

2.2.2 Model for particle aggregation and size-dependent sinking

Different approaches have been applied to simulate particle aggregation in the marine environment. A detailed representation of the particle size spectrum can be accomplished by explicitly simulating many different size classes, which interact with each other via collision-based aggregation, particle sinking, remineralisation and breakup (Burd, 2013; Jackson, 1990). This flexible approach captures the details of the size spectrum and its spatio-temporal variation in a very detailed way. However, it is computationally expensive and thus prohibitive to be applied to large spatial and long temporal scales.

The aggregation module applied in MOPS parameterises a continuous log–log-linear size distribution of particles via the spectral slope ε calculated from number and mass of particles (Kriest and Evans, 2000). The particle size distribution is influenced by size-dependent particle aggregation and sinking (Kriest, 2002; Kriest and Evans, 2000). Because aggregation reduces particle numbers (but not mass), and sinking preferentially removes large particles, number and mass change independently. By assuming a log–log-linear size spectrum, the slope ε of this spectrum can, at each time step and grid point, be computed from the particle number and total particle mass.

The model requires parameters for the power-law relationships between particle diameter, d, and mass, m ($m = Cd^\zeta$), and between particle diameter and sinking speed, w ($w = Bd^\eta$), to be specified. In our model experiments, we assign fixed values for the minimum diameter and mass of a primary particle of size of $d_1 = 0.002$ cm and $m_1 = 0.00075$ nmol P. The exponent for the relationship between size and mass is set to $\zeta = 1.62$, as proposed for marine aggregates in Kriest (2002), which is in line with more recent findings (Burd

Table 1. Model runs of sensitivity study, their parameter combinations and the calculated misfit of tracers (J_{RMSE}) and OMZs (J_{OMZ}) for MIT2.8 and the ECCO1.0 configurations. The 25 % best simulations with regard to J_{RMSE} and J_{OMZ} are highlighted in yellow and the worst 25 % in red (relative to $RMSE^{ECCO1.0^*}$ and $OMZ^{ECCO1.0^*}$). The simulations in between are coloured in two orange gradations (bright orange is medium good and dark orange is medium bad). The best simulation of each resolution with regard to J_{RMSE} and J_{OMZ} is bold. OMZ is defined as 50 mmol m^{-3}. Parameter η denotes the exponent for size-dependent sinking, α the stickiness, w_1 the minimum sinking speed, D_L the maximum diameter for size-dependent sinking and aggregation, and w_{max} the maximum sinking velocity in the spectral computations.

Run	η	α	w_1	D_L	w_{max}	J_{RMSE} MIT2.8	J_{RMSE} ECCO1.0	J_{OMZ} MIT2.8	J_{OMZ} ECCO1.0
1	0.62	0.2	0.7	1.0	33	0.894	0.631	0.817	0.754
2	0.62	0.2	0.7	2.0	51	0.730	0.499	0.791	0.739
3	0.62	0.2	0.7	4.0	78	0.531	0.440	0.817	0.710
4	0.62	0.2	1.4	1.0	66	0.938	0.735	0.836	0.767
5	0.62	0.2	1.4	2.0	101	0.823	0.640	0.805	0.748
6	0.62	0.2	1.4	4.0	156	0.655	0.535	0.791	0.736
7	0.62	0.2	2.8	1.0	132	1.033	0.879	0.919	0.844
8	0.62	0.2	2.8	2.0	203	1.032	0.877	0.919	0.844
9	0.62	0.2	2.8	4.0	312	1.030	0.874	0.817	0.845
13	0.62	0.5	0.7	1.0	33	0.714	0.510	0.771	0.737
14	0.62	0.5	0.7	2.0	51	0.561	0.441	0.730	0.601
15	0.62	0.5	0.7	4.0	78	0.618	0.567	0.919	0.585
16	0.62	0.5	1.4	1.0	66	0.603	0.457	0.778	0.721
17*	0.62	0.5	1.4	2.0	101	0.508	0.443	0.759	0.580
18	0.62	0.5	1.4	4.0	156	0.848	0.627	0.919	0.652
19	0.62	0.5	2.8	1.0	132	0.775	0.693	0.828	0.760
20	0.62	0.5	2.8	2.0	203	0.570	0.566	0.805	0.745
21	0.62	0.5	2.8	4.0	312	**0.493**	0.459	0.817	0.737
25	0.62	0.8	0.7	1.0	33	0.690	0.495	0.748	0.719
26*	0.62	0.8	0.7	2.0	51	0.570	0.465	0.723	**0.551**
27	0.62	0.8	0.7	4.0	78	0.667	0.622	0.936	0.644
28	0.62	0.8	1.4	1.0	66	0.522	**0.431**	0.758	0.605
29	0.62	0.8	1.4	2.0	101	0.661	0.560	**0.620**	0.578
30	0.62	0.8	1.4	4.0	156	1.011	0.791	0.936	0.814
31	0.62	0.8	2.8	1.0	132	0.501	0.456	0.788	0.727
32	0.62	0.8	2.8	2.0	203	0.682	0.443	0.708	0.728
33	0.62	0.8	2.8	4.0	312	1.004	0.597	0.805	0.656
10	1.17	0.2	0.7	1.0	1007	0.780	0.654	0.927	0.868
11	1.17	0.2	1.4	1.0	2013	0.945		0.936	
12	1.17	0.2	2.8	1.0	4027	1.028		0.919	
22	1.17	0.5	0.7	1.0	1007	0.606	0.506	0.932	0.927
23	1.17	0.5	1.4	1.0	2013	0.677		0.912	
24	1.17	0.5	2.8	1.0	4027	0.930		0.911	
34	1.17	0.8	0.7	1.0	1007	0.698	0.521	0.947	0.949
35	1.17	0.8	1.4	1.0	2013	0.595		0.894	
36	1.17	0.8	2.8	1.0	4027	0.784		0.895	
noAgg					234	0.529	0.426	0.791	0.640

and Jackson, 2009; Jouandet et al., 2014). For the relationship between size and sinking speed we test two alternative values for η, namely $\eta = 0.62$ and $\eta = 1.17$ for the exponent, and w_1 between 0.7 and 2.8 m d^{-1} for the minimum sinking speed (see below). Assuming a constant degradation rate, the average sinking speed of all particles combined would increase with depth due to higher sinking speed of large particles and their higher proportion in the deeper ocean interior. To prevent instabilities at very large sinking speeds (very flat size distributions), as in Kriest and Evans (2000) and Kriest (2002), we restrict the size dependency of sinking and aggregation to a maximum diameter of D_{L}. Beyond D_{L}, these processes do not vary with particle size any more. In our model experiments, we let this parameter vary between 1, 2 and 4 cm.

Changes in the number of marine particles are dependent on particle aggregation, described by the collision rate, and the probability that two particles stick together, α. In our model experiments we vary α between 0.2 and 0.8. The collision rate depends on turbulent shear and differential sinking and is parameterised as in Kriest (2002). We assume that the turbulent shear is high in the euphotic layers and 0 in the deeper ocean layers.

To avoid complications and non-linear feedbacks, in the experiments presented here, we assume that plankton mortality and zooplankton egestion as well as quadratic zooplankton mortality produce new detritus particles but do not change the size spectrum.

By using this setup, the module is similar to parameterisations of particle size applied in other large-scale or global models (Gehlen et al., 2006; Oschlies and Kähler, 2004; Schwinger et al., 2016).

2.3 Model simulations and experiments

2.3.1 MOPS without aggregation

As a reference scenario, we used MOPS as described by Kriest and Oschlies (2015). The model has been implemented in both global configurations MIT2.8 (hereafter called noAgg$^{\mathrm{MIT2.8}}$) and in the finer resolution, ECCO1.0 (noAgg$^{\mathrm{ECCO1.0}}$).

2.3.2 Adjustment of biogeochemical model parameters

Introducing aggregates and a dynamic particle flux profile to the global model MOPS has a strong impact on biogeochemical model dynamics. Starting from parameter values of the calibrated model setup (without aggregation) of Kriest (2017), we calibrated parameters relevant for phytoplankton and zooplankton growth and turnover as described in Kriest et al. (2017) against observed global distributions of nutrients and oxygen.

Parameters to be calibrated for this new model were the light and nutrient affinities of phytoplankton, zooplankton quadratic mortality, detritus remineralisation rate, particle stickiness and the exponent η that relates particle sinking speed to particle size (see Table 2). After introduction of particle aggregation, the calibrated nutrient affinity of phytoplankton is now much higher, with a half-saturation constant for phosphate of $K_{\mathrm{PHY}} = 0.11$ mmol PO$_4$ m^{-3} instead of 0.5 mmol PO$_4$ m^{-3} in Kriest et al. (2017), very likely because the optimisation compensates for the higher export (and lower recycling) of phosphorus and nitrogen. Possibly for the same reason, detritus remineralisation rate in the optimised model is increased from 0.05 to 0.25 d^{-1}. Light affinity of phytoplankton deviates less from the value in the model without particle aggregation, but the quadratic mortality of zooplankton is strongly reduced (1.6 (mmol P m^{-3})$^{-1}$ instead of 4.55 (mmol P m^{-3})$^{-1}$); the latter might be regarded as an attempt of the optimisation to reduce the export of organic matter from the euphotic zone. The two parameters that affect aggregation and particle sinking remained at moderate values of $\alpha = 0.42$ and $\eta = 0.72$, i.e. close to those applied in earlier model experiments with aggregation (e.g. Kriest, 2002). The residual cost function J_{RMSE} of this pre-calibrated model with aggregation was 0.472, i.e. lower than noAgg$^{\mathrm{MIT2.8}}$ ($J_{\mathrm{RMSE}} = 0.529$), but somewhat higher than achieved with a model version optimised against nutrient and oxygen concentrations (Kriest et al., 2017), which resulted in a misfit of $J_{\mathrm{RMSE}} = 0.439$. In the sensitivity experiment described below we will examine whether this remaining misfit can be reduced even further and evaluate the model sensitivity to changes in the parameters of this highly complex module.

2.3.3 Sensitivity experiments at coarse resolution (MIT2.8)

In the coarser model configuration of MOPS, MIT2.8, a first sensitivity study of 36 model simulations with different aggregation parameters was performed (see Table 1). We varied the values of four aggregation parameters, which control the rate of aggregation and the sinking behaviour of particles. The first parameter is the stickiness α, i.e. the probability that after collision two particles stick together, which was set to values of 0.2, 0.5 and 0.8, respectively. The second parameter is the maximum particle diameter for size-dependent aggregation and sinking, D_{L}, set to values of 1, 2 and 4 cm. A small value of D_{L} reduces the maximum possible sinking speed of the detrital pool and vice versa. Parameter w_1 describes the sinking speed of a primary particle with values of 0.7, 1.4 and 2.8 m d^{-1}. One effect of a small value of w_1 is that it reduces the loss of organic matter from surface layers, and thus it has a direct effect on the recycling of nutrients at the surface. At the same time, it also affects the maximum possible sinking speed of the entire detritus pool. Finally, the exponent that relates particle sinking to diameter, η, is set to values of either 0.62 and 1.17. A high η represents dense particles and a fast increase of particle sinking speed with size; a

Table 2. Model adjustment of biogeochemistry with aggregates compared to Kriest et al. (2017) and new parameters in this study.

Parameters that remain fixed	Kriest et al. (2017)	This study	Unit	Description
ro2ut	171.7	171.7	mol O_2 : mol P	Redfield ratio
Subdin	15.8	15.8	mmol NO_3 m^{-3}	no denitrification below this level
Nfix	1.19	1.19	µmol N m^{-3} d^{-1}	N fixation
ACkbaco2	1.00	1.00	mmol O_2 m^{-3}	half-saturation constant for oxic degradation
ACkbacdin	31.97	31.97	mmol NO_3 m^{-3}	half-saturation constant for suboxic degradation
ACmuzoo	1.89	1.89	1 d^{-1}	maximum grazing rate
Parameters that changed compared to Kriest et al. (2017)				
ACik	9.65	6.52	W m^{-2}	light half-saturation constant
ACkpo4	0.5	0.106	mmol P m^{-3}	half-saturation constant for PO_4 uptake
AComniz	4.55	1.6	m^3 (mmol P d)$^{-1}$	quadratic zooplankton mortality
detlambda	0.05	0.25	1 d^{-1}	detritus remineralisation rate
New parameters for the aggregation model (further modified in this study)				
SinkExp	–	0.7164		exponent that relates particle sinking speed to diameter
Stick	–	0.4162		stickiness for interparticle collisions

low value stands for more porous particles, which show only a weak relationship between size and sinking speed (Kriest, 2002).

2.3.4 Sensitivity experiments at fine resolution (ECCO1.0)

The occurrence of aggregates, and their transport to the ocean interior, can furthermore depend on physical dynamics (e.g. Kiko et al., 2017). Therefore, in a second step, we repeated some of the experiments presented above in the finer-resolution version ECCO1.0 to investigate possible improvements at higher resolution. In particular, we repeated all MIT2.8 simulations with $\eta = 0.62$ in this finer-resolution configuration. Additionally, we carried out three more simulations with $\eta = 1.17$ but with the smallest $D_L = 1$ cm to prevent particles from sinking through more than one box per time step (see Table 1). All simulations together lead to 30 model runs in the finer-resolution configuration. To compare the ECCO1.0 simulations directly with results from MIT2.8, we re-gridded the result from ECCO1.0 simulations onto the coarser MIT2.8 grid.

2.4 Model assessment and diagnostics

Because observational data of particle flux are either limited with regard to space and time (e.g. Gehlen et al., 2006) or are combined with assumptions that yield no clear patterns (Gehlen et al., 2006; Henson et al., 2012; McDonnell and Buesseler, 2010), this study restricts the model assessment to observations of nutrients and oxygen, in combination with the model fit to volume and location of oxygen minimum zones.

2.4.1 Root mean squared error of tracers

After a spinup of 3000 years into a seasonally cycling equilibrium state, the model results are evaluated in terms of annual means of oxygen, phosphate and nitrate. As in previous studies (e.g. Kriest et al., 2017) the misfit is calculated by the deviation between simulated results, m, and observed properties taken from the World Ocean Atlas (WOA), o (Garcia et al., 2006). The deviations are weighted by volume of each grid box V_i, expressed as the fraction of the total ocean volume V_T. The sum of the weighted deviations is normalised by the observed global mean concentration of each tracer:

$$J_{\mathrm{RMSE}} = \sum_{j=1}^{3} J(j) = \sum_{j=1}^{3} \frac{1}{o_j} \sqrt{\sum_{i=1}^{N} \left(m_{i,j} - o_{i,j}\right)^{2*} \frac{V_i}{V_T}}. \quad (1)$$

In this equation, $j = 1, 2, 3$ describes the respective tracer (i.e. PO_4, NO_3 and O_2). N is the total number of model

grid boxes and o_j is the global average observed concentration of each tracer (Kriest et al., 2017). Thus, a low misfit value represents a good agreement between model and observations ($J_{\mathrm{RMSE}} = 0$ would be a perfect fit), which enables a prediction about the model accuracy with regard to these tracers. The model runs with the lowest J_{RMSE} in the coarse and the fine resolution are hereafter called $\mathrm{RMSE}^{\mathrm{MIT2.8^*}}$ and $\mathrm{RMSE}^{\mathrm{ECCO1.0^*}}$, respectively.

2.4.2 Fit to oxygen minimum zones

To evaluate the extent and location of OMZs, we follow the approach of Cabré et al. (2015) by calculating the overlap between modelled and observed (Garcia et al., 2006; hereafter referred to as "WOA") OMZs. As several marine processes are oxygen-dependent but have heterogeneous criteria for their minimum oxygen threshold, in this study, the OMZs are calculated for different oxygen threshold concentrations, C. Therefore, low-oxygen waters are characterised as $O_2 < c$, with c ranging from 0 to 100 mmol $O_2\,m^{-3}$. To calculate the overlap between simulated and observed OMZs, we use the following equation (Sauerland et al., 2019):

$$C = \frac{V^{\cap}(c)}{V_{\cup}(c)} = \frac{V^{\cap}(c)}{V^{m}(c) + V^{o}(c) - V^{\cap}(c)}. \quad (2)$$

In this equation, $V^{\cap}(c)$ is the volume of overlap of suboxic waters between model and observations, with regard to the defined oxygen threshold concentration c. This overlap is divided by the union (total volume of low-oxygen waters occupied in the model or in the observations) and results in a value between 0, equal to zero overlap between model and observations, and 1, which represents an optimal overlap. To adjust the scale to J_{RMSE}, we calculated the following:

$$J_{\mathrm{OMZ}} = 1 - C. \quad (3)$$

In this equation, J_{OMZ} varies between 0 and 1. Consequently, the scale of J_{OMZ} is equivalent to the scale of J_{RMSE}, which implies that a low misfit corresponds to a good agreement between model and observational data and vice versa. The model simulations with regard to the lowest J_{OMZ} are called $\mathrm{OMZ}^{\mathrm{MIT2.8^*}}$ and $\mathrm{OMZ}^{\mathrm{ECCO1.0^*}}$ hereafter. In calculating the overlap, we distinguish between the global ocean and the Pacific as well as the Atlantic Ocean.

2.4.3 Estimation of particle flux length scale *b*

To investigate, if, and how, the model reproduced observed maps of the particle flux length scale, b, that relates particle flux and depth via $F(z) \propto z^{-b}$ and derived from data by Marsay et al. (2015) and Guidi et al. (2015), we log-transformed $F(z)$, the simulated annual average flux of particulate organic matter as a function of depth, and carried out a linear regression of these values. The highest b values correspond to short particle flux length scale, i.e. many small particles, and thus a low sinking speed, shallow remineralisation and high oxygen consumption in shallow waters. For the reference models without aggregation these global maps should, in areas with shallow mixed layers, show spatially uniform values, as imposed by the model's prerequisites. Deviations from uniform values can be ascribed either to oxidant limitation of remineralisation (see above model description) or to physical processes such as mixing or upwelling, which can result in an additional vertical transport of particles.

The parameterisation of the aggregation model assumes a constant sinking speed for an upper size limit D_{L} (see above), and therefore average particle sinking speed will remain constant below some depth. Also, the assumption of a particle size spectrum, size-dependent sinking and constant remineralisation will result in particle flux profiles that do not fully agree with those predicted by a power law (see Kriest and Oschlies, 2008). Thus, because the aggregation model's prerequisites do not fully agree with a continuous increase of sinking speed with depth, we confine the regression of log-transformed particle flux to a vertical range between 100 and 1000 m, where the aggregation model still shows an increase of average sinking speed with depth (see also Kriest and Oschlies, 2008).

3 Results

3.1 Global patterns of particle flux profiles

As could be expected, $\mathrm{noAgg}^{\mathrm{ECCO1.0}}$ shows almost no spatial pattern of b, with values around the prescribed nominal value of $b = 0.858$ (global mean: 0.64; Fig. 1a; please note the different scaling in a and d) indicating long particle flux length scales and deep remineralisation. Regions with particularly low diagnosed b values (< 0.2) result either from decreased remineralisation in OMZs (e.g. eastern tropical Pacific OMZ) or are found in areas of deep mixing (in the model mainly high latitudes or western boundary currents), where vertical mixing increases the inferred particle flux length scales. However, for the best simulation with regard to the sum of J_{RMSE} and J_{OMZ} of the aggregation model (called ECCO1.0* hereafter) we find the highest b values, corresponding to short particle flux length scales, or shallow remineralisation, in the oligotrophic subtropical gyres. In contrast, b is the smallest in the equatorial upwelling and in the shelf regions (Fig. 1d and g). This pattern is in accordance with the observed spatial pattern derived by Marsay et al. (2015). In our model, this very deep flux penetration (b close to 0) in the equatorial upwelling can be explained with low oxygen concentrations, which reduce the remineralisation rate. In contrast, when deriving the particle flux length scale from a similar model but with oxygen-independent remineralisation (Kriest and Oschlies, 2013), we find a b

close to the prescribed b value of 0.858 (Fig. S1 in the Supplement).

In the subtropical and the equatorial region, the spatial variance (marked transparent red; Fig. 1g) of model-derived b values is quite high, which is caused by spatial variations in the physical environment, i.e. permanently stratified subtropical gyres and upwelling regions with low oxygen and reduced remineralisation. However, besides ECCO1.0* the four best model simulations with respect to the sum of J_{RMSE} and J_{OMZ} (simulation nos. 14, 17, 28 and 29; Table 1) show essentially the same pattern of b (Fig. S2), although these four simulations include quite different parameterisations (see Table 1).

Regions with high b values are characterised by a high spectral slope of the size distribution and therefore a high abundance of small particles, leading to slow sinking speeds (Fig. 7) and low export rates in ECCO1.0* (Fig. 1f). ECCO1.0* simulates the highest export rates at high latitudes and in the upwelling region and the lowest export rates in the subtropical gyres (Fig. 1f and i). Although the spatial pattern of export rates is similar for both model simulations with and without aggregation, ECCO1.0* shows a 1.6-fold higher global mean export rate (10.1 mmol P $\mathrm{m}^{-2}\,\mathrm{a}^{-1}$) than $\mathrm{noAgg}^{\mathrm{ECCO1.0}}$ (6.1 mmol P $\mathrm{m}^{-2}\,\mathrm{a}^{-1}$). In ECCO1.0* export rates show a higher regional variability than in $\mathrm{noAgg}^{\mathrm{ECCO1.0}}$ (Fig. 1c, f and i), which is due to blooms in the high latitudes during summer season accelerating the size-dependent aggregation and thus the export signal.

The oxygen concentration at a depth of 100 m shows the same global pattern in both simulations, with high oxygen concentrations at high latitudes and decreasing concentrations towards the Equator (Fig. 1b and e). However, the oxygen concentration at high latitudes is slightly higher in $\mathrm{noAgg}^{\mathrm{ECCO1.0}}$ than in ECCO1.0* (Fig. 1h). Moreover, the global suboxic volume (for a criterion $c = 50\,\mathrm{mmol\,m^{-3}}$) in ECCO1.0* ($7.3 \times 10^{16}\,\mathrm{m^3}$) is larger than in $\mathrm{noAgg}^{\mathrm{ECCO1.0}}$ ($3.7 \times 10^{16}\,\mathrm{m^3}$). Comparing our model results with the dataset of Garcia et al. (2006), which yields a volume of $5.6 \times 10^{16}\,\mathrm{m^3}$, we find an underestimation of the suboxic volume for $\mathrm{noAgg}^{\mathrm{ECCO1.0}}$ by 34 % and an overestimation for ECCO1.0* by 30 %.

3.2 Representation of oxygen minimum zones

The finer-resolution and data-assimilated circulation of ECCO1.0 in general improves the representation of OMZs in comparison to MIT2.8 with regard to the overlap of OMZs for a criterion of $50\,\mathrm{mmol\,m^{-3}}$ (Fig. 2). Both simulations without explicit particle dynamics, namely $\mathrm{noAgg}^{\mathrm{MIT2.8}}$ and $\mathrm{noAgg}^{\mathrm{ECCO1.0}}$, clearly underestimate the extent of the OMZ at a depth of 500 and 1000 m for an OMZ criterion of $50\,\mathrm{mmol\,m^{-3}}$ in the Pacific basin (Fig. 2). The simulations including particle dynamics that are the best with respect to the OMZ metric, $\mathrm{OMZ}^{\mathrm{MIT2.8^*}}$ and $\mathrm{OMZ}^{\mathrm{ECCO1.0^*}}$, exhibit a larger OMZ area for both resolutions (Fig. 2). Despite the improved representation of OMZs, all models including the particle aggregation module still tend to merge the OMZs of the Northern Hemisphere (NH) and the Southern Hemisphere (SH) at a depth of 500 m, which does not agree with the well-separated northern and southern OMZ shown by the observations (Figs. 2 and S3 in the Supplement). As reflected in a plot that shows the extent of OMZ in the NH and SH, similar to Fig. 1a and 1b of Cabré et al. (2015), all models fail to represent the double structure of OMZ north and south of the Equator. However, in our model the northern Pacific OMZ is fitted quite well (Figs. 2 and S3).

Aggregation improves the representation of OMZs with respect to a criterion of $c = 50\,\mathrm{mmol\,m^{-3}}$ compared to the simulations without aggregation for both resolutions in the NH, but not in the SH (Fig. 3). In $\mathrm{noAgg}^{\mathrm{ECCO1.0}}$ the OMZ simulated in the NH is too small and too shallow (Fig. 3a). Even though $\mathrm{OMZ}^{\mathrm{ECCO1.0^*}}$ tends to underestimate the suboxic area between ~ 700 and 1300 m, it shows a considerably higher overlap of model results and observations compared to $\mathrm{noAgg}^{\mathrm{ECCO1.0}}$ (Fig. 3b). However, in the SH $\mathrm{noAgg}^{\mathrm{ECCO1.0}}$ represents the OMZs better than $\mathrm{OMZ}^{\mathrm{ECCO1.0^*}}$, which tends to overestimate the suboxic area in this hemisphere. In addition to differences caused by particle dynamics, circulation affects the performance in the two hemispheres: $\mathrm{OMZ}^{\mathrm{ECCO1.0^*}}$ represents the highest overlap between ~ 100 and 500 m depth in the SH, but this is surpassed by $\mathrm{OMZ}^{\mathrm{MIT2.8^*}}$ between 500 and 900 m depth. In the NH, $\mathrm{OMZ}^{\mathrm{ECCO1.0^*}}$ outcompetes $\mathrm{OMZ}^{\mathrm{MIT2.8^*}}$ between 300 and 900 m depth as far as overlap is concerned (Fig. 3b).

However, the improvement of the representation of OMZs in the simulations with aggregation depends on the criterion for OMZs. As could be expected, a higher oxygen threshold for the OMZ criterion enhances the overlap between model simulations and observational data (Fig. 4). As for the fixed criterion of $50\,\mathrm{mmol\,m^{-3}}$, globally and in the Pacific the better circulation and finer resolution of ECCO1.0 improves the overlap for varying OMZ criteria in comparison to MIT2.8 (Fig. 4a and c). While the $\mathrm{OMZ}^{\mathrm{ECCO1.0^*}}$ simulation reaches globally a maximum overlap of 65.9 % (for $c = 100\,\mathrm{mmol\,m^{-3}}$), $\mathrm{OMZ}^{\mathrm{MIT2.8^*}}$ culminates only in a maximum of 58.7 % for the same criterion.

In the Pacific basin $\mathrm{OMZ}^{\mathrm{ECCO1.0^*}}$ reaches an agreement with observations of 19.9 % overlap for a criterion of $20\,\mathrm{mmol\,m^{-3}}$ (Fig. 4c). The overlap then increases strongly until the $100\,\mathrm{mmol\,m^{-3}}$ criterion (68.2 %). It is noteworthy that globally and in the Pacific area $\mathrm{noAgg}^{\mathrm{ECCO1.0}}$ outperforms all models for a criterion of $20\,\mathrm{mmol\,m^{-3}}$, where it shows an agreement of almost 31 %. The Atlantic basin shows an inverse trend (Fig. 4b): here, $\mathrm{OMZ}^{\mathrm{MIT2.8^*}}$ represents the OMZ better than $\mathrm{OMZ}^{\mathrm{ECCO1.0^*}}$ (26 % and 12.2 %, respectively, for a criterion of $70\,\mathrm{mmol\,m^{-3}}$). Further, in this region, the ECCO1.0 model that performs best with respect to RMSE ($\mathrm{RMSE}^{\mathrm{ECCO1.0^*}}$) outperforms $\mathrm{OMZ}^{\mathrm{ECCO1.0^*}}$ over the full range of criteria (Fig. 4b). Thus, there are large regional differences in the model's response to different circu-

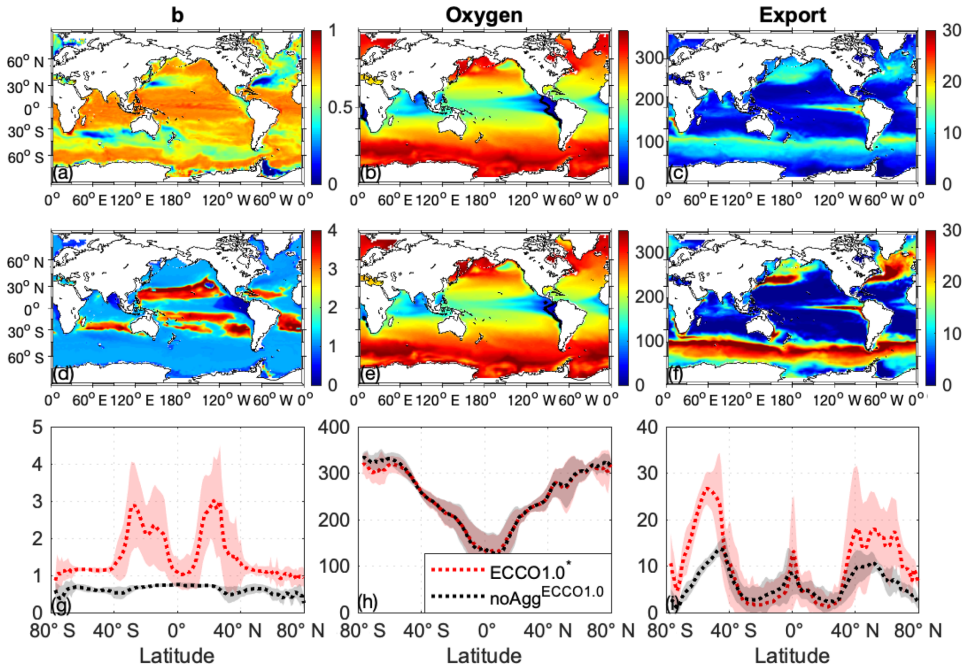

Figure 1. Global maps of b **(a, d)**, O_2 at 100 m (mmol m^{-2}, **b, e**) and export at 100 m (mmol P m^{-2} a^{-1}, **c, f**) for noAgg$^{ECCO1.0}$ **(a, b, c)** and for the best aggregation model with regard to the sum of J_{RMSE} and J_{OMZ} (simulation no. 26; **d, e, f**). The black line indicates the OMZ for a criterion of 50 mmol m^{-3}. Lower panels: Global mean (dotted line) and standard deviation (transparent shaded) of b **(g)**, O_2 **(h)** and export **(i)** of noAgg$^{ECCO1.0}$ (black) and the best aggregation model with regard to the sum of J_{RMSE} and J_{OMZ} (simulation no. 26; red). Please note the different scaling for b values **(a, d)**.

Table 3. Number of simulations with different parameters for D_L, α and w_1 for the porous ($\eta = 0.62$) and dense ($\eta = 1.17$) particles which outperform the corresponding other size. The numbers are given with respect to two different criteria, J_{RMSE} and J_{OMZ}.

	$\eta = 0.62$	$\eta = 1.17$	Resolution
J_{RMSE}	6	3	MIT2.8
J_{OMZ}	8	1	MIT2.8
J_{RMSE}	2	1	ECCO1.0
J_{OMZ}	2	0	ECCO1.0

lations and particle dynamics. Because the dataset of observations used for comparison does not contain any concentrations below 30 mmol m^{-3} in the Atlantic, all models show no overlap at all in this basin.

In summary, the improvement of model fit with regard to J_{OMZ} depends not only on particle dynamics but also on the definition of OMZs (i.e. the OMZ criterion c), the model resolution as well as the region considered (Figs. 2, 3, 4).

3.3 Sensitivity of nutrient and oxygen distributions to aggregation parameters

Table 3 shows that in six cases out of nine (MIT2.8), a model that represents porous particles ($\eta = 0.62$) outperforms the corresponding model with a sinking speed that describes rather dense, cell-like particles ($\eta = 1.17$). The same applies for the higher resolution (ECCO1.0), where in two cases out of three a porous parameterisation improves the fit with regard to J_{RMSE} (see Table 1). Also, both J_{RMSE} and J_{OMZ} of the "dense" parameterisations are never among the best five models with respect to either metric (see Table 1). Thus, in the following we focus on model simulations with $\eta = 0.62$.

Among the sensitivity experiments performed, the best model with respect to J_{RMSE} (hereafter referred to as RMSE$^{MIT2.8^*}$) is characterised by an intermediate stickiness α of 0.5, the largest diameter for size-dependent aggregation and sinking, D_L, of 4 cm and a minimum particle sinking speed w_1 of 2.8 m d^{-1}, representing a rather fast organic matter transport to the ocean interior. However, many other models with medium stickiness perform about equally well (Fig. 5b). Models with lower stickiness perform best with slow minimum sinking speed w_1 and a large maximum size $D_L = 4$ cm for size-dependent sinking and aggregation

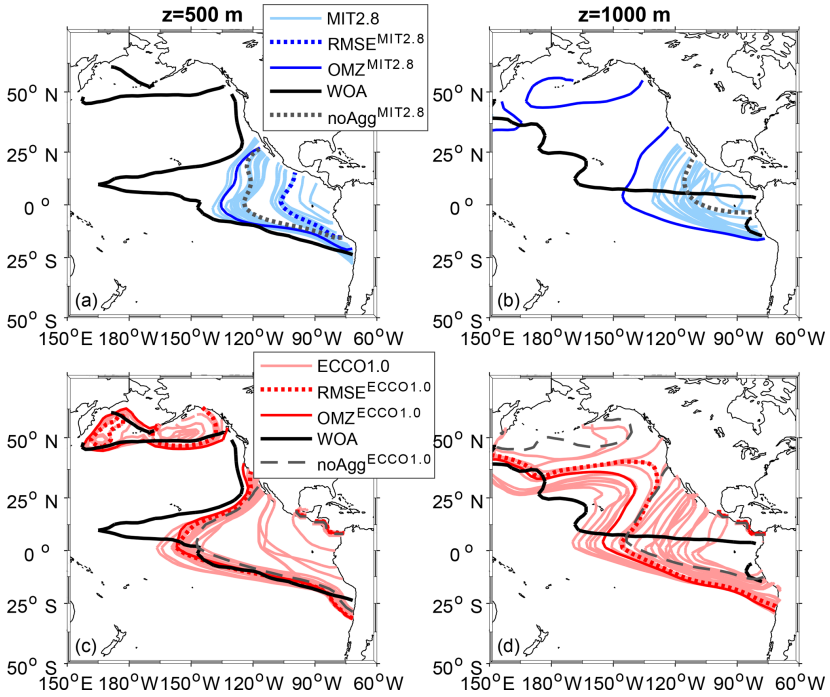

Figure 2. Comparison of Pacific Ocean OMZ ($O_2 \leq 50\,\mathrm{mmol\,m^{-3}}$) between model simulations and observations. Panels **(a)** and **(b)** show the OMZ at a depth of 500 and 1000 m for the coarse resolution, MIT2.8, and panels **(c)** and **(d)** for the fine resolution, ECCO1.0.

(Fig. 5a). In contrast, a large stickiness (which facilitates the formation of aggregates in surface layers) requires either small w_1 or D_L, which reduces the export of particles out of the euphotic zone, and into the ocean interior.

Oxygen concentrations contribute most to the global J_{RMSE} (Kriest et al., 2017). The influence of oxygen on global tracer misfit is dominated by the deep concentrations (Fig. S4) and thus to a large extent by the large-scale circulation. The OMZs, because of their small regional extent, contribute less to the global misfit (Kriest et al., 2017). This is confirmed by Fig. S4d, e and f, showing that, in the eastern tropical Pacific region, deep (> 300 m) mesopelagic and deep oxygen concentrations scatter strongly among the different models (Fig. S4a), despite their good global match in shallow waters. Likewise, although global mean profiles of nutrients are quite similar among the different circulations, and agree quite well with observations, their concentrations scatter strongly in the eastern tropical Pacific. Most of the simulations tend to underestimate the oxygen and nitrate concentration in this region (Fig. S4a and c). Oxygen concentrations that are too low lead to denitrification that is too high and thus widespread nitrate depletion in the eastern tropical Pacific region, which explains the simultaneous underestimate of oxidants in this region.

To sum up, a moderate stickiness enhances the chance of a good model fit to nutrients and oxygen (J_{RMSE}), but there is no unique trend for the parameters or combination of parameters, with the exception of the exponent that relates particle sinking speed to its size: here, we find an advantage of a parameterisation characteristic for porous marine aggregates. In the optimal scenario, the misfit is less than that of a model without aggregates, when this is simulated with fixed reference parameters ($noAgg^{MIT2.8}$). Because of the small spatial extent of OMZs, the model fit to nutrient and oxygen concentrations is mainly caused by the large-scale tracer distribution, even if some models show a considerable mismatch to these tracers in OMZs.

The pattern for J_{RMSE} does not change very much when applying a different, more highly resolved and data-assimilated circulation (see Table 1 and Fig. 6). Now, the optimal model ($RMSE^{ECCO1.0^*}$) is improved with respect to J_{RMSE} by about 13 %, but many other almost equally good solutions can be found with moderate to high stickiness. Introducing aggregates in this coupled model system does not improve the model fit to nutrient and tracer concentrations, as evident from the comparison of $RMSE^{ECCO1.0^*}$ ($J_{RMSE} = 0.431$) against a model without aggregate dynamics ($J_{RMSE} = 0.426$; Table 1). The lack of improvement can likely be explained by the fact that the biogeochemical parameters of MOPS with particle dynamics were adjusted in the circulation of MIT2.8, and thus they are not optimal

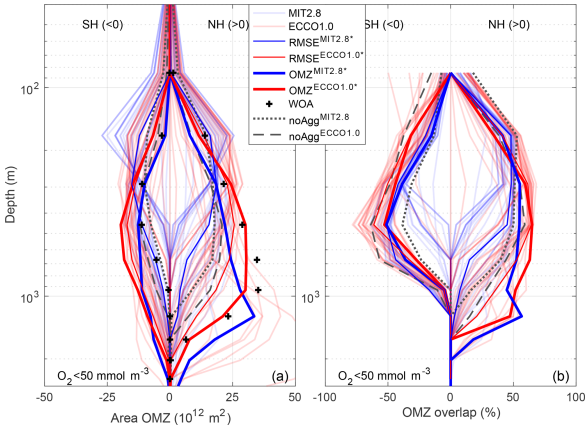

Figure 3. Area of OMZ **(a)** and overlap of OMZs between model and observations following Cabre et al. (2015) **(b)**. In both panels, the left-hand side shows the Southern Hemisphere (0–40° S); the right shows the Northern Hemisphere (0–40° N), plotted against the logarithmic depth. OMZs are defined as regions with $O_2 < 50\,\mathrm{mmol\,m^{-3}}$.

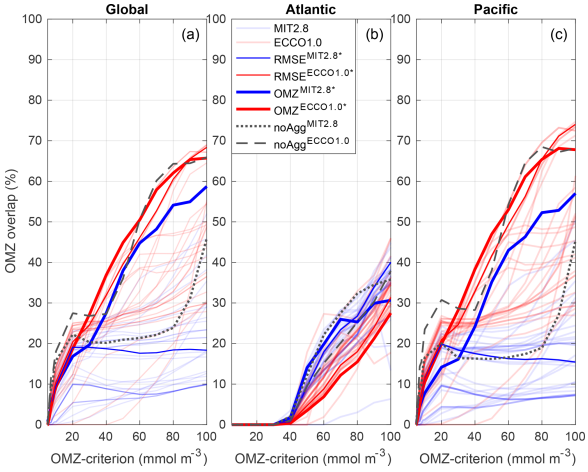

Figure 4. Overlap between modelled and observed OMZs (Eq. 2) for varying criteria c, ranging from $0 < c < 100\,\mathrm{mmol\,m^{-3}}$) on a global scale **(a)**, for the Atlantic Ocean **(b)** and for the Pacific Ocean **(c)**.

for the model when simulated in the physical dynamics of ECCO1.0.

The sensitivity to the metric for OMZs differs from the sensitivity to the metric for nutrients and oxygen. Now, for the fit to oxygen minimum zones (J_{OMZ}), a large stickiness (α), in combination with D_{L} of 2 cm and slow-to-moderate minimum sinking speed w_1, is of advantage (Figs. 5 and 6). Thus, a high rate of aggregation, and a maximum sinking speed of about 50–100 $\mathrm{m\,d^{-1}}$, improves the model with respect to OMZs. This is also evident from comparison of the optimal models ($\mathrm{OMZ}^{\mathrm{MIT2.8}^*}$ and $\mathrm{OMZ}^{\mathrm{ECCO1.0}^*}$) to models without aggregate dynamics ($\mathrm{noAgg}^{\mathrm{MIT2.8}}$ and $\mathrm{noAgg}^{\mathrm{ECCO1.0}}$), shown in Figs. 3 and 4 and Sect. 3.2. Nevertheless, even the models that perform best with respect to J_{OMZ} underestimate mesopelagic oxygen when averaged over the eastern tropical Pacific (Fig. S4a).

The sensitivity patterns with regard to J_{OMZ} among both configurations MIT2.8 and ECCO1.0 diverge considerably from each other, which is in contrast to the patterns for J_{RMSE} noted above (compare Fig. 5 with Fig. 6). Thus, model performance with respect to J_{OMZ} seems to depend much more on circulation and physical details than the large-scale dynamics reflected in J_{RMSE}.

4 Discussion

In our sensitivity study, we used a similar parameterisation of particle aggregation as Oschlies and Kähler (2004) applied in their biogeochemical-circulation model for the North Atlantic Ocean. The difference compared to our model consists in aggregates, which are composed of phytoplankton and detritus, the parameterisation, which is based on dense particles (dSAM, Kriest, 2002) and a biogeochemical model, which is different. We found high values for the spectral slope of the size distribution (i.e. high abundance of small particles) and thus a low particle sinking speed in the subtropical gyres (Fig. 7), which corresponds with the findings by Oschlies and Kähler (2004) and Dutay et al. (2015). This, in turn, leads to the highest b values in the oligotrophic subtropical gyres and the lowest ones in the high latitudes and the upwelling region, in agreement with the pattern as shown in Marsay et al. (2015). These findings imply that such a b pattern can result not only from temperature-dependent remineralisation – as suggested by Marsay et al. (2015) – but also from particle dynamics and temperature-independent remineralisation. However, if temperature-dependent remineralisation, as suggested by Marsay et al. (2015) or Iversen and Ploug (2013), was also included in our model, this would likely enhance horizontal variations in the particle flux profile, with even deeper flux penetration in the cold waters of the high latitudes and upwelling areas. Besides particle dynamics, the low b values in upwelling regions found in our study (Fig. 1d) are also caused by the suboxic conditions, which suppress remineralisation in subsurface waters. Such a tight link between suboxia and deep flux penetration is supported by the observations reported by Devol and Hartnett (2001) and Van Mooy et al. (2002). Therefore, two different processes – particle aggregation and/or temperature-dependent remineralisation – suggest low b values and deep flux penetration in the very productive areas of high latitudes. A third process, which consists in oxygen-dependent remineralisation, is superimposed on these in OMZs, causing the steepest particle profiles in these areas.

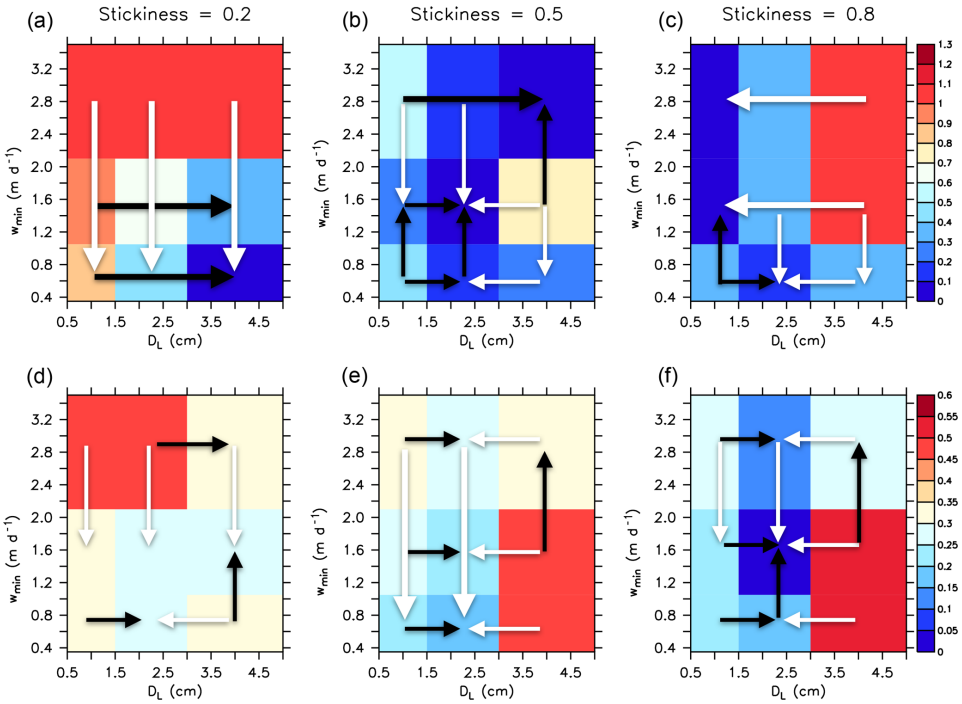

Figure 5. Sensitivity of J_{RMSE} (Eq. 1); **(a, b, c)** and J_{OMZ} (Eq. 3); **(d, e, f)** to minimum sinking speed w_1 and maximum size D_{L} for the coarse resolution, MIT2.8, for three different values of stickiness **(a–f)**, and $\eta = 0.62$ ("porous" particles). The colour bar shows J_{RMSE} and J_{OMZ} (blue – good fit, red – bad fit), normalised by its minimum value across all model experiments. Black arrows indicate an improvement of J_{RMSE} or J_{OMZ} with increasing parameter values, while white arrows show an improvement with decreasing values.

However, it should be noted that although the maximum sinking speed of our best simulations (101 (no. 17) and 51 m d^{-1} (no. 26), see Table 1) agrees with observations (Alldredge and Gotschalk, 1988; Nowald et al., 2009; Jouandet et al., 2011), the range of b values in our model is almost twice as large as suggested by most empirical studies (Berelson, 2001; Buesseler et al., 2007; Martin et al., 1987; Van Mooy et al., 2002). However, as there is no common depth range to determine the particle flux length scale b, the depth range spreads over a wide range in various studies and thus impedes the comparability (Marsay et al., 2015), which might explain some divergence between observations and model results. In particular, our model simulates too large a fraction of small particles and therefore too steep a particle size spectrum in the subtropical gyres, which causes b values that are too high in these areas. Other processes that modify the size spectrum, like grazing by zooplankton, and the subsequent egestion of large fecal pellets, might also play a role in these regions. Additionally, the model tends to underestimate the number of large particles (size range 0.14 to 16.88 mm) in the surface of the tropical Atlantic Ocean (23° W), compared to observations (Kiko et al., 2017; Fig. S6). On the other hand, a first, direct comparison to the UVP 5 dataset (Kiko et al., 2017, their Fig. 1) exhibits a correct magnitude regarding the number of particles within this size range (0.14 to 16.88 mm) in our model (Fig. S5) along the 151° W section. One possible explanation for the mismatch at 23° W could consist in a not sufficiently resolved equatorial current system, which also will be discussed below. Also, additional biological processes, such as the downward transport of organic matter through vertically migrating zooplankton (Kiko et al., 2017) or particle breakup of aged, fragile particles at depth (e.g. Biddanda et al., 1988), could improve the model. However, introducing this additional complexity is beyond the scope of this paper. In future studies, consideration of these processes, in conjunction with a comprehensive model calibration against observed particle abundances and size spectra (e.g. Stemmann et al., 2002), may help not only to improve the representation of OMZs but also to better constrain the contributions of individual processes such as aggregation, vertical migration and temperature-dependent remineralisation, as well as to validate simulated particle dynamics.

However, model calibration against observed particle dynamics has to account for characteristics and limitations of observations. For example, the size spectrum assumed in our model is of infinite upper size and also contains particles with a diameter larger than, for example, 4 cm (the upper limit for size dependency of aggregation and sinking). While these

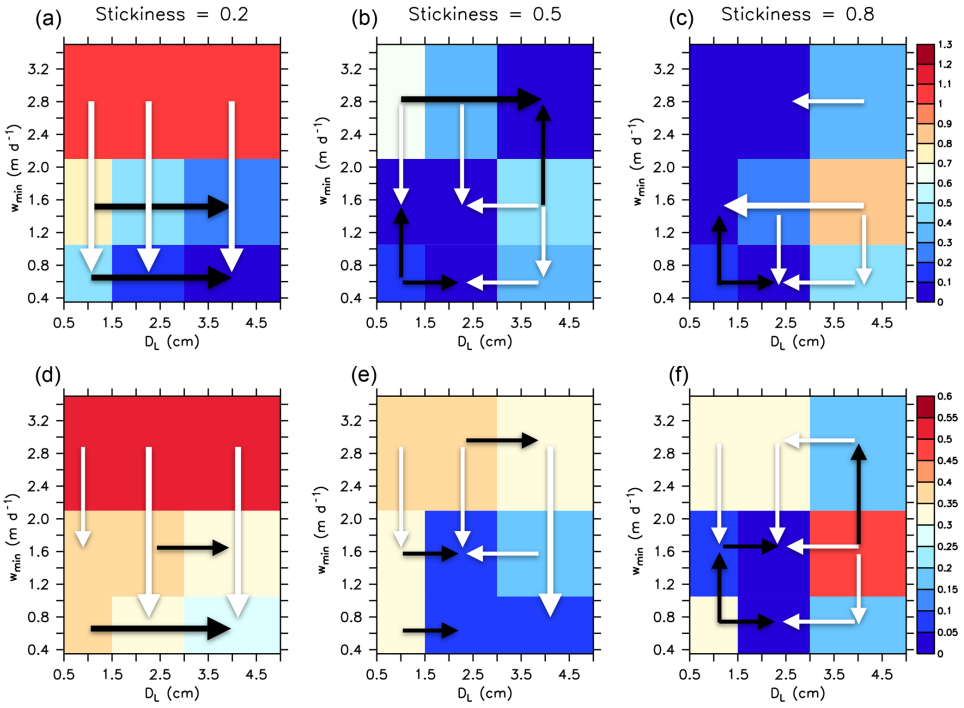

Figure 6. As Fig. 5 but for simulations with ECCO1.0.

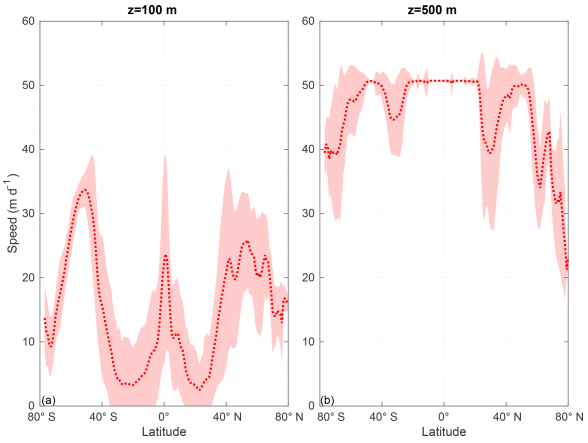

Figure 7. Zonal mean sinking speed of detritus (m d^{-1}; dotted line) and its standard deviation (shaded) of ECCO1.0* for a depth of 100 m **(a)** and for a depth of 500 m **(b)**.

particles exist (e.g. Bochdansky and Herndl, 1992), they are very rare (in the model, and likely also in the observations) and might not be observed with standard methods, which usually rely on a sample size of a few litres. The rare occurrence of large particles (and the limited sample size) has, for example, consequences for estimated size spectra parameters (Blanco et al., 1994). Thus, any model calibration against observations of particle abundance and size has to account for a proper match between simulated and observed quantities.

As we used on the one hand two different model grid resolutions and on the other hand varied model parameterisations with regard to particle aggregation, changes in the location and extension of OMZs and the distribution of tracers within each resolution are exclusively driven by the aggregation parameters. A good parameterisation of particle aggregation parameters can therefore have a major influence on the representation of OMZs. Furthermore, a higher model resolution improves the depiction of equatorial currents and therefore the oxygen transport (Cabré et al., 2015; Duteil et al., 2014), which, in turn, results in an improved representation of OMZs in the finer-resolution configuration, ECCO1.0, compared to the coarser resolution, MIT2.8. However, as physical processes at smaller scales affect the simulated shallow to mesopelagic oxygen and nutrient concentrations for the eastern tropical Pacific (Getzlaff and Dietze, 2013), the finer ($1° \times 1°$) resolution of ECCO1.0 is not sufficient to resolve the details of the equatorial current system (Duteil et al., 2014). This can explain the still high residual misfit of these simulations and the missing double structure of OMZs in the eastern tropical Pacific. We therefore suggest that the difference in improving the representation of OMZs between NH and SH is more affected by physics than by biology.

Furthermore, the results of our sensitivity study confirm that dense particles do not constitute a realistic representation of particles, as indicated by Karakaş et al. (2009) and Kriest (2002). Porous particles seem to constitute a more appropriate parameterisation for good model fit with regard to J_{RMSE} and J_{OMZ} (Table 1). Although the observed stickiness ranges between almost 0 and 1 (e.g. Alldredge and McGillivary, 1991; Kiørboe et al., 1990), in our study a moderate stickiness, α, between 0.5 and 0.8 leads the model towards a good fit to observed nutrients, oxygen and OMZs.

In summary, our study supports the results of Schwinger et al. (2016), who found an improved representation of nutrient distribution and OMZs when switching from constant particle sinking to either a power law or particle dynamics, similar to those presented here. However, the difference between the two latter schemes in that study were only small. A more extensive search of the parameter space within a given circulation may further improve the model. Additionally, we optimised $noAgg^{MIT2.8}$ against the same misfit function as $MOPS^{oD}$ of Kriest et al. (2017) and found that even though including an aggregation module improves our model, utilising an appropriate parameter optimisation would further enhance our model fit. Thus, without a comprehensive calibration of biogeochemical and aggregation parameters, there only seems to be a slight advantage when using this more complex model of particle dynamics.

Finally, we found a steep particle size spectrum in the subtropical oligotrophic region (Fig. 1d), which does not agree with observational data. Potentially, there are processes taking place that are not considered in our model, i.e. particle repackaging and active transport by zooplankton (vertical migration) (Kiko et al., 2017) based on a modified food web. Thus, particle aggregation alone so far seems not to be sufficient for a correct representation of the particle size spectrum.

5 Conclusion and outlook

Najjar et al (2007) applied different model circulations to the same biogeochemical model and found that physical processes are an important factor for modelling marine biogeochemistry. Our study furthermore showed that also biogeochemical parameterisations – in particular, those related to particle flux – can have an important impact on the representation of dissolved inorganic tracers, in line with earlier studies (e.g. Kriest et al., 2012; Kwon and Primeau, 2006, 2008). These earlier studies applied and varied a globally uniform particle flux length scale, whereas it has been suggested that this parameter should vary in space and time (e.g. Guidi et al., 2015; Marsay et al., 2015). The sensitivity study presented here constitutes a first approach to systematically estimate the impact of marine particle aggregation – and thus a spatially and temporally variable flux length scale – on the location and extent of OMZs as well as the representation of phosphate, nitrate and oxygen under steady-state conditions in a global three-dimensional biogeochemical ocean model.

We have shown that the assumptions inherent in the model confirm the general pattern of the spatial map of b values proposed by Marsay et al. (2015) (Fig. 1a and d). This, in turn, shows that the pattern of Martin's b can be depicted not only by a particulate organic carbon flux dependent on temperature but also by simulating explicit particle dynamics.

We furthermore found that even though there are still a lot of gaps in understanding several processes (e.g. the variation of export rates, particle stickiness and particle flux profile over space and time, as well as the link between particle diameter and sinking speed), the comparisons against observational data show a trend towards a model improvement by integrating particle dynamics (Table 1). While the parameterisation of aggregation leads the model towards an improved fit to OMZs for both model resolutions, this increase in model fit with regard to phosphate, nitrate and oxygen is only detectable in the coarse-resolution MIT2.8, but not in the finer-resolution and data-assimilated circulation of ECCO1.0. Moreover, model simulations show that besides effects of grid resolution, the model fit with regard to J_{RMSE} and J_{OMZ} is mainly driven by the particles' porosity. Our results indicate that a best fit to both tracers as well as OMZs (50 mmol O_2 m^{-3} criterion) is achieved by parameterising porous particles in combination with an intermediate-to-large maximum particle diameter for size-dependent aggregation and sinking, a moderate-to-high stickiness ranging between 0.5 and 0.8, and an intermediate-to-high initial sinking speed ranging between 1.4 and 2.8 m d^{-1} (Fig. 5). The strong sensitivity of the model fit to aggregation parameters may point towards the importance of a spatially and temporally varying flux length scale; however, they also show that the dynamics of the model depend strongly on the assumptions we make with respect to particle properties and processes.

Finally, we have shown that uncertainties in the parameterisation of particle aggregation remain, leading to the inference that dissolved inorganic tracers offer only insufficient observational constraints for global particle parameterisation. Therefore, for an accurate representation it will be necessary to calibrate the model not only against observed phosphate, nitrate, oxygen distributions and volume and location of OMZs (Sauerland et al., 2019) but also against number and size of particles, using comprehensive datasets of observations (as in Guidi et al., 2015).

Code and data availability. The source code of MOPS including the aggregation module coupled to TMM as well as the model output are available at: https://data.geomar.de/thredds/catalog/open_access/niemeyer_et_al_2019_bg/catalog.html (Niemeyer, 2019). The source code of the TMM is available at: https://github.com/samarkhatiwala/tmm (Khatiwala, 2019).

Supplement. The supplement related to this article is available online at: https://doi.org/10.5194/bg-16-3095-2019-supplement.

Author contributions. DN, IK and AO conceived the study. DN performed and analysed the simulations. All authors discussed and wrote the manuscript.

Competing interests. The authors declare that they have no conflict of interest.

Acknowledgements. This work is a contribution to DFG-supported project SFB 754 (https://www.sfb754.de, last access: 13 August 2019). Parallel supercomputing resources have been provided by the North-German Supercomputing Alliance (HLRN) and the computing centre at Kiel University. We thank two anonymous reviewers for their helpful comments.

Financial support. The article processing charges for this open-access publication were covered by a Research Centre of the Helmholtz Association.

Review statement. This paper was edited by Fortunat Joos and reviewed by two anonymous referees.

References

Alldredge, A. L. and Gotschalk, C.: In situ settling behavior of marine snow, Limnol. Ocean., 33, 339–351, 1988.

Alldredge, A. L. and McGillivary, P.: The attachment probabilities of marine snow and their implications for particle coagulation in the ocean, Deep-Sea Res. Pt. A, 38, 431–443, https://doi.org/10.1016/0198-0149(91)90045-H, 1991.

Armstrong, R. A., Lee, C., Hedges, J. I., Honjo, S., and Wakeham, S. G.: A new, mechanistic model for organic carbon fluxes in the ocean based on the quantitative association of POC with ballast minerals, Deep-Sea Res. Pt. II, 49, 219–236, https://doi.org/10.1016/S0967-0645(01)00101-1, 2002.

Banse, K.: New views on the degradation and disposition of organic particles as collected by sediment traps in the open sea, Deep-Sea Res. Pt. A, 37, 1177–1195, https://doi.org/10.1016/0198-0149(90)90058-4, 1990.

Berelson, W.: The flux of particulate organic carbon into the ocean interior, Oceanography, 14, 59–67, https://doi.org/10.5670/oceanog.2001.07, 2001.

Berelson, W. M.: Particle settling rates increase with depth in the ocean, Deep-Sea Res. Pt. II, 49, 237–251, https://doi.org/10.1016/S0967-0645(01)00102-3, 2002.

Biddanda, B. A. and Pomeroy, L. R.: Microbial aggregation and degradation of pyhtoplankton-derived detritus in seawater, I. Microbial succession, Mar. Ecol. Prog. Ser., 42, 79–88, 1988.

Blanco, J. M., Echevarria, F., and Garcia, C. M.: Dealing with size-spectra: Some conceptual and mathematical problems, Sci. Mar., 58, 17–29, 1994.

Bochdansky, A. B. and Herndl, G. J.: Ecology of amorphous aggregations (marine snow) in the Northern Adriatic Sea, III. Zooplankton interactions with marine snow, Mar. Ecol. Prog. Ser., 87, 135–146, 1992.

Boyd, P. W. and Trull, T. W.: Understanding the export of biogenic particles in oceanic waters: Is there consensus?, Prog. Oceanogr., 72, 276–312, https://doi.org/10.1016/j.pocean.2006.10.007, 2007.

Buesseler, K. O., Lamborg, C. H., Boyd, P. W., Lam, P. J., Trull, T. W., Bidigare, R. R., Bishop, J. K. B., Casciotti, K. L., Dehairs, F., Elskens, M., Honda, M., Karl, D. M., Siegel, D. A., Silver, M. W., Steinberg, D. K., Valdes, J., Mooy, B. Van, and Wilson, S.: Revisiting Carbon Flux Through the Ocean's Twilight Zone, Science, 316, 567–570, https://doi.org/10.1126/science.1137959, 2007.

Burd, A. B.: Modeling particle aggregation using size class and size spectrum approaches, J. Geophys. Res.-Ocean., 118, 3431–3443, https://doi.org/10.1002/jgrc.20255, 2013.

Burd, A. B. and Jackson, G. A.: Particle aggregation, Annu. Rev. Mar. Sci., 1, 65–90, https://doi.org/10.1146/annurev.marine.010908.163904, 2009.

Cabré, A., Marinov, I., Bernardello, R., and Bianchi, D.: Oxygen minimum zones in the tropical Pacific across CMIP5 models: Mean state differences and climate change trends, Biogeosciences, 12, 5429–5454, https://doi.org/10.5194/bg-12-5429-2015, 2015.

Cocco, V., Joos, F., Steinacher, M., Frölicher, T. L., Bopp, L., Dunne, J., Gehlen, M., Heinze, C., Orr, J., Oschlies, A., Schneider, B., Segschneider, J., and Tjiputra, J.: Oxygen and indicators of stress for marine life in multi-model global warming projections, Biogeosciences, 10, 1849–1868, https://doi.org/10.5194/bg-10-1849-2013, 2013.

Devol, A. H. and Hartnett, H. E.: Role of the oxygen-deficient zone in transfer of organic carbon to the deep ocean, Limnol. Ocean., 46, 1684–1690, https://doi.org/10.4319/lo.2001.46.7.1684, 2001.

Dutay, J. C., Tagliabue, A., Kriest, I., and van Hulten, M. M. P.: Modelling the role of marine particle on large scale 231Pa, 230Th, Iron and Aluminium distributions, Prog. Oceanogr., 133, 66–72, https://doi.org/10.1016/j.pocean.2015.01.010, 2015.

Duteil, O., Böning, C. W., and Oschlies, A.: Variability in subtropical-tropical cells drives oxygen levels in the tropical Pacific Ocean, Geophys. Res. Lett., 41, 8926–8934, https://doi.org/10.1002/2014GL061774, 2014.

Engel, A. and Schartau, M.: Influence of transparent exopolymer particles (TEP) on sinking velocity of Nitzschia closterium aggregates, Mar. Ecol. Prog. Ser., 182, 69–76, https://doi.org/10.3354/meps182069, 1999.

Garcia, H. E., Locarnini, R. A., Boyer, T. P., and Antonov, J. I.: World Ocean Atlas 2005, Volume 3: Dissolved Oxygen, Apparent Oxygen Utilization, and Oxygen Saturation, edited by: Levitus, S., NOAA Atlas NESDIS 63, US Gov. Print. Off. Washington, DC, 3, 342 pp., 2006.

Gehlen, M., Bopp, L., Emprin, N., Aumont, O., Heinze, C., and Ragueneau, O.: Reconciling surface ocean productivity, export fluxes and sediment composition in a global

biogeochemical ocean model, Biogeosciences, 3, 521–537, https://doi.org/10.5194/bg-3-521-2006, 2006.

Getzlaff, J. and Dietze, H.: Effects of increased isopycnal diffusivity mimicking the unresolved equatorial intermediate current system in an earth system climate model, Geophys. Res. Lett., 40, 2166–2170, https://doi.org/10.1002/grl.50419, 2013.

Guidi, L., Legendre, L., Reygondeau, G., Uitz, J., Stemmann, L., and Henson, S. A.: A new look at ocean carbon remineralization for estimating deepwater sequestration, Global Biogeochem. Cy., 29, 1044–1059, https://doi.org/10.1002/2014GB005063, 2015.

Hansen, J. L. S. and Kiørboe, T.: Quantifying interspecific coagulation efficiency of phytoplankton, Mar. Ecol. Prog. Ser., 159, 75–79, https://doi.org/10.3354/meps159075, 1997.

Henson, S. A., Sanders, R., Madsen, E., Morris, P. J., Le Moigne, F., and Quartly, G. D.: A reduced estimate of the strength of the ocean's biological carbon pump, Geophys. Res. Lett., 38, 10–14, https://doi.org/10.1029/2011GL046735, 2011.

Henson, S. A., Sanders, R., and Madsen, E.: Global patterns in efficiency of particulate organic carbon export and transfer to the deep ocean, Global Biogeochem. Cy., 26, GB1028, https://doi.org/10.1029/2011GB004099, 2012.

Henson, S. A., Yool, A., and Sanders, R.: Variability in efficiency of particulate organic carbon export: A model study, Global Biogeochem. Cy., 29, 33–45, https://doi.org/10.1002/2014GB004965, 2015.

Honjo, S., Manganini, S. J., Krishfield, R. A., and Francois, R.: Particulate organic carbon fluxes to the ocean interior and factors controlling the biological pump: A synthesis of global sediment trap programs since 1983, Prog. Oceanogr., 76, 217–285, https://doi.org/10.1016/j.pocean.2007.11.003, 2008.

Iversen, M. H. and Ploug, H.: Temperature effects on carbon-specific respiration rate and sinking velocity of diatom aggregates – potential implications for deep ocean export processes, Biogeosciences, 10, 4073–4085, https://doi.org/10.5194/bg-10-4073-2013, 2013.

Jackson, G. A.: A model of the formation of marine algal flocs by physical coagulation processes, Deep-Sea Res. Pt. A, 37, 1197–1211, https://doi.org/10.1016/0198-0149(90)90038-W, 1990.

Jouandet, M.-P., Trull, T. W., Guidi, L., Picheral, M., Ebersbach, F., Stemmann, L., and Blain, S.: Optical imaging of mesopelagic particles indicate deep carbon flux beneath a natural iron-fertilized bloom in the Southern Ocean, Limnol. Oceanogr., 56, 1130–1140, https://doi.org/10.4319/lo.2011.56.3.1130, 2011.

Jouandet, M.-P., Jackson, G. A., Carlotti, F., Picheral, M., Stemmann, L., and Blain, S.: Rapid formation of large aggregates during the spring bloom of Kerguelen Island: observations and model comparisons, Biogeosciences, 11, 4393–4406, https://doi.org/10.5194/bg-11-4393-2014, 2014.

Karakaş, G., Nowald, N., Schäfer-Neth, C., Iversen, M., Barkmann, W., Fischer, G., Marchesiello, P., and Schlitzer, R.: Impact of particle aggregation on vertical fluxes of organic matter, Prog. Oceanogr., 83, 331–341, https://doi.org/10.1016/j.pocean.2009.07.047, 2009.

Keller, D. P., Oschlies, A., and Eby, M.: A new marine ecosystem model for the University of Victoria Earth System Climate Model, Geosci. Model Dev., 5, 1195–1220, https://doi.org/10.5194/gmd-5-1195-2012, 2012.

Khatiwala, S.: A computational framework for simulation of biogeochemical tracers in the ocean, Global Biogeochem. Cy., 21, GB3001, https://doi.org/10.1029/2007GB002923, 2007.

Khatiwala, S.: Transport Matrix Method software for ocean biogeochemical simulations, available at: https://doi.org/10.5281/zenodo.1246300 (last access: 13 August 2019), 2018.

Khatiwala, S.: Transport Matrix Method (TMM) code repository, available at: https://github.com/samarkhatiwala/tmm, last access: 13 August 2019.

Khatiwala, S., Visbeck, M., and Cane, M. A.: Accelerated simulation of passive tracers in ocean circulation models, Ocean Model., 9, 51–69, https://doi.org/10.1016/j.ocemod.2004.04.002, 2005.

Kiko, R., Biastoch, A., Brandt, P., Cravatte, S., Hauss, H., Hummels, R., Kriest, I., Marin, F., McDonnell, A. M. P., Oschlies, A., Picheral, M., Schwarzkopf, F. U., Thurnherr, A. M., and Stemmann, L.: Biological and physical influences on marine snowfall at the equator, Nat. Geosci., 10, 852–858, https://doi.org/10.1038/ngeo3042, 2017.

Kiørboe, T., Andersen, K. P., and Dam, H. G.: Coagulation efficiency and aggregate formation in marine phytoplankton, Mar. Biol., 107, 235–245, https://doi.org/10.1007/BF01319822, 1990.

Kriest, I.: Different parameterizations of marine snow in a 1D-model and their influence on representation of marine snow, nitrogen budget and sedimentation, Deep-Sea Res. Pt. I, 49, 2133–2162, https://doi.org/10.1016/S0967-0637(02)00127-9, 2002.

Kriest, I. and Evans, G. T.: A vertically resolved model for phytoplankton aggregation, Proc. Indian Acad. Sci. Earth Planet. Sc., 109, 453–469, https://doi.org/10.1007/BF02708333, 2000.

Kriest, I. and Oschlies, A.: On the treatment of particulate organic matter sinking in large-scale models of marine biogeochemical cycles, Biogeosciences, 5, 55–72, https://doi.org/10.5194/bg-5-55-2008, 2008.

Kriest, I. and Oschlies, A.: Swept under the carpet: organic matter burial decreases global ocean biogeochemical model sensitivity to remineralization length scale, Biogeosciences, 10, 8401–8422, https://doi.org/10.5194/bg-10-8401-2013, 2013.

Kriest, I. and Oschlies, A.: MOPS-1.0: towards a model for the regulation of the global oceanic nitrogen budget by marine biogeochemical processes, Geosci. Model Dev., 8, 2929–2957, https://doi.org/10.5194/gmd-8-2929-2015, 2015

Kriest, I., Sauerland, V., Khatiwala, S., Srivastav, A., and Oschlies, A.: Calibrating a global three-dimensional biogeochemical ocean model (MOPS-1.0), Geosci. Model Dev., 10, 127–154, https://doi.org/10.5194/gmd-10-127-2017, 2017.

Kriest, I., Oschlies, A., and Khatiwala, S.: Sensitivity analysis of simple global marine biogeochemical models, Global Biogeochem. Cy., 26, GB2029, https://doi.org/10.1029/2011GB004072, 2012.

Kwon, E. Y. and Primeau, F.: Optimization and sensitivity study of a biogeochemistry ocean model using an implicit solver and in situ phosphate data, Global Biogeochem. Cy., 20, GB4009, https://doi.org/10.1029/2005GB002631, 2006.

Kwon, E. Y. and Primeau, F.: Optimization and sensitivity of a global biogeochemistry ocean model using combined in situ DIC, alkalinity, and phosphate data, J. Geophys. Res.-Ocean, 113, C08011, https://doi.org/10.1029/2007JC004520, 2008.

Kwon, E. Y., Primeau, F., and Sarmiento, J. L.: The impact of remineralization depth on the air-sea carbon balance, Nat. Geosci., 2, 630–635, https://doi.org/10.1038/NGEO612, 2009.

Laws, E. A., Ducklow, H., and McCarthy, J. J.: Temperature effects on export production in the open ocean, Global Biogeochem. Cy., 14, 1231–1246, https://doi.org/10.1029/1999GB001229, 2000.

Le Moigne, F. A. C., Henson, S. A., Sanders, R. J., and Madsen, E.: Global database of surface ocean particulate organic carbon export fluxes diagnosed from the ^{234}Th technique, Earth Syst. Sci. Data, 5, 295–304, https://doi.org/10.5194/essd-5-295-2013, 2013.

Lutz, M., Dunbar, R., and Caldeira, K.: Regional variability in the vertical flux of particulate organic carbon in the ocean interior, Global Biogeochem. Cy., 16, 1037, https://doi.org/10.1029/2000GB001383, 2002.

Marsay, C. M., Sanders, R. J., Henson, S. A., Pabortsava, K., Achterberg, E. P., and Lampitt, R. S.: Attenuation of sinking particulate organic carbon flux through the mesopelagic ocean, P. Natl. Acad. Sci. USA, 112, 1089–1094, https://doi.org/10.1073/pnas.1415311112, 2015.

Martin, J. H., Knauer, G. A., Karlt, D. M., and Broenkow, W. W.: VERTEX: carbon cycling in the northeast Pacific, Deep-Sea Res., 34, 267–285, 1987.

McDonnell, A. M. P. and Buesseler, K. O.: Variability in the average sinking velocity of marine particles, Limnol. Oceanogr., 55, 2085–2096, https://doi.org/10.4319/lo.2010.55.5.2085, 2010.

Metcalfe, A. M., Stoll, S., and Burd, A.: The effect of inhomogeneous stickiness on polymer aggregation, J. Colloid Interf. Sci., 298, 629–638, https://doi.org/10.1016/j.jcis.2005.12.045, 2006.

Najjar, R. G., Jin, X., Louanchi, F., Aumont, O., Caldeira, K., Doney, S. C., Dutay, J. C., Follows, M., Gruber, N., Joos, F., Lindsay, K., Maier-Reimer, E., Matear, R. J., Matsumoto, K., Monfray, P., Mouchet, A., Orr, J. C., Plattner, G. K., Sarmiento, J. L., Schlitzer, R., Slater, R. D., Weirig, M. F., Yamanaka, Y., and Yool, A.: Impact of circulation on export production, dissolved organic matter, and dissolved oxygen in the ocean: Results from Phase II of the Ocean Carbon-cycle Model Intercomparison Project (OCMIP-2), Global Biogeochem. Cy., 21, GB3007, https://doi.org/10.1029/2006GB002857, 2007.

Niemeyer, D.: Source code repository of MOPS including the aggregation module, available at: https://data.geomar.de/thredds/catalog/open_access/niemeyer_et_al_2019_bg/catalog.html, last access: 13 August 2019.

Nowald, N., Fischer, G., Ratmeyer, V., Iversen, M., Reuter, C., and Wefer, G.: In-situ sinking speed measurements of marine snow aggregates acquired with a settling chamber mounted to the Cherokee ROV, Ocean, '09 IEEE Bremen Balanc. Technol. with Futur, Needs, 1286–1291, https://doi.org/10.1109/OCEANSE.2009.5278186, 2009.

Oschlies, A.: Model-derived estimates of new production: New results point towards lower values, Deep-Sea Res. Pt. II, 48, 2173–2197, https://doi.org/10.1016/S0967-0645(00)00184-3, 2001.

Oschlies, A. and Kähler, P.: Biotic contribution to air-sea fluxes of CO_2 and O_2 and its relation to new production, export production, and net community production, Glob. Biogeochem. Cy., 18, GB1015, https://doi.org/10.1029/2003GB002094, 2004.

Paulmier, A., Kriest, I., and Oschlies, A.: Stoichiometries of remineralisation and denitrification in global biogeochemical ocean models, Biogeosciences, 6, 923–935, https://doi.org/10.5194/bg-6-923-2009, 2009.

Ploug, H., Iversen, M. H., and Fischer, G.: Ballast, sinking velocity, and apparent diffusivity within marine snow and zooplankton fecal pellets: Implications for substrate turnover by attached bacteria, Limnol. Oceanogr., 53, 1878–1886, https://doi.org/10.4319/lo.2008.53.5.1878, 2008.

Roth, R., Ritz, S. P., and Joos, F.: Burial-nutrient feedbacks amplify the sensitivity of atmospheric carbon dioxide to changes in organic matter remineralisation, Earth Syst. Dynam., 5, 321–343, https://doi.org/10.5194/esd-5-321-2014, 2014.

Sauerland, V., Kriest, I., Oschlies, A., and Srivastav, A.: Multi-objective Calibration of a Global Biogeochemical Ocean Model against Nutrients, Oxygen and Oxygen Minimum Zones, J. Adv. Model. Earth Sy., 11, 1285–1308, https://doi.org/10.1029/2018MS001510, 2019.

Schwinger, J., Goris, N., Tjiputra, J. F., Kriest, I., Bentsen, M., Bethke, I., Ilicak, M., Assmann, K. M., and Heinze, C.: Evaluation of NorESM-OC (versions 1 and 1.2), the ocean carbon-cycle stand-alone configuration of the Norwegian Earth System Model (NorESM1), Geosci. Model Dev., 9, 2589–2622, https://doi.org/10.5194/gmd-9-2589-2016, 2016.

Smayda, T. J.: The suspension and sinking of phytoplankton in the sea, Ocean. Mar. Biol. Ann. Rev., 8, 353–414, 1970.

Stammer, D., Ueyoshi, K., Köhl, A., Large, W. G., Josey, S. A., and Wunsch, C.: Estimating air-sea fluxes of heat, freshwater, and momentum through global ocean data assimilation, J. Geophys. Res., 109, C05023, https://doi.org/10.1029/2003JC002082, 2004.

Stemmann, L., Gorsky, G., Marty, J.-C., Picheral, M., and Miquel, J.-C.: Four-year study of large-particle vertical distribution (0–1000 m) in the NW Mediterranean in relation to hydrology, phytoplankton, and vertical flux, Deep-Sea Res. Pt. II, 49, 2143–2162, https://doi.org/10.1016/S0967-0645(02)00032-2, 2002.

Van Mooy, B. A. S., Keil, R. G., and Devol, A. H.: Impact of suboxia on sinking particulate organic carbon: Enhanced carbon flux and preferential degradation of amino acids via denitrification, Geochim. Cosmochim. Ac., 66, 457–465, https://doi.org/10.1016/S0016-7037(01)00787-6, 2002.

Volk, T. and Hoffert, M. I.: Ocean carbon pump: Analysis of relative stregths and efficiencies in ocean-driven atmospheric CO_2 changes, Geophys. Monogr., 32, 99–110, 1985.

Supplement of Biogeosciences, 16, 3095–3111, 2019
https://doi.org/10.5194/bg-16-3095-2019-supplement

Biogeosciences Open Access EGU

Supplement of

The effect of marine aggregate parameterisations on nutrients and oxygen minimum zones in a global biogeochemical model

Daniela Niemeyer et al.

Correspondence to: Daniela Niemeyer (dniemeyer@geomar.de)

This file provides additional figures to the manuscript 'The effect of marine aggregate parameterisations on nutrients and oxygen minimum zones in a global biogeochemical model'. It contains the following figures:

Figure S1: Global maps of b for $noAgg^{ECCO1.0}$ (a) (same as Fig. 1a) and simulation BUR (b) from Kriest and Oschlies (2013), where remineralisation does not depend on oxygen.

Figure S2: Global map of b for the four best model simulations with regard to the sum of J_{RMSE} and J_{OMZ} in ECCO1.0: (a) simulation #14; (b) simulation #17; (c) simulation #28; (d) simulation #29).

Figure S3: As Fig. 2, but for O_2 <= 30 mmol m^{-3}.

Figure S4: Profiles of average nutrient and oxygen concentrations for the eastern tropical Pacific (upper panels) and globally (lower panels).

Figure S5: Simulated particle abundance (in # L^{-1}) in the surface layer (upper), for the 23°W section (lower left) and 151°W section (lower right) as a depth-profile for a particle size range of 0.14 to 16.88 mm diameter, following Kiko et al. (2017).

Supplement Figures

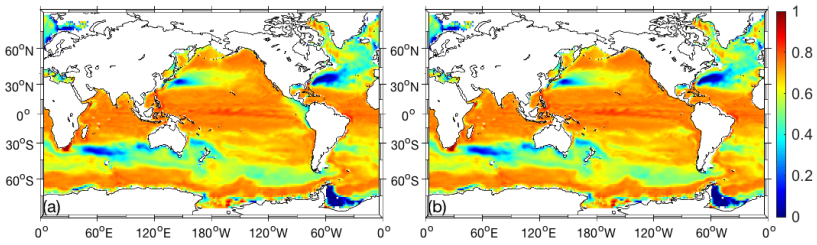

Figure S1: Global maps of *b* for noAgg$^{ECCO1.0}$ (a) (same as Fig. 1a) and simulation BUR (b) from Kriest and Oschlies (2013), where remineralisation does not depend on oxygen.

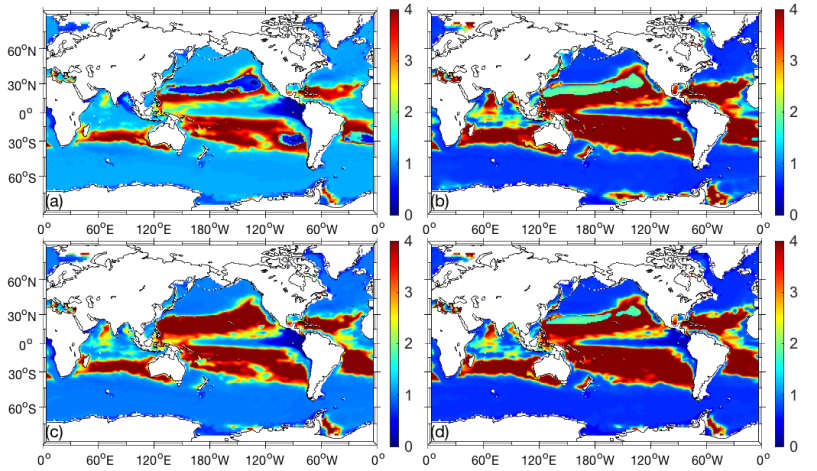

Figure S2: Global map of *b* for the four best model simulations with regard to the sum of J_{RMSE} and J_{OMZ} in ECCO1.0: (a) simulation #14; (b) simulation #17; (c) simulation #28; (d) simulation #29).

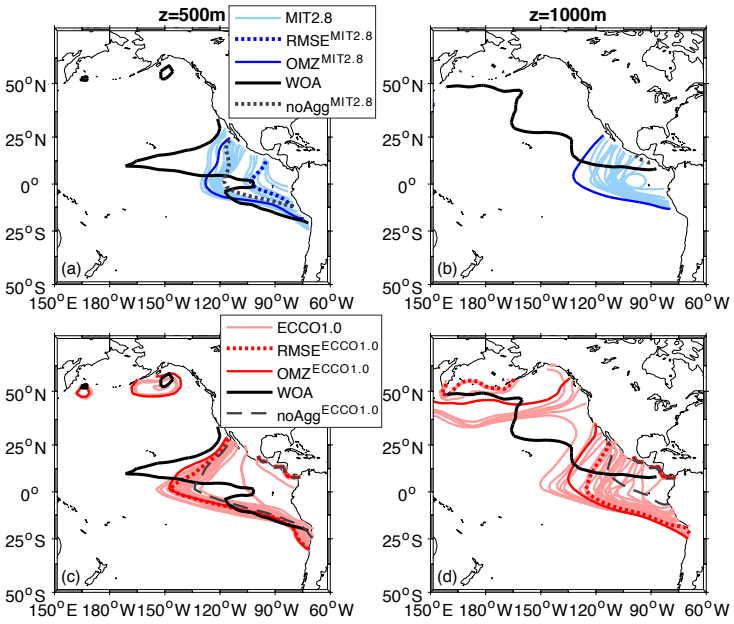

Figure S3: As Fig. 2, but for O_2 <= 30 mmol m^{-3}.

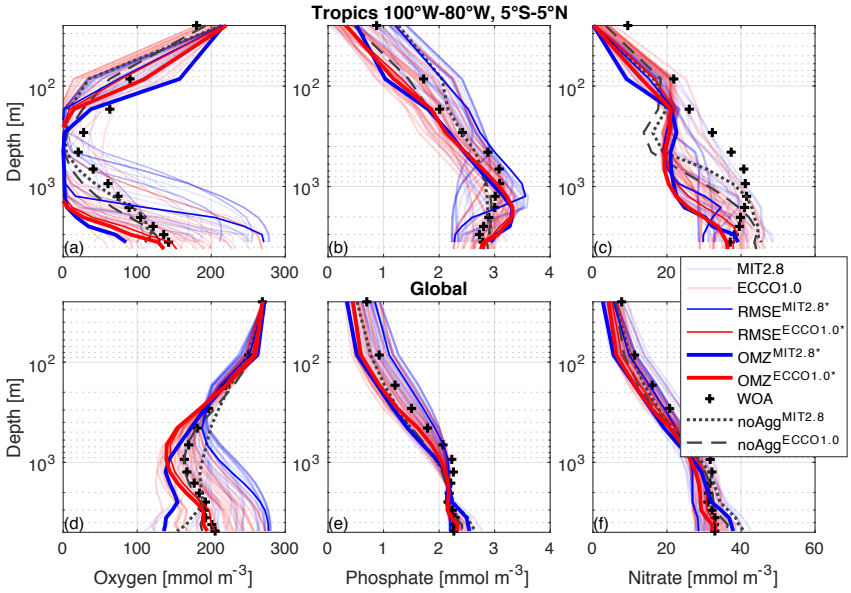

Figure S4: Profiles of average nutrient and oxygen concentrations for the eastern tropical Pacific (upper panels) and globally (lower panels).

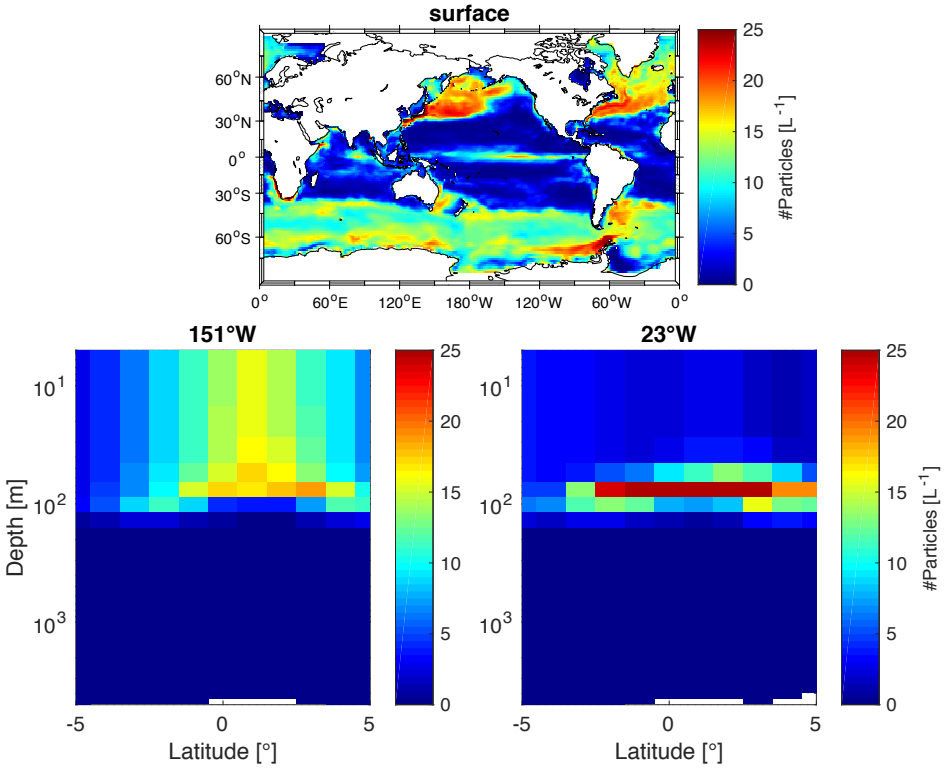

Figure S5: Simulated particle abundance (in # L^{-1}) in the surface layer (upper) and for the 23°W section (lower left) and 151°W section (lower right) as a depth-profile for a particle size range of 0.14 to 16.88 mm diameter, following Kiko et al. (2017).

4 Parameter optimisation against observed marine particles, nutrients and oxygen minimum zones in a global biogeochemical model

This chapter is a manuscript in preparation entitled 'Parameter optimisation against observed marine particles, nutrients and oxygen minimum zones in a global biogeochemical model' by Niemeyer, D., Kriest, I., Kiko, R., and Oschlies, A. and with potential contributions by Guidi, L., Hauss, H., McDonnell, A., Picheral, M., Rogge, A., Sauerland, V., Stemmann, L. and Waite, A.

Abstract Marine biogenic particles play an important role in the transport of carbon and other biogeochemical elements from the surface into the ocean interior. They can aggregate into larger particles, breakup into smaller components and also interact with marine zooplankton that itself can migrate vertically and thereby actively contribute to particle transport. Here, we integrate explicit descriptions of particle dynamics in a global biogeochemical model, which is optimised against a global dataset of observed marine particles as well as dissolved inorganic tracers and the vertical and horizontal extent of OMZs. The results show that integrating more processes into the optimisation against marine particles lead the model towards an improved fit to observed particles. However, a parameterisation that targets on the fit to marine particles deteriorates the representation of dissolved inorganic tracers, namely phosphate, nitrate and oxygen. Thus, we also optimise the model against observed particles as well as dissolved inorganic tracers and find a best compromise solution for both objectives. Nevertheless, the model still tends to underestimate especially the deep particles. This indicates that another important process determining marine particle dynamics is still missing in the global biogeochemical model.

4.1 Introduction

Based on the large size of its carbon reservoir, the ocean plays an important role in the global carbon cycle. The marine biological carbon pump ensures that carbon is efficiently moved from the sea surface in contact with the atmosphere into the ocean interior. Without the action of the biological carbon pump, CO_2 concentrations in the surface water, and hence in the atmosphere, would be about twice as high as today [Maier-Reimer et al., 1996]. The ocean also plays an important role in the uptake of anthropogenic CO_2 emissions: So far, the ocean has absorbed about 48% of total cement-manufactured and fossil

fuelled emissions [Sabine et al., 2004]. This uptake has been realized predominantly by the so-called physical solubility pump [Volk and Hoffert, 1985], while contributions from a possibly changing biological carbon pump are not well known.
This carbon, which is absorbed at the surface, is consumed by phytoplankton producing organic matter and biominerals and is transported in the deeper ocean interior as detritus. These detritus particles are exported either passively by gravitational sinking [Volk and Hoffert, 1985] or actively by migrating zooplankton [Longhurst et al., 1990; Steinberg et al., 2002].
On their way downwards by passive gravitational sinking, the sinking speed is determined by size and density of particles [Engel and Schartau, 1999], the presence of inorganic ballast of the particles [Ploug et al., 2008; Bach et al., 2016] and density and viscosity of seawater, which is determined by temperature and salinity [Bach et al., 2012]. As the particles are also simultaneously degraded by remineralisation, the passive transport of particles is a competition between sinking and remineralisation. Ballast [Ploug et al., 2008; Bach et al., 2016] and temperature [Segschneider and Bendtsen, 2013; Marsay et al., 2015; Iversen and Ploug, 2013] not only determine the sinking of particles, but also the remineralisation. Moreover, the remineralisation rate is determined by oxygen concentrations [Ploug, 2001; Tiano et al., 2014; Robinson, 2019].
Active transport into the deeper ocean is caused by diurnal vertical migration (DVM) by zooplankton and nekton, which feed on particles, phytoplankton and other zooplankton organisms at the surface during night and descend to depths of several hundred meters during daytime [Kiko et al., 2017]. Thus, particulate organic carbon (POC) is removed from the particle sinking pool in near-surface waters. In deeper layers, the zooplankton defecates the particles during daytime, which provides fresh and dense fecal pellets, possibly including mineral ballast [Ploug et al., 2008]. As those particles are dense and heavy, they reach very high sinking speeds [Ploug et al., 2008] and thus potentially provide an important amount of particle flux reaching the deep ocean interior [Kelly et al., 2019; Hernández-León et al., 2019; Kiko et al., 2020]. Depending on the geographical location [Rutherford et al., 1999] and day- or night-time, the abundance of zooplankton is highly variable in space and time. As, depending on the species, not all organisms migrate to deeper ocean layers to hide from predators, the fraction of migrating zooplankton as well as the migration depth are highly variable and still remain unclear [Archibald et al., 2019]. Kiko et al. [2017] showed that zooplankton processes seem to be important for a correct representation of particle number and size and thus should be integrated into models that include particle dynamics.
In addition, observations showed that beside large particles also small particles are available in the deep ocean, which indicates another process, i.e. the particle breakup into smaller components [Ruiz and Izquierdo, 1997; Dilling and Alldredge, 2000; Burd and Jackson, 2009]. This process is assumed to be induced by particle shear and reduces the particle size but not its mass [Stemmann et al., 2004; Turner, 2015].
Although there are observed particle datasets available [Guidi et al., 2015; Kiko et al., 2017, 2020], these observations are limited in space and time and extrapolations to global scales are difficult. Global models are therefore a useful tool to investigate the effect of particle interactions and help to extrapolate these processes on global scale. However,

there is a large number of parameters to take into account and specify, and the interdependencies of those parameters remain unclear. Thus, in Niemeyer et al. [2019] we tested the parameter sensitivity of six model parameters that impact particle dynamics, and compared the model output to observed distributions of nutrients and oxygen. As this approach allows only a limited exploration of the parameter space, and did not account for the model's fit to observed particle concentrations, in this study we apply objective parameter optimisation against a dataset of observed particle size distributions. In particular, we aim to answer the following questions:

1. Does optimisation against observed particle concentrations improves the model fit, and does it help to constrain the uncertain model parameters?

2. Is the model able to fit particulate organic and dissolved inorganic tracers at the same time?

3. Does simulation of active particle transport by migrating zooplankton and particle breakup improve particle dynamics?

4.2 Model description and methods

In this study, we used the Model of Oceanic Pelagic Stoichiometry (MOPS) including an aggregation module [Niemeyer et al., 2019] and added two new processes: particle breakup (shedding) and the effect of particle transport via implicit zooplankton migration and its fecal pellet egestion in deeper ocean layers ('gut flux'). The biogeochemical model was coupled to an offline circulation by applying the Transport Matrix Method (TMM) [Khatiwala et al., 2005; Khatiwala, 2007, 2018], which will be described below.

4.2.1 The physical model

We use the 'Transport Matrix Method', hereafter called TMM [Khatiwala et al., 2005; Khatiwala, 2007, 2018], describing an offline approach to simulate biogeochemical tracer transport. Advection and mixing are represented by monthly mean transport matrices (TMs). Additionally, salinity, temperature and wind are used for simulating air-sea gas exchange of oxygen as well as for the parameterisation of temperature-dependent growth of phytoplankton.
As the TMs and forcing fields of a circulation model with a higher resolution of 1.0° x 1.0° and 23 depth layers in general improve the model fit [Niemeyer et al., 2019], we focussed in this study on this data-constrained circulation, called ECCO1.0, and neglected any coarser resolution. For physical transport, we used a time step length of 1/2 day and for biogeochemical interaction 1/40 day.

4.2.2 The biogeochemical model

We build upon the coupled model setup presented by Niemeyer et al. [2019], experiment ECCO1.0, and describe the biogeochemical and particle aggregation model only briefly here, with focus on the parameters to be optimised. In particular, we apply the phosphorus-based Model of Oceanic Pelagic Stoichiometry, called MOPS, [Kriest and Oschlies, 2015], which represents eight tracers: phosphate, dissolved organic matter, oxygen, phytoplankton, zooplankton, detritus, nitrate and the number of detrital particles. The P-, N- and O_2-cycles are coupled via constant stoichiometric ratios, following Paulmier and Ruiz-Pino [2009]. In the model, detritus is produced through linear phytoplankton and quadratic zooplankton mortality. Additionally, the amount of food not ingested by zooplankton, ε_{zoo}, feeds into the detritus pool. Detritus sinks with a sinking speed determined by particle dynamics, and remineralises with a constant rate, r. However, remineralisation of particulate and dissolved organic matter depends on oxygen, and ceases when oxygen becomes too low. With decreasing oxygen nitrate is used as electron acceptor for denitrification. If neither oxygen nor nitrate is available, remineralisation does not occur any more. On a global scale, the loss of fixed nitrogen via denitrification is compensated via temperature-dependent nitrogen fixation. A fraction of sinking detritus that reaches the seafloor is resuspended back into the water column, and the other fraction is buried into the sediment. Buried P and N are resupplied via river runoff, and the P budget is thus globally stable, while N and O_2 adjust to the biogeochemical parameters and boundary conditions (nitrogen fixation and air-sea gas exchange, respectively; see Kriest and Oschlies [2015]). The biogeochemical model is complemented by a model for particle aggregation and size-dependent sinking as described in Niemeyer et al. [2019] (see section 4.2.2.1). In addition, we also included parameterisations for aggregate breakup (section 4.2.2.2) and the effect of zooplankton vertical migration and egestion at depth ('gut flux', section 4.2.2.3).

4.2.2.1 Particle aggregation and size dependent sinking

As in Niemeyer et al. [2019], the aggregation module simulates size-dependent properties of detritus particles by assuming power-law relationships between particle diameter, d, and mass, m, ($m = Cd^{\zeta}$) and between particle diameter and sinking speed, w ($w = Bd$). The minimum diameter and mass of a primary particle is set to $d_1 = 0.002$ and $m_1 = 0.00075$ mmol P, respectively. Following Kriest [2002] and Niemeyer et al. [2019], we set the relationship between size and mass, ζ, to 1.62. To enable very fast sinking speeds, we set an upper limit for size dependent processes and aggregation of $D_L = 20$ cm, i.e. particles larger than D_L exhibit no increase in sinking speed anymore. The model calculates the time- and space-varying spectral slope ε of the particle size distribution from the number N and mass M of particles for each time step [Kriest and Evans, 2000], via $N = A \int_{d_1}^{\infty} d^{-\varepsilon} dd$ and $M = AC \int_{d_1}^{\infty} d^{\zeta-\varepsilon} dd$. This log-log-linear particle size distribution is affected by particle aggregation processes and sinking

4.2.2.2 Particle breakup

Kiko et al. [2017] found in their observations lots of small particles in the deep ocean supported by the findings by Cavan et al. [2017]. In addition, Bianchi et al. [2018] showed in their modelling study an improvement by integrating particle breakup. Thus, a new component in our model consists in particle breakup, ρ, and is described as the particle breakup into smaller particles (given in d^{-1}). We assume that aggregates with at least twice the mass of a primary particle (of diameter d_1), given by $d_2 = d_1 2^{1/\zeta}$ disaggregate into primary particles with a rate ρ (d^{-1}). Thus, the number of particles breaking up, b_N (numbers cm^{-3} d^{-1}), over the size range from d_2 to infinity is given by

$$b_N = \rho A \int_{d_2}^{\infty} d^{-\varepsilon} dd = \rho N 2^{\frac{1-\varepsilon}{\zeta}} \tag{4.1}$$

where N (numbers cm^{-3}) is the total number of particles, defined by

$$N = A \int_{d_1}^{\infty} d^{-\varepsilon} dd \tag{4.2}$$

(see Kriest and Evans [1999]). This process decreases the number of particles larger than d_2, while it increases the number of primary particles of size mass m_1. The mass gain of small primary particles is then computed from the mass of particles that breakup, b_M , via

$$b_M = \rho AC \int_{d_2}^{\infty} d^{\zeta-\varepsilon} dd = \rho 2M 2^{\frac{1-\varepsilon}{\zeta}} \tag{4.3}$$

where M (mmol P m^{-3}) is the total mass of aggregates defined by

$$M = AC \int_{d_1}^{\infty} d^{\zeta-\varepsilon} dd \tag{4.4}$$

(see Kriest and Evans [1999]). These particles resulting from the breakup of a large particle into primary particles will all have a mass of m_1; thus, the total change in numbers is given by

$$\triangle N = \frac{b_M}{m_1} - b_N = \rho 2^{\frac{1-\varepsilon}{\zeta}} \left[\frac{2M}{m_1} - N \right]. \tag{4.5}$$

Dividing by the number of particles, N, we obtain the rate of breakup B:

$$B = \frac{\triangle N}{N} = \rho 2^{\frac{1-\varepsilon}{\zeta}} \left[\frac{2M}{Nm_1} - 1 \right]. \tag{4.6}$$

According to this formulation the gain of particles due to aggregate breakup is largest when the size distribution is "flat" (small ε), i.e. when there is a high proportion of large aggregates (equivalently: when the ratio of mass to numbers is large). Theoretically, the particle breakup rate ρ can range between zero and one, whereas zero represents no breakup at all and one describes such a high breakup that every particle is disintegrated into its primary compounds. Consequently, aggregate breakup, ρ, is a process, which possibly enables small particles to be available in deep ocean layers.

4.2.2.3 Zooplankton vertical migration

We take into account the effects of vertically migrating zooplankton, which feeds during night at the surface and migrates to the mesopelagic during daytime to hide from predators. Instead of explicitly including this diurnal vertical migration, we parameterise the effect of this migration and the egestion of faecal pellets in the mesopelagic, as follows: we assume that zooplankton migration has two controlling factors, namely the migration depth of the zooplankton, which is set in our study to 400 m [Kiko et al., 2017; Bianchi et al., 2013], and the fraction of zooplankton that migrates and evacuates its gut at depth. The egestion at depth thus creates a 'gut flux' to 400 m.
As described in Kriest and Oschlies [2015], the amount of detritus produced by grazing G and subsequent egestion E is described by

$$E = (1 - \sigma_{DOP})(1 - \varepsilon_{zoo})G \tag{4.7}$$

where σ_{DOP} is the fraction of the flux that is routed to dissolved organic matter, and ε_{ZOO} is the ingestion efficiency of zooplankton. We assume that for every layer in the euphotic zone (the upper 100 m, from depth layer k=1 to k=6) a fraction of this flux, θ is not released as detritus in the local depth layer, but is immediately shifted to the detritus pool at 400 m depth (k=11). We further assume that the size distribution of this flux is the same

as in the depth layer of the origin, implying that zooplankton and their feces in the originating layer track the size distribution of aggregates, i.e. when there are large aggregates there is also large zooplankton (as in Kriest [2002]). Thus, the rate of change of aggregate mass and numbers due to this implicit gut flux at 400 m (i.e. depth layer k_{gut}) is given by

$$\triangle M(k_{gut}) = \frac{1}{\triangle z(k_{gut})} \theta \sum_{k=1}^{k=6} E(k) \triangle z(k) \tag{4.8}$$

$$\triangle N(k_{gut}) = \frac{1}{\triangle z(k_{gut})} \theta \sum_{k=1}^{k=6} E(k) \frac{\zeta + 1 - \varepsilon(k)}{m_1(1-\varepsilon(k))} \triangle z(k). \tag{4.9}$$

The fraction of migrating zooplankton, θ, might - again - theoretically range between zero and one, where zero describes no zooplankton migration at all and one defines that all zooplankton organisms migrate to deeper layers during daytime.

4.2.3 Observations

The observed particle dataset is collected with the Underwater Vision Profiler (UVP 5), which enables the in situ quantification of marine particles with diameter > 0.06 mm in a water volume of 0.93 L per image [Picheral et al., 2010]. After recording, all thumbnails are extracted via ImageJ [Gorsky et al., 2010] and grouped into the size classes by equivalent spherical diameter (ESD).
The global dataset used in this study has a range in particle diameter between 0.16 mm and 26.00 mm, i.e. 22 particle size classes. The observed dataset is gridded onto the 1° model resolution by calculating the mean number of particles per size class and gridpoint. Afterwards, the particles are separated into MiPs, small microscopic particles (0.16-0.51 mm), and MaPs, large macroscopic particles (0.51-26.00 mm).

4.2.4 Optimisation

Most of the biogeochemical model parameters remain fixed at the values of configuration ECCO1.0 described in Niemeyer et al. [2019]. However, based on preceding tests and experiments in the configuration presented here we set w_1, the minimum sinking speed of a primary particle, to 0.33 m d^{-1} and the maximum diameter for size-dependent sinking and aggregation, D_L, to 20 cm (see Tab. 4.1) to enable very high sinking speeds. In addition to Niemeyer et al. [2019], this model configuration includes three more parameters as described above: the migration depth of zooplankton, the fraction of migrating zooplankton, θ, and particle breakup rate, ρ. As shown in Tab. 4.1, we fixed the migration depth of

zooplankton to a value of 400 m, which is thus independent from oxygen concentrations, and optimised the other two additional parameters as detailed below.

4.2.4.1 Optimised parameters

In this study, we carried out six different model optimisations, which differ with respect to the number of objectives to be optimised and the number of optimised parameters. As shown in Niemeyer et al. [2019], α, the probability that two particles stick together, and η, the exponent that relates particle sinking to diameter influence the particle size spectrum, the sinking speed and thus the overall particle flux. Based on these findings, these parameters are subject to optimisation. A large value of these parameters may lead to a high export of particles, and thus cause nutrient depletion especially in the surface layer. The detritus remineralisation rate, r, affects the nutrient turnover and decreases the particle abundance at the same time. Therefore this parameter was also subject to optimisation.

Parameters that are fixed	**Niemeyer et al. (2019)**	**this study**	**unit**	**description**
w_1	0.7	0.33	m d^{-1}	minimum sinking speed of a primary particle
D_L	2.0	20.0	cm	diameter for size-dependent aggregation and sinking
zmigrate	-	400	m	zooplankton migration depth
Range of optimised parameters				
α	-	0.5 – 0.9		stickiness for interparticle collision
η	-	0.5 – 1.8		exponent that relates particle sinking speed to diameter
ε_{zoo}	-	0.5 – 1.0		zooplankton ingestion efficiency
r	-	0.001 – 0.2	1 d^{-1}	detritus remineralisation rate
θ	-	0.01 – 0.9	m d^{-1}	fraction of migrating zooplankton
ρ	-	0.001 – 0.1	1 d^{-1}	break-up rate of particles

Tab. 4.1: *Model adjustments and new parameters used in this study compared to Niemeyer et al. [2019] and range of optimised parameters. Please note, that in the simulation* $Base_3{}_P^{UVP}$*, where r is not included in the optimisation algorithm, this parameter is fixed to 0.05* d^{-1}.

As noted above, Kiko et al. [2017] found in their observations a large number of small particles in the deep ocean, pointing towards processes that reduce the particle size in the ocean interior. To examine the impact of this process regarding the model fit to observations, we also optimised breakup rates of particles, ρ. As Kiko et al. [2017] and Aumont et al. [2018] stressed the importance of zooplankton, its vertical migration and effect on particle flux, we furthermore added two zooplankton parameters to the optimisation: the zooplankton ingestion efficiency, ε_{zoo}, which influences the detritus pool and the proportion of migrating zooplankton that egests particles into deeper ocean layers, θ.
By setting an upper and lower limit for the parameters to be optimised we reduce the parameter space and guide the model towards a good fit to observations, thereby increasing the efficiency of the - computationally expensive - optimisation. We followed Niemeyer et al. [2019] who found that the model fit to dissolved inorganic tracers is best with an intermediate to high α and set the boundaries for α, the probability that two particles stick together, to a range between 0.5 and 0.9 (see Tab. 4.1). Although the sensitivity study exhibited a best fit for a weak increase of sinking speed with aggregate size (corresponding to porous aggregates), i.e. $\eta = 0.62$, we enable the model to range between 0.5 to 1.8 (see Tab. 4.1). Remineralisation, r, and particle breakup rate, ρ, have been assigned between 0.001 d^{-1} and 0.2 and 0.001 and 0.1 d^{-1}, respectively (see Tab. 4.1). To prevent zooplankton from extinction, the lower limit of ε_{zoo} is set to 0.5 and the upper one to the maximum possible limit of 1.0. As the fraction of migrating zooplankton seems to be an important shuttle for the particles to reach deeper ocean layers, we set a very broad range, i.e. 0.01 to 0.9 (see Tab. 4.1).

4.2.4.2 Objectives of optimisation

With regard to the objectives, we distinguish between three different types of optimisations: (1) single-objective optimisation against a global particle dataset assembled from UVP data (J_{UVP}), and two types of multi-objective optimisations. The first case of multi-objective optimisation (2) is against a dataset of the underwater vision profiler, UVP, J_{UVP}, as the first objective, and the root mean square error, RMSE, of dissolved inorganic tracers (including phosphate, nitrate and oxygen), J_{RMSE}, as the second objective. The second case of multi-objective optimisation consists in an optimisation, where the UVP-dataset is - again - the first objective and the sum of J_{RMSE} of dissolved inorganic tracers and the overlap of OMZs, J_{OMZ}, between model and observations (following the approach by Cabré et al. [2015]; see also Niemeyer et al. [2019]) is the second objective (see Tab. 4.2).

4.2.4.2.1 Objective 1: Fit to number and size of particles

As the aim consists in improving the particle abundance and size distribution in our model, we chose the deviation of number and size of particles between model simulations and

observations as our first objective. As observational reference, we used a dataset of the UVP 5 [Picheral et al., 2010], mapped onto our model geometry. Afterwards, we calculated the deviation for each grid point between simulated and observed mean MiPs, small micrometric particles ranging in diameter between 0.16 mm and 0.51 mm, and MaPs, large macroscopic particles ranging between 0.51 mm and 26.0 mm (taking into account Kiko et al. [2017]; but please note the different boundaries of particle size classes in our study).
There are many more particles at the sea surface than at greater depths, and any absolute deviation would therefore focus on shallow waters, and not consider phenomena such as the 'marine equatorial snowfall' [Kiko et al., 2017]. To avoid such bias, the squared deviation of MiPs and MaPs is weighted by the squared number of both observed particle size classes at the corresponding location, thereby enhancing the mismatch at small concentrations at depth:

$$J_{UVP} = \sum_{j=1}^{2} J(j) = \sum_{j=1}^{2} \frac{1}{N_j} \sqrt{\sum_{i=1}^{N_j} \frac{(m_{i,j} - o_{i,j})^2}{o_{i,j}^2}}. \tag{4.10}$$

In this equation, $j = 2$ represents number of particle size classes, MiPs (small micrometric particles) and MaPs (large macroscopic particles), and i=1...N describes the number of ocean grid boxes, where observations of MiPs and MaPs exist. Furthermore, o represents the observational dataset and m the model results. To force the optimisation to reproduce small particles in the deeper ocean, the relative deviation has been chosen at this point. In summary, the lower J_{UVP} is, the better the model fits the observed particle dataset of the UVP 5.

4.2.4.2.2 Objective 2: RMSE to dissolved inorganic tracers

Following Kriest et al. [2017], the second objective of our model optimisation consists in the root mean squared error (RMSE) to dissolved inorganic tracers, namely phosphate, nitrate and oxygen between modelled, m, and observed, o, [Garcia et al., 2006] (hereafter named WOA) concentrations. We calculate the deviation between modelled, m, and observed, o, tracer concentration of phosphate, nitrate and oxygen, squared it up and weighted it by the relative volume of each grid box:

$$J_{RMSE} = \sum_{j=1}^{3} J(j) = \sum_{j=1}^{3} \frac{1}{\overline{o_j}} \sqrt{\sum_{i=1}^{N} (m_{i,j} - o_{i,j})^2 \cdot \frac{V_i}{V_T}}. \tag{4.11}$$

$j = 3$ describes the number of tracers, namely phosphate, nitrate and oxygen and i is again the number of ocean grid boxes. To emphasize on large deviations in the deep ocean, the

fit is weighted by the volume fraction as explained in Kriest et al. [2017]. J_{RMSE}, mostly varies between 0.4 and 1.0 (and is usually around 0.5 [Sauerland et al., 2019]), whereby a low value corresponds to a good model fit.

4.2.4.2.3 Objective 3: Fit to oxygen minimum zones

Following the approach by Cabré et al. [2015], we calculated the horizontal and vertical overlap between modelled and observed (WOA) OMZs for the fit to OMZs, J_{OMZ}. In this study, we defined OMZs by waters with oxygen concentrations lower than an oxygen threshold, c, set to 50 mmol m^{-3}. In this equation by Sauerland et al. [2019]

$$C = \frac{V^{\cap}(c)}{V_{\cup}(c)} = \frac{V^{\cap}(c)}{V^{m}(c) + V^{o}(c) - V^{\cap}(c)} \tag{4.12}$$

the overlap volume between modelled and observed OMZs, $V^{\cap}(c)$, is divided by the total volume, where either model or observations are suboxic, $V_{\cup}(c)$. This results in a fit ranging between zero, no overlap at all, and one, a perfect fit. We moreover calculated

$$J_{OMZ} = 1 - C \tag{4.13}$$

to adjust the scale to J_{RMSE}, i.e. zero is equal to the best fit and a high J_{OMZ} corresponds with a low overlap between modelled and observed OMZs. However, the fit to oxygen minimum zones was not treated as an independent third objective. Instead we calculated the sum of J_{RMSE} and J_{OMZ}, which constitutes one combined objective (see also Sauerland et al. [2019], who examined a single-objective optimisation against the sum of J_{RMSE} and J_{OMZ}).

4.2.4.2.4 Best compromise solution between two objectives

Sauerland et al. [2019] described in their study that the output of a multi-objective optimisation is a set of compromise solutions between the considered objectives. In this case, the misfit between model output and observations on both axes representing the two objectives ranges between zero, the best possible fit, and one. As the associated parameter set represents a 'knee' of the Pareto Front, the best compromise solution between both objectives is the minimum distance to the coordinate origin.
Thus, we calculated the minimum Euclidean distance, d, between data points a_i and coordinate origin, b_i, in a two-dimensional space for the two objectives (1^{st} objective, J_{UVP},

and 2^{nd} objective, J_{RMSE} (+ J_{OMZ})):

$$d(a,b) = \sqrt{(a_1 - b_1)^2 + (a_2 - b_2)^2}. \tag{4.14}$$

The minimum distance describes a compromise solution for both equally-weighted objectives.

4.2.5 Experiments

In this study, we used six different model simulations which vary regarding their number of optimised parameters and objectives (see Tab. 4.2):

Base$_3^{UVP}$: three optimised parameters: particle stickiness, α, sinking exponent, η, zooplankton ingestion efficiency, ε_{zoo}; single-objective optimisation against J_{UVP} (Eq. 4.10)

Base$_4^{UVP}$: as Base$_3^{UVP}$, but adding the remineralisation rate of detritus r to optimised parameters

Base$_5^{UVP}$: as Base$_4^{UVP}$, but adding the fraction of migrating zooplankton θ to optimised parameters

All^{UVP}: as Base$_5^{UVP}$, but adding the particle breakup rate ρ to optimised parameters

All$^{UVP\&RMSE}$: as All^{UVP} but with multi-objective optimisation against UVP and RMSE (Eq. 4.10 and 4.11, respectively)

All$^{UVP\&RMSE+OMZ}$: as All$^{UVP\&RMSE}$ but with multi-objective optimisation against UVP and RMSE+OMZ (Eq. 4.10 and 4.11 + 4.13)

We limited the optimisations to a maximum of 300 generations, where each generation includes 10 individuals, i.e. different parameter sets. As the optimisation is computationally expensive, we ran short-term optimisations, where we integrated the model solutions of each generation over 10 years. This length of simulation was regarded as sufficient to propagate the parameter information, e.g. enhanced particle aggregation to the ocean interior via particle sinking. However, after 10 years the model has not yet reached an equilibrium state with respect to the combined effects of particle production, its flux to the ocean interior and the effect of the large-scale circulation on the global distribution of nutrients and oxygen.

Therefore, after short-term optimisation we took the parameters of the best simulation and integrated the model over another 3000 years to run the model into equilibrium state. This allows us to determine the effects of parameterisation on global scale biogeochemistry.

4.3 Results

The optimisation convergence depends on the number of objectives. While the four single-objective optimisations against a global observed dataset of marine particles converge after 54, 74, 200 and 179 generations, respectively, the multi-objective optimisations did not converge with the given maximum number of 300 generations. Please note, that each simulation has been integrated over 3000 years into a steady state after optimisation. This output after 3000 has always been used in the following.

	$Base_{3P}^{UVP}$	$Base_{4P}^{UVP}$	$Base_{5P}^{UVP}$	All^{UVP}	$All^{UVP\ \&\ RMSE}$	$All^{UVP\ \&\ RMSE+OMZ}$
α	0.9	0.9	0.9	0.9	0.9/**0.9**/0.9	0.9/**0.84**/0.67
η	0.92	1.8	0.68	0.91	0.91/**1.3**/0.5	0.9/**0.63**/1.33
ε_{zoo}	1.0	1.0	0.63	1.0	1.0/**1.0**/1.0	1.0/**1.0**/0.89
r	0.05	0.001	0.001	0.02	0.02/**0.08**/0.08	0.02/**0.13**/0.08
θ			0.02	0.38	0.01/**0.01**/0.19	0.32/**0.05**/0.74
ρ				0.001	0.001/**0.04**/0.04	0.001/**0.001**/0.06
J_{UVP}	1.67	1.6	1.45	1.29	1.22/**1.68**/5.0	1.22/**1.6**/1.8
J_{RMSE}	1.56	1.67	2.1	1.08	0.3/**0.2**/0.18	0.3/**0.22**/0.2
J_{OMZ}	1.0	1.0	1.0	0.95	0.35/**0.31**/0.35	0.35/**0.29**/0.29

Tab. 4.2: *Model simulations, their optimised parameters and the calculated misfit of particles (J_{UVP}), dissolved inorganic tracers (J_{RMSE}) and OMZs (J_{OMZ}) with regard to the weighted best simulation of the last generation of each optimisation (please note, that the given fit is after optimisation and after running the model into steady state). OMZ is defined as 50 mmol m^{-3}. The first value in the multi-objective optimisations describes the best simulation regarding J_{UVP}, the second, bold value is the best compromise solution of both objectives (the associated parameterisation is used in this study) and the third value constitutes the best fit to the second objective (i.e. J_{RMSE} or J_{RMSE}+J_{OMZ}). As in $Base_{3P}^{UVP}$ the detritus remineralisation is fixed to 0.05 d^{-1}, it is depicted in this table in grey.*

4.3.1 Model fit to observed particles

Optimising the basic parameters, namely α, η and ε_{zoo}, in our global biogeochemical model against the UVP 5 dataset, simulation $Base_{3P}^{UVP}$, the parameterisation of the last generation does not lead the model towards a good fit to J_{UVP} (1.67) compared to the

following simulations (see Tab. 4.2). As the model parameterisation exhibits a η of 0.92 and thus simulates rather porous particles with a low sinking speed of large particles and moreover a very high ε_{zoo} (1.0) leading to no zooplankton egestion feeding into the particle pool, the model tends to underestimate the number of particles especially in the deeper ocean (see Fig. 4.1). This also results in a too low POC flux in 2000 m depth (see Fig. 4.2) compared to observations. This pattern is also shown in the equatorial Atlantic along 23°W and in the Pacific along 151°W, where particles in the deep ocean for both particle size classes, MiPs and MaPs, are underestimated (see Fig. 4.3 and 4.4). Especially in the equatorial region, i.e. 23°W, the model is not able to reproduce the IPM, intermediate particle maximum, indicated by observations [Kiko et al., 2017]. However, compared to the best simulation, ECCO*, from the sensitivity study by Niemeyer et al. [2019], both particle size classes are improved in both sections as the model now includes a higher number of particles – especially in shallow waters (see Fig. 4.3 and 4.4).

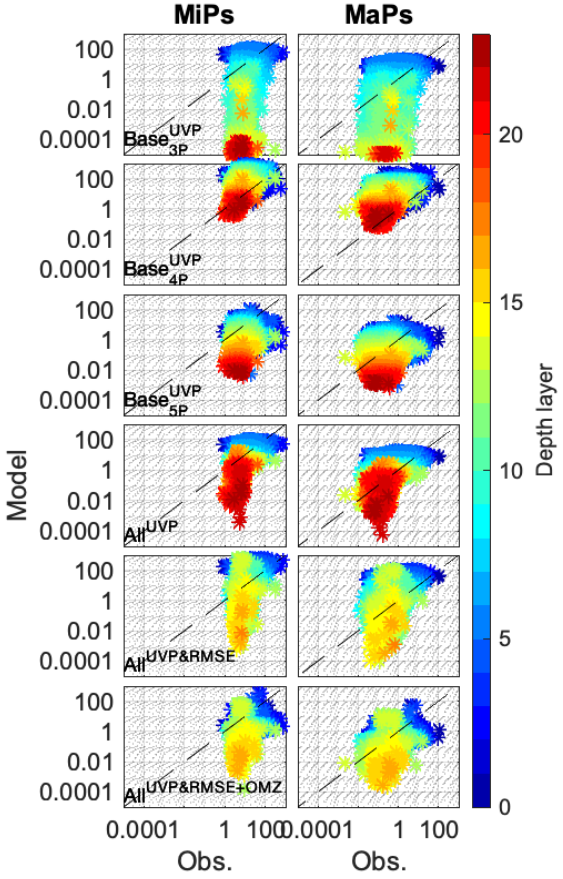

Fig. 4.1: *MiPs and MaPs (mean particles l^{-1} per model grid box) model vs. observations (from UVP 5 dataset). The colorbar represents the depth layer from the model (blue=shallow waters, red=deep ocean).*

Including one more parameter in the optimisation, namely the detritus remineralisation rate, r, slightly improves J_{UVP} (1.6) in Base_4^{UVP} compared to the previous simulation,

Base_{3P}^{UVP} (see Tab. 4.2). The probability of two particles sticking together, α, as well as the zooplankton ingestion efficiency, ε_{zoo}, are almost unchanged compared to the previous simulation. As the exponent between diameter and sinking speed is doubled (1.8) compared to Base_{3P}^{UVP} (see Tab. 4.2), the simulated particles exhibit very high sinking speeds leading to an improved fit to observed very deep particles and POC flux in 2000 m depth (see Fig. 4.1 and 4.2). However, particles in shallow ocean layers are considerably overestimated in both particle size classes (see Fig. 4.1), likely owing to the very low optimal remineralisation rate r. This particle overestimation is also represented in both modelled sections, at 23°W and 151°W respectively (see Fig. 4.3 and 4.4).

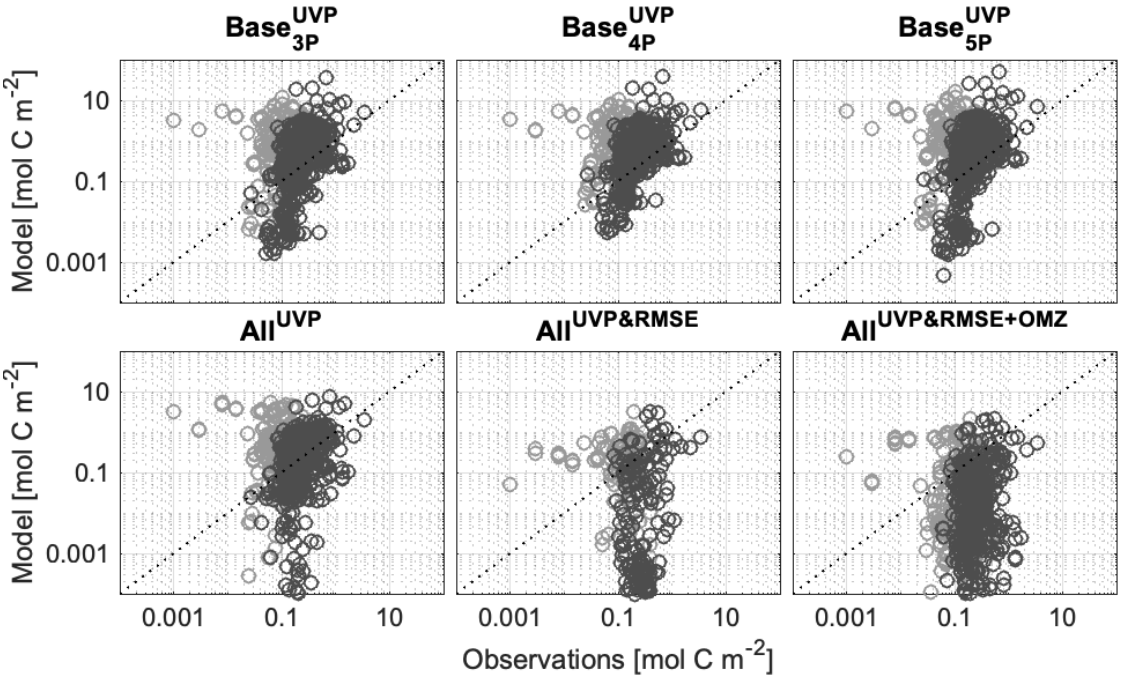

Fig. 4.2: *POC-flux (in mol C m^{-2}) in 2000 m depth model results plotted versus observations from UVP5 dataset (dark grey) and dataset from Honjo et al. [2008] (light grey).*

Base_{5P}^{UVP}, which moreover includes the fraction of migrating zooplankton in the optimisation (formerly set to zero), further improves the model regarding J_{UVP} (1.45). Contrary to the previous simulations, ε_{zoo} has an intermediate value of 0.63 and thus zooplankton contributes to the particle flux by egestion. As the fraction of migrating zooplankton, θ, is very low (0.02), ε_{zoo} has however a very limited impact on particle flux. Moreover, a low η of 0.68, i.e. corresponding to porous particles and a low sinking speed, leads the model towards an underestimation of particles – especially in the deeper ocean interior (see Fig. 4.1) - and of the particle flux in 2000 m depth (see Fig. 4.2). As shown in Fig. 4.3 and 4.4, the model tends to underestimate the number of particles in both size classes and both sections; however, the spatial pattern of deep particles in the Pacific basin is matched quite well by the model.
Including all parameters into the optimisation, i.e. adding the particle breakup into smaller

components further improves the model regarding J_{UVP} (1.29) in simulation All^{UVP}. Although the fraction of migrating zooplankton is much larger (0.38) than in the previous simulations, ε_{zoo} is at the upper boundary (1.0) and zooplankton egestion thus does not feed into the particle pool. The optimal parameters lead the model towards an underestimation of the number of particles in the deep ocean, while particles in the shallow layers globally fit to observations (see Fig. 4.1). Although the model exhibits a pattern of underestimating the POC flux in 2000 m depth for a few grid points, the general pattern fits to observations (see Fig. 4.2). As shown in Fig. 4.3 and 4.4, the model tends to overestimate the number of particles in shallow waters and underestimates particles in the deep ocean for both particle size classes and both considered sections.

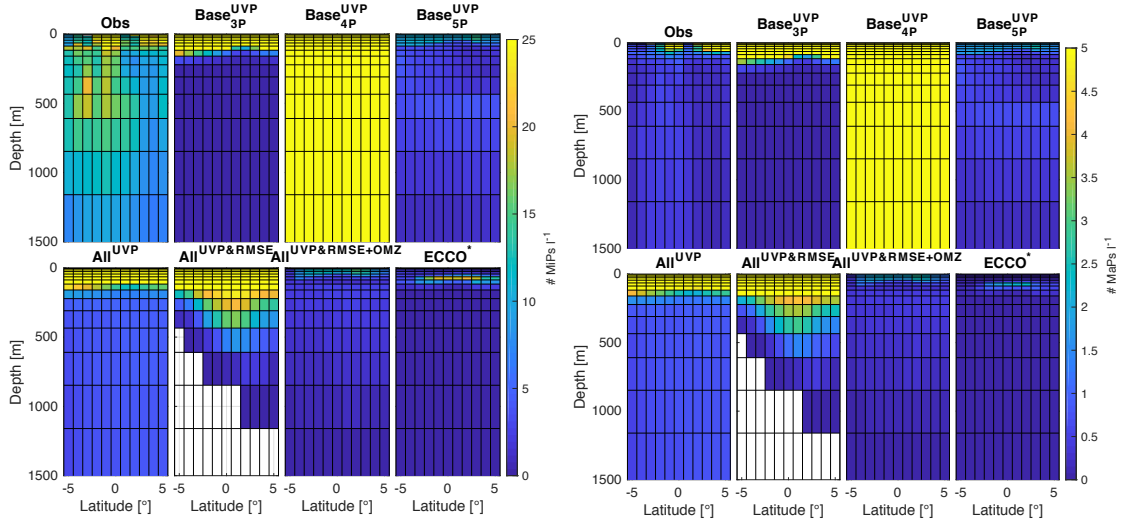

Fig. 4.3: *Mean MiPs (left), the small particle size class, and MaPs (right), the large particle size class, of observations and all model simulations at 23°W. ECCO* is the best simulation of the sensitivity study by Niemeyer et al. [2019]. White boxes depict very low particle concentrations.*

Although the model is not able to find an appropriate parameterisation for particles in shallow waters (best representation in Base$_{5P}^{UVP}$, Fig. 4.1) and in the deep ocean interior (best representation in Base$_{4P}^{UVP}$, Fig. 4.1) at the same time, an increasing number of model processes generally improves the fit to particles, J_{UVP} (see Tab. 4.2, which decreases from 1.67 to 1.29). However, in most cases optimisation causes the ingestion efficiency of zooplankton to approach its upper boundary – therefore, production of detritus happens mostly through zooplankton quadratic mortality (and, to a lesser extent, linear phytoplankton mortality). As a consequence, the parameter for the effect of zooplankton vertical migration appears only weakly constrained, which might explain its large variation between Base$_{5P}^{UVP}$ and All^{UVP}.

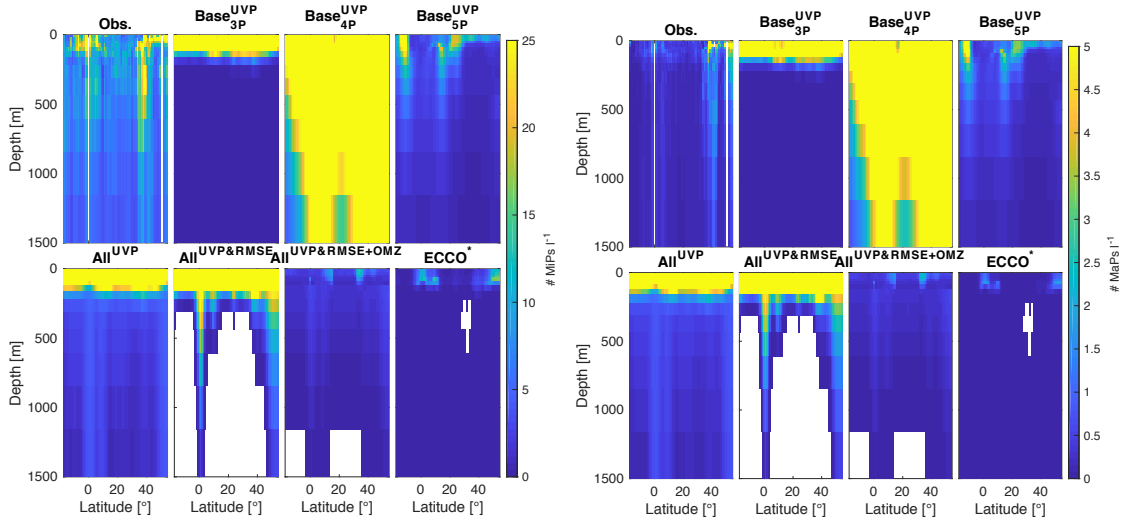

Fig. 4.4: *Mean MiPs (left), the small particle size class, and MaPs (right), the large particle size class, of observations and all model simulations at 151°W. ECCO* is the best simulation of the sensitivity study by Niemeyer et al. [2019]. White boxes depict very low particle concentrations.*

4.3.2 Model fit to dissolved inorganic tracers and OMZs

As not only particles but also dissolved inorganic tracers, i.e. nutrients and oxygen, and also the representation of OMZs, may be important to determine the model fit to observations, this section investigates the fit to observed dissolved inorganic tracers and the overlap between modelled and observed OMZs. Both are not included in the single-objective optimisations and are thus independent from the optimisation.
The parameterisation of Base_{3P}^{UVP} and Base_{4P}^{UVP} neither leads the model towards a good fit to particles nor to dissolved inorganic tracers (J_{RMSE}=1.56 and J_{RMSE}=1.67, respectively) or OMZs (J_{OMZ}=1.0 for both simulations) (see Tab. 4.2) compared to the following simulations. This results in an underestimation of nutrients in epi- and mesopelagic waters and in an overestimation of oxygen concentrations (see Fig. 4.5). Therefore, this parameterisation does not enable the formation of OMZs for a criterion of 50 mmol m^{-3} in both simulations (see Fig. 4.5). As shown in Fig. 4.5 an optimisation against observed particles leads the model towards a considerable decline regarding the fit of dissolved inorganic tracers and OMZs to observations compared to ECCO*, which constitutes the best simulation regarding J_{RMSE} and J_{OMZ} by Niemeyer et al. [2019].
Simulation Base_{5P}^{UVP} moreover exhibit a similar pattern for nutrients (i.e. an underestimation of phosphate and nitrate in epi- and mesopelagic waters; J_{RMSE}=2.1) but shows an even stronger overestimation of oxygen concentrations between 100 m and 1500 m (see Fig. 4.5) compared to Base_{3P}^{UVP} and Base_{4P}^{UVP}. As oxygen concentrations are considerably too high compared to observations, the model is still not able to reproduce the observed OMZs (see Fig. 4.5), which results in a fit to J_{OMZ} of 1.0 (see Tab. 4.2). The final single-objective optimisation, which includes the full number of parameters, All^{UVP}, represents not only the best fit to particles (see previous section), but also to dissolved

inorganic tracers and OMZs (J_{RMSE}=1.29 and J_{OMZ}=0.95, respectively). However, the model still tends to underestimate the phosphate and nitrate concentrations in epi- and mesopelagic waters (see Fig. 4.5). Oxygen concentrations are lower than in the previous simulations, and the model now underestimates the oxygen concentrations >1000 m depth (see Fig. 4.5).

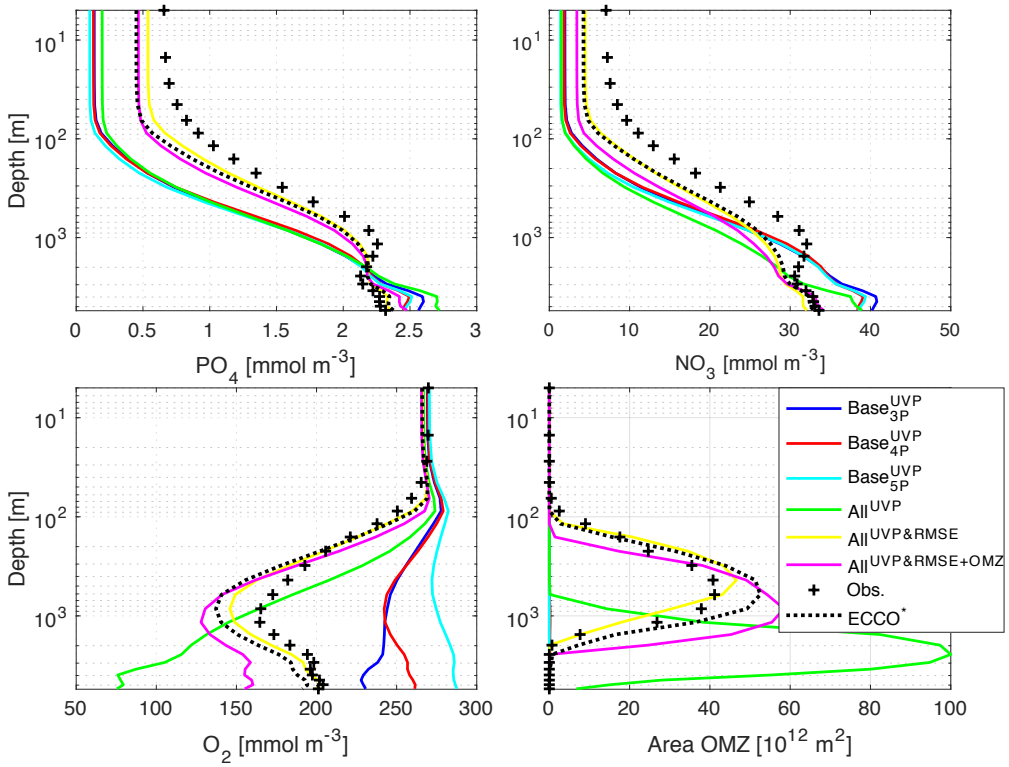

Fig. 4.5: *Global average depth profiles of phosphate, nitrate, oxygen and the area of OMZ (40°N to 40°S) following the approach by Cabré et al. [2015]. OMZs are defined as O_2<50 mmol m^{-3}. ECCO* constitutes the best simulation regarding J_{RMSE} and J_{OMZ} from the sensitivity study by Niemeyer et al. [2019].*

Thus, it can be concluded that the model is not able to fit particulate and dissolved tracers using a single-objective optimisation against observed particles. Based on these findings, we integrated in the following the fit to J_{RMSE} as well as the sum of J_{RMSE} and J_{OMZ} in the optimisation algorithm as a second objective.

4.3.3 Model fit to particulate and dissolved tracers

As described in Sauerland et al. [2019], a multi-objective optimisation gives out a set of (in our case) 10 different parameterisations and model fits, which follows a Pareto Front between both objectives. As those different parameterisations cover a broad range of fits

to both objectives, in this study always the best compromise solution between both objectives has been chosen, i.e. the minimum distance between data points and coordinate origin.
Adding one more objective, the fit to dissolved inorganic tracers, J_{RMSE}, into the optimisation, simulation All$^{UVP\&RMSE}$ describes the best compromise solution between J_{UVP} and J_{RMSE} (see Tab. 4.2), calculated as given in Eq. 11. The parameterisation for the best compromise solution between both objectives reduces the fit to J_{UVP} (1.67) compared to the previous single-objective optimisation, All^{UVP} (see Tab. 4.2). As the parameterisation exhibits beside a high η of 1.3 also a high r (0.08) and θ (0.04) compared to the previous simulations, the model tends to overestimate the number of particles in shallow waters but underestimates the deep ones (see Fig. 4.1) as well as the POC flux (see Fig. 4.2). This results in no particles at all in the deepest ocean layers (see Fig. 4.1). However, the model is now able to improve the representation of particles in both sections, at 23°W and 151°W, and both particle size classes (see Fig. 4.3 and 4.4) and moreover exhibits an improved representation of the IPM compared to the previous simulations (see Fig. 4.3). Contrary to the previous single-objective optimisations, the parameterisation of the best compromise solution is now able to fit dissolved inorganic tracers as well as OMZs (see Fig. 4.5) and constitutes the best representation of dissolved inorganic tracers compared to the previous simulations. Compared to the 'hand-tuned' sensitivity study by Niemeyer et al. [2019], simulation ECCO*, the fit to dissolved inorganic tracers and OMZs is slightly improved (see Fig. 4.5).
In the final optimisation All$^{UVP\&RMSE+OMZ}$, where the sum of the best compromise solution of J_{RMSE} and J_{OMZ} constitutes the second objective, the fit to J_{UVP} (1.76) is reduced compared to the previous multi-objective optimisation excluding the overlap between modelled and observed OMZs. Porous particles and a reduced sinking speed (0.63) in combination with a doubled r (0.13) leads the model towards a good fit of shallow particles compared to All$^{UVP\&RMSE}$. However, the model tends to underestimate deep particles (see Fig. 4.1) and POC flux at 2000 m depth (see Fig. 4.2). Fig. 4.3 and 4.4 show an underestimation of particles in both size classes and considered sections in shallow but also in deep waters. Although the fit to J_{UVP} (1.76) and J_{RMSE} (0.63) is reduced compared to All$^{UVP\&RMSE}$, the fit to J_{OMZ} (0.59) is improved leading, however, to a too large area of modelled OMZs compared to observations (see Fig. 4.5) as the model underestimates the oxygen concentration from a depth of 400 m, which, in turn, leads to an overestimation of the OMZ volume (see Fig. 4.5). It can be concluded that the parameterisation of the best compromise solution between J_{UVP} and J_{RMSE}, All$^{UVP\&RMSE}$, represents dissolved inorganic tracers and OMZs best (see Fig. 4.5). However, the parameterisation is not appropriate for a correct representation of particles in the deep ocean interior.

4.3.4 Model fit to observed zooplankton data and global biogeochemical fluxes

In Base$_3^{UVP}_P$, the model tends to underestimate the primary production (see Fig. 4.6) compared to observations by Lutz et al. [2007] due to low global average phosphate and nitrate concentrations in epi- and mesopelagic waters (see Fig. 4.5). Although zooplank-

ton is overestimated compared to observations by Moriarty et al. [2013], ε_{zoo} is at the upper boundary and thus zooplankton does not contribute to the particle pool via egestion leading to an underestimation of the small particles, MiPs (see Fig. 4.1). However, the large particles, MaPs, are overestimated leading to a slight overestimation of the particle flux in 100 m depth and a strong overestimation in 2000 m depth. As remineralisation is very low, the oxygen concentration over the full water column is very high (see Fig. 4.5). Base_{4P}^{UVP} exhibits a lower primary production (see Fig. 4.6), which is – again – due to low nutrient concentrations over the full water column (see Fig. 4.5), and lower zooplankton grazing compared to the previous simulation (see Fig. 4.6). The remineralisation is strongly increased, which reduces the export in shallow and also in deep waters, i.e. 100 m and 2000 m depth respectively (see Fig. 4.6).
In Base_{5P}^{UVP}, the model underestimates the primary production compared to observations leading to a too low number of particles in both size classes (see Fig. 4.1). Although the zooplankton ingestion efficiency, ε_{zoo}, is lower than in the other simulations, θ is also very low (0.02) and thus only has a limited impact on particle dynamics (see Tab. 4.2). Despite the underestimation of particles in both size classes (see Fig. 4.1), the export in shallow and also in deep waters is overestimated (see Fig. 4.6).

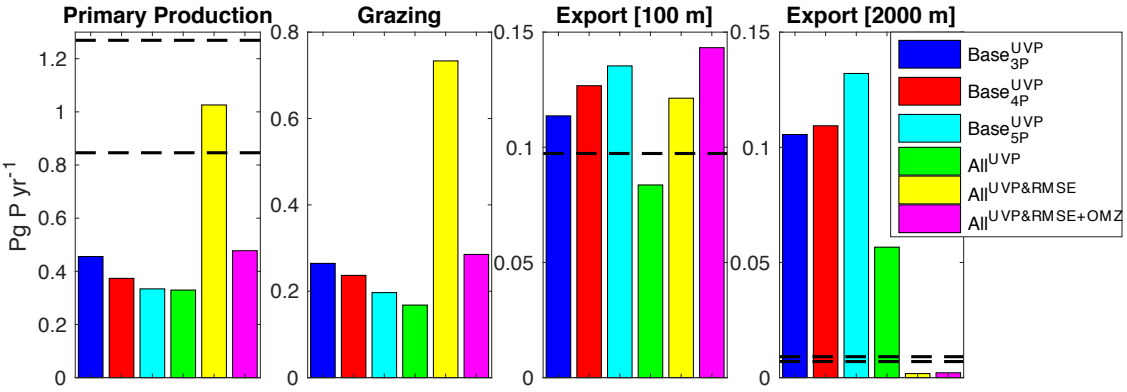

Fig. 4.6: *Global integral of primary production, zooplankton grazing, export at 100 m and 2000 m depth in Pg P yr^{-1} of all simulations. Dashed lines denote observations (primary production from Carr et al. [2006]; export 100 m from Lutz et al. [2007]; export 2000 m from Honjo et al. [2008] and Guidi et al. [2015].*

Adding the fit to dissolved inorganic tracers in the optimisation, namely $\text{All}^{UVP\&RMSE}$, r is tripled compared to All^{UVP}, which leads to an increased availability of nutrients (see Fig. 4.5) and thus strongly enhances the primary production and zooplankton grazing (see Fig. 4.6). The high biological activity, in turn, increases the number of particles in both size classes (see Fig. 4.1), which is strongly overestimated, leading to a slight overestimation of the export flux in shallow waters (see Fig. 4.6). However, the deep export flux in 2000 m depth moves towards zero (see Fig. 4.6).
As in $\text{All}^{UVP\&RMSE+OMZ}$ also J_{OMZ} is included in the optimisation, the model now exhibits the highest r (0.13) compared to the previous simulations (see Tab. 4.2). However,

the number of particles of the large particle size class targets the observations quite well (see Fig. 4.1). The export in shallow waters is slightly overestimated by the model compared to observations, the deep flux is underestimated (see Fig. 4.6).

4.4 Discussion

In this study, in five out of six optimisations, the zooplankton ingestion efficiency, ε_{zoo}, in our model is at the upper boundary of its parameter space and might be overestimated compared to observations (61-77% zooplankton ingestion efficiency off South Georgia; Atkinson et al. [1996]). Because the particle size distribution is tightly linked to zooplankton mortality and egestion to the particle pool, optimisation might thus neglect the contribution of zooplankton migration (θ) and egestion. One approach to circumvent this effect could consist in reducing the upper limit of ε_{zoo}, which could lead to an enhanced particle egestion in the deeper ocean by migrating zooplankton.
Although the fraction of migrating zooplankton is in three out of four cases at the lower boundary of the parameter space (except for simulation All^{UVP}), it should be noted that the fraction of vertical migrating zooplankton is strongly dependent on the region [Décima et al., 2011; Steinberg et al., 2008] and that the model parameterises a globally constant fraction. Moreover, in the observations very small zooplankton is not represented – contrary to our model. As zooplankton migration (θ) is in most cases very low, it could potentially be assumed that the model implicitly considers non-migrating microzooplankton. Furthermore, Bianchi et al. [2013] and Aumont et al. [2018] indicate that oxygen-dependency plays an important role regarding zooplankton migration. Bianchi et al. [2013] shows that especially the subtropics and Southern Ocean exhibit deep migration to 600 m depth, which could potentially contribute to the deep particle flux. Thus, implementing oxygen-dependent zooplankton migration could potentially further improve the representation especially of deep particles. Kiko et al. [2020] contradict the hypothesis of oxygen-dependent migration and show that the depth of several migrating zooplankton species coincide with the depth of OMZs. However, the behaviour of zooplankton in low oxygen waters, i.e. feeding and egestion, remain unclear. Another approach could thus consist in the implementation of oxygen-dependent egestion. In conclusion, due to the coarse depicted equatorial current system, the seasonality especially in the higher latitudes, the tight link to the considered region (which also impacts the particle flux [Romero et al., 2020]) and the limited number of observations, the comparison between modelled and observed zooplankton, and its impact on particle production and transformation are highly uncertain and need to be further investigated.
This study indicates that the model is not able to represent the equatorial intermediate particle maximum, IPM, at 23°W, as shown from observations [Kiko et al., 2017]. As this is a small-scale feature and limited on a few grid points mainly in the equatorial region, this effect may have been neglected in the cost function of the optimisation in our global model. Moreover, as shown in Cabré et al. [2015] and Duteil et al. [2014], a high model resolution improves the representation of the equatorial currents, which are not

sufficiently represented in our global 1° resolution model. Both aspects thus could impact the representation of marine particles.
It has shown that integrating a high particle breakup rate ρ as in simulation All$^{UVP\&RMSE}$, improves the representation of the oxygen distribution (see Tab. 4.2 and Fig. 4.5). It seems that different objectives favour different model parameterisations: An optimisation against the global marine particle dataset targets on high export rates (single-objective simulations; see Fig. 4.6) to prevent particles from remineralisation in shallow waters, while a model, which is additionally optimised against dissolved inorganic tracers, All$^{UVP\&RMSE}$, shows higher remineralisation at shallower depths. One possible explanation could consist in the consideration of different depths dependent on the considered objective: As the model is able to find a good parameterisation for shallow particles (see Fig. 4.1), the parameterisation seems not appropriate for the deep particles as well. However, as OMZs are located in the mesopelagic, the optimisation also including e.g. J_{OMZ} potentially concentrates on shallower waters, which possibly leads to neglecting the deep particles (see Fig. 4.1).
Guidi et al. [2015], Marsay et al. [2015] and Henson et al. [2015] found b values ranging between 0.4 and 1.75, indicating that processes associated with particle flux and remineralisation are highly variable and strongly dependent on the considered region, depth and season. The model presented here is capable of simulating temporal and spatial variability of particle flux through aggregation, but it does not represent a simultaneous fit to large and small particles at the surface and in the deep ocean. One possible explanation could be a missing representation of particle lability or age. Aumont et al. [2017] showed in their model study that integrating a variable reactivity of particles increases the particle concentration in the deep ocean interior. Moreover, Stemmann et al. [2004] suggested that the impact of microbial degradation on particles is increasing with depth, which is expected to be anti-correlated to zooplankton concentrations as zooplankton gets rare with increasing depth.
Besides the age, or lability, of particles, other important processes that determine particle dynamics might be missing in our global biogeochemical model: For example, by applying a constant exponent for the size dependency of particle sinking speed in this study, we assume that the particle characteristics (such as porosity or density) are equal over the full water column from the sea surface down to the sediment, which is likely incorrect. It remains unclear if the assumption of size-dependent sinking used in this study is sufficient and applies for the full water column or depth-dependent processes need to be integrated in future studies.

4.5 Conclusion and Outlook

In this study, we present an objective model optimisation and conduct a comparison with global observed datasets of marine particles, dissolved inorganic tracers and the vertical and horizontal extent of OMZs. Comparison of four optimisations with different numbers of free parameters suggest that including more processes that impact particle dynamics

improve their representation. However, enhancing the fit to observed marine particles decreases the fit to dissolved inorganic tracers in the ocean. Thus, in a second step, we optimised the global biogeochemical model against both objectives and found a compromise solution improving the representation of surface marine particles as well as nutrients, oxygen concentration and OMZ extent. The best compromise solution however represents an underestimation of deep particles. Moreover, all considered objectives target on different depths as e.g. OMZs are located in shallower waters but particles are considered from the surface down to the sea floor. As multi-objective optimisations constitute a compromise solution between the considered objectives, we can conclude that the model accuracy is not only dependent on the considered objective, depth and location but also on the question to be answered.
Finally, we showed in our study that an increasing number of processes that determine particle dynamics improve the representation of marine particles. However, the model still has problems to represent shallow and deep particles at the same time using the same parametrisation. One step to overcome this gap could consist in including changing particle characteristics, e.g. variable particle reactivity, or zooplankton migration characteristics, e.g. oxygen-dependent migration, over the water column.

Acknowledgements

This work has been supported and financed by the Collaborative Research Center 754 “Climate-Biogeochemistry Interactions in the Tropical Ocean”; (www.sfb754.de; grant no. 27542298 of the German Science Foundation DFG). RK acknowledges support via a “Make Our Planet Great Again” grant of the French National Research Agency within the “Programme d’Investissements d’Avenir”; reference ANR-19-MPGA-0012. Parallel supercomputing resources have been provided by the North-German Supercomputing Alliance (HLRN).

5 Conclusion and Outlook

5.1 Summary and Conclusion

This thesis investigates processes of the biological pump that determine the global marine oxygen distribution. The findings provide the basis to advance our knowledge of potential driving factors of future ocean deoxygenation. In chapter 2 possible feedback loops between projected future global change conditions and benthic processes, were investigated. In chapter 3 and chapter 4 the impact of particle dynamics on oxygen distribution under preindustrial steady state conditions has been explored.

As outlined in section 1.6, this thesis focusses on the following three questions:

1. Under a business as usual global change scenario, which is the dominant feedback determining the expansion of OMZs - the positive feedback between benthic release of phosphorus and marine biological production or the negative one between marine uptake of CO_2 and air temperature?

To answer this question, the potential feedback between low-oxygen water and responding benthic fluxes under a business-as-usual global change scenario enhancing the phosphorus weathering is investigated in chapter 2. This study finds that the negative feedback due to increased phosphorus weathering on land increases the marine productivity, thereby facilitating the marine uptake of atmospheric CO_2, reducing the air temperature and thus potentially limiting the expansion of OMZs. This phosphorus-weathering feedback dominates over the assumed feedback between increased export and remineralisation, expanding OMZs and thereby promoting the release of benthic phosphorus. It can therefore be concluded that enhanced weathering input of phosphorus seems not to trigger a self-reinforcing runaway process regarding marine deoxygenation on millennial timescales in the UVic Earth System Climate Model of intermediate complexity.

2. Does a global biogeochemical model that includes particle dynamics improve the representation of OMZs under steady state conditions?

As shown by Duteil et al. [2014], the representation of OMZs depends on circulation and model resolution. Marsay et al. [2015] and Guidi et al. [2015] moreover show in their studies conflicting patterns of global particle flux profiles and Kriest and Oschlies [2015] find a strong dependence between the OMZ volume and the particle flux profile. Thus, in

chapter 3 two different model resolutions as well as a broad range of model parameterisations regarding the particle export have been tested.
The simulations show that adding an aggregation module into a global marine biogeochemical model enhance the overlap between observed and modelled OMZs compared to a model without particle aggregation. The representation of OMZs moreover strongly depends on the given threshold for OMZs. In addition to a fine spatial resolution of the model physics, a suitable biogeochemical parameterisation of the particle aggregation module is required for an improved model fit, namely an intermediate-to-high sinking speed, porous particles and a moderate-to-high particle stickiness. Finally, this study also find that model calibration against a global observed dataset of marine organic particles is needed.

3. Does calibration against observed particle abundance and size help to improve simulated oxygen distribution, and are additional model processes besides aggregation necessary to improve the model fit?

To answer this question, a systematic calibration against an observed particle dataset was performed in chapter 4. In addition, the model is optimised against dissolved inorganic tracers and OMZ distribution patterns and moreover includes two new processes, namely zooplankton migration and particle breakup. This study demonstrates that an increasing number of processes regarding particle dynamics is able to improve the representation of OMZs. Although a model optimisation against the overlap between modelled and observed OMZs improves the fit with increasing model complexity, the particle dynamics are not correctly represented over the full water column, i.e. the model is not able to find a good parameterisation for shallow and deep particles at the same time. This indicates that some processes on the way of organic matter from the surface to the deep ocean is not well parameterised in the model and could potentially lead to a more realistic representation of the OMZs.

In conclusion, this thesis investigates different processes regarding the biological pump that can impact the representation of OMZs. It is shown that the representation of OMZs is improved by integrating particle dynamics. However, this improvement is based on a mismatch between modelled and observed particles. As an improved representation of particles in the water column can potentially induce a shift in the strength of the feedbacks investigated in chapter 2, improved particle dynamics can lead to a further understanding of processes that determine the representation of OMZs.

5.2 Outlook

The biological pump is highly variable due to complex physical, chemical and biological interactions and depends on several factors that may alter under global change conditions, which, in turn, potentially also determines the vertical and lateral extent of OMZs. Even under current conditions, processes of the biological pump that determine the oxygen distribution are not well quantified.
Chapter 4 shows that the model especially tends to underestimate the number of particles of both size classes in the deep ocean leading to the assumption that other processes that lead to efficient export of both particle size classes to the deep ocean are still missing. Following this assumption, two aspects that increase the number of particles in the ocean interior could be implemented in future studies, which are discussed below: implementing additional processes that determine particle characteristics and thus the overall vertical particle flux, or increasing the complexity of zooplankton dynamics.
Previous studies show a wide range of particle flux profiles indicating high uncertainties in the associated particle flux profile [Guidi et al., 2015; Marsay et al., 2015; Henson et al., 2015]. It is assumed that the particle flux depends on the considered region, the associated seasonality as well as depth. As the model is able to simulate regionally variable particle dynamics, one step towards an improved representation of particles would be to include depth-dependent particle characteristics over the water column. For example, Aumont et al. [2017] show in their study that including a variable particle reactivity enhances the particle concentration in the ocean interior. Moreover, the particle density is constant over the full water column in our modelling study, which might not be the case in observations [Berelson, 2002]. Thus, including changes in the particle density and reactivity across the water column could potentially lead to a more realistic representation of OMZs under steady state conditions.
Observations of migrating zooplankton and zooplankton-related fluxes are sparse and the contribution of the active flux by migrating zooplankton to total particulate flux is still highly uncertain (18% - 84%; [Kiko et al., 2020; Kelly et al., 2019; Hernández-León et al., 2019]). However, zooplankton dynamics could potentially constitute a driving factor for a more realistic representation of particles and thus oxygen. Existing studies assume that zooplankton migration depends - possibly among others - on the considered region [Décima et al., 2011; Steinberg et al., 2008], the zooplankton composition including their specific migration and egestion characteristics [Passow and Carlson, 2012] as well as mesopelagic oxygen concentrations [Seibel, 2011; Wishner et al., 2018; Kiko and Hauss, 2019]. Although the fraction of migrating zooplankton is calibrated and enabled to range between 0.01 and 0.9 in our study, the migration depth is fixed to 400 m and thus the overall process of zooplankton migration is highly simplified compared to observational findings.
Moreover, diurnal vertical migration of makrozooplankton and nekton are not considered in this model. As their implementation could increase the active particle transport into the ocean interior, this could consist an objective of a future study.
Changes in the oxygen concentrations - as suggested under global change conditions - can moreover induce shifts in the biomass [Wishner et al., 2018] and the regional zoo-

plankton composition [Passow and Carlson, 2012]. As different species influence particle dynamics by fragmentation or egestion in very different ways [Turner, 2015], changing oxygen conditions can directly impact the zooplankton composition and thus the future particle flux profile [Passow and Carlson, 2012], which is, however, beyond the scope of this thesis.

Oxygen is also suggested to be a primary driver for zooplankton migration [Bianchi et al., 2013; Aumont et al., 2018], although the approach of oxygen-dependent zooplankton migration is controversially discussed in literature. Thus, another step forward could consist in the additional implementation of oxygen-dependent zooplankton migration. Although an oxygen-dependency could lead to shallower zooplankton migration above OMZs, especially in the subtropical gyres and Southern Ocean deep vertical migration down to 600 m depth as observed by Bianchi et al. [2013] could be considered by the model. Although Aumont et al. [2018] investigate in their modelling study relatively low active transport of carbon by migrating zooplankton in the subtropics, the scarce number of observations in this region contradict those findings and exhibit an intermediate active transport by migrating zooplankton [Buitenhuis et al., 2013].

Moreover, as the zooplankton migration depth is assumed to be shallower in expanding OMZs, this could also result in shallower respiration, which potentially constitutes a positive feedback loop and thus increases the oxygen depletion in those regions [Bianchi et al., 2013] under global change conditions. Thus, beside the influence of zooplankton migration on particle dynamics, the altered zooplankton respiration could also play an important role in the representation of OMZs in biogeochemical models, which is still highly uncertain [Cabré et al., 2015].

Controversial to the hypothesis above, Kiko et al. [2020] show that the daytime depth of several migrating zooplankton species coincides with the core of the OMZ suggesting that zooplankton migrates into the OMZ. This indicates that metabolic rates are potentially reduced under low oxygen conditions. It remains uncertain if zooplankton feeds and egests inside the OMZ during daytime, which could directly influence the particle flux into the deeper ocean [Kiko et al., 2020]. Thus, implementing e.g. oxygen-dependent feeding and egestion could potentially contribute to an improved representation of deep particles.

In conclusion, it seems that more detailed global observations regarding the transport by zooplankton and nekton and passive particle dynamics and their sinking on total particle flux are necessary for future studies. Moreover, integrating even more depth-dependent particle characteristics and more complex zooplankton dynamics as oxygen-dependent migration, feeding or gutflux, could potentially further improve the representation of the marine particle flux profile. As this increases the model complexity and the number of estimated parameters, a systematic model optimisation is a useful tool for a detailed investigation of the full parameter space. An improved representation of marine particles, in turn, could lead to an extended understanding of the oxygen distribution - under steady state and global change conditions. A recent study by Bisson et al. [2020] aims to get a deeper insight into different export processes via a satellite-based food-web model and will be published soon.

Finally, this thesis shows that the impact of single processes or a combination of possible feedbacks regarding the biological pump and its effect on OMZs can to some extent be

predicted. Nevertheless, it is still unclear if the biological pump will strengthen or weaken under global change conditions [Passow and Carlson, 2012] due to the high number of uncertain processes and feedbacks. An adequate representation of the particle flux from the euphotic zone into the aphotic is a necessary prerequisite for the representation of the benthic fluxes at the seafloor. It seems that in particular the transport from the euphotic to the aphotic zone can be further improved. Thus, the ability to resolve driving factors of the biological pump that determine the representation of OMZs in global models still remain limited.

Bibliography

Alldredge, A. (1998). The carbon, nitrogen and mass content of marine snow as a function of aggregate size. *Deep. Res. Part I Oceanogr. Res. Pap.*, 45:529–541.

Alldredge, A. L. and Gotschalk, C. (1988). In situ settling behavior of marine snow. *Limnol. Ocean.*, 33(3):339–35.

Alldredge, A. L., Granata, T. C., Gotschalk, C. C., and Dickey, T. D. (1990). The physical strength of marine snow and its implications for particle disaggregation in the ocean. *Limnol. Ocean.*, 35(7):1415–1428.

Alldredge, A. L. and McGillivary, P. (1991). The attachment probabilities of marine snow and their implications for particle coagulation in the ocean. *Deep Sea Res. Part A, Oceanogr. Res. Pap.*, 38(4):431–443.

Archibald, K. M., Siegel, D. A., and Doney, S. C. (2019). Modeling the Impact of Zooplankton Diel Vertical Migration on the Carbon Export Flux of the Biological Pump. *Global Biogeochem. Cycles*, 33(2):181–199.

Arhonditsis, G. B., Adams-Vanharn, B. A., Nielsen, L., Stow, C. A., and Reckhow, K. H. (2004). Evaluation of the current state of mechanistic aquatic biogeochemical modeling. *Environ. Sci. Technol.*, 271:13–26.

Armstrong, R. A., Peterson, M. L., Lee, C., and Wakeham, S. G. (2009). Settling velocity spectra and the ballast ratio hypothesis. *Deep. Res. Part II Top. Stud. Oceanogr.*, 56:1470–1478.

Atkinson, A., Ward, P., and Murphy, E. J. (1996). Diel periodicity of subantarctic copepods: Relationships between vertical migration, gut fullness and gut evacuation rate. *J. Plankton Res.*, 18(8):1387–1405.

Aumont, O. and Bopp, L. (2006). Globalizing results from ocean in situ iron fertilization studies. *Global Biogeochem. Cycles*, 20:1–15.

Aumont, O., Ethé, C., Tagliabue, A., Bopp, L., and Gehlen, M. (2015). PISCES-v2: An ocean biogeochemical model for carbon and ecosystem studies. *Geosci. Model Dev.*, 8(8):2465–2513.

Aumont, O., Maury, O., Lefort, S., Bopp, L., and Aumont, O. (2018). Evaluating the potential impacts of the diurnal vertical migration by marine organisms on marine biogeochemistry. *Global Biogeochem. Cycles*, 32:1622–1643.

Aumont, O., Van Hulten, M., Roy-Barman, M., Dutay, J. C., Éthé, C., and Gehlen, M. (2017). Variable reactivity of particulate organic matter in a global ocean biogeochemical model. *Biogeosciences*, 14:2321–2341.

Bacastow, R., Jolla, L., and Maier-Reimer, C. E. (1991). Dissolved organic carbon in modeling oceanic new production. *Global Biogeochem. Cycles*, 5(1):71–85.

Bach, L. T., Boxhammer, T., Larsen, A., Hildebrandt, N., Schulz, K. G., and Riebesell, U. (2016). Influence of plankton community structure on the sinking velocity of marine aggregates. *Global Biogeochem. Cycles*, 30:1145–1165.

Bach, L. T., Riebesell, U., Sett, S., Febiri, S., Rzepka, P., and Schulz, K. G. (2012). An approach for particle sinking velocity measurements in the 3-400 um size range and considerations on the effect of temperature on sinking rates. *Mar. Biol.*, 159:1853–1864.

Béné, C., Barange, M., Subasinghe, R., Pinstrup-Andersen, P., Merino, G., Hemre, G.-H., and Williams, M. (2015). Feeding 9 billion by 2050 – Putting fish back on the menu. *Food Secuirty*, 7:261–274.

Berelson, W. M. (2002). Particle settling rates increase with depth in the ocean. *Deep. Res. Part II Top. Stud. Oceanogr.*, 49:237–251.

Berner, R. A. (1992). Weathering, plants, and the long-term carbon cycle. *Geochim. Cosmochim. Acta*, 56(8):3225–3231.

Bianchi, D., Dunne, J. P., Sarmiento, J. L., and Galbraith, E. D. (2012). Data-based estimates of suboxia, denitrification, and N2O production in the ocean and their sensitivities to dissolved O2. *Global Biogeochem. Cycles*, 26:1–13.

Bianchi, D., Galbraith, E. D., Carozza, D. A., Mislan, K. A., and Stock, C. A. (2013). Intensification of open-ocean oxygen depletion by vertically migrating animals. *Nat. Geosci.*, 6(7):545–548.

Bianchi, D., Weber, T. S., Kiko, R., and Deutsch, C. (2018). Global niche of marine anaerobic metabolisms expanded by particle microenvironments. *Nat. Geosci.*, 11(4):263–268.

Biddanda, B. A. and Pomeroy, L. R. (1988). Microbial aggregation and degradation of phytoplankton-derived detritus in seawater. I. Microbial succession. *Mar. Ecol. Prog. Ser.*, 42:79–88.

Bisson, K., Siegel, D., and Devries, T. (2020). Diagnosing mechanisms of ocean carbon export in a satellite-based food web model. *Front. Mar. Sci.*, accepted.

Bopp, L., Le Quere, C., Heimann, M., Manning, A. C., and Monfray, P. (2002). Climate-induced oceanic oxygen fluxes: Implications for the contemporary carbon budget. *Global Biogeochem. Cycles*, 16(2):1022–1035.

Bopp, L., Resplandy, L., Orr, J. C., Doney, S. C., Dunne, J. P., Gehlen, M., Halloran, P., Heinze, C., Ilyina, T., Séférian, R., Tjiputra, J., and Vichi, M. (2013). Multiple stressors of ocean ecosystems in the 21st century: Projections with CMIP5 models. *Biogeosciences*, 10:6225–6245.

Boyd, P. W., Sherry, N. D., Berges, J. A., Bishop, J. K., Calvert, S. E., Charette, M. A., Giovannoni, S. J., Goldblatt, R., Harrison, P. J., Moran, S. B., Roy, S., Soon, M., Strom, S., Thibault, D., Vergin, K. L., Whitney, F. A., and Wong, C. S. (1999). Transformations of biogenic particulates from the pelagic to the deep ocean realm. *Deep. Res. Part II Top. Stud. Oceanogr.*, 46:2761–2792.

Breitburg, D. (2002). Effects of hypoxia, and the balance between hypoxia and enrichment, on coastal fishes and fisheries. *Estuaries*, 25(4b):767–781.

Buesseler, K. O., Lamborg, C. H., Boyd, P. W., Lam, P. J., Trull, T. W., Bidigare, R. R., Bishop, J. K. B., Casciotti, K. L., Dehairs, F., Elskens, M., Honda, M., Karl, D. M., Siegel, D. a., Silver, M. W., Steinberg, D. K., Valdes, J., Mooy, B. V., and Wilson, S. (2007). Revisiting Carbon Flux Through the Ocean 's Twilight Zone. *Science (80)*, 316:567–570.

Buitenhuis, E. T., Vogt, M., Moriarty, R., Bednarsek, N., Doney, S. C., Leblanc, K., and Al., E. (2013). MAREDAT: Towards a world atlas of MARine Ecosystem DATa. *Earth Syst. Sci. Data*, 5(2):227–239.

Burd, A. B. and Jackson, G. A. (2009). Particle Aggregation. *Ann. Rev. Mar. Sci.*, 1:65–90.

Cabré, A., Marinov, I., Bernardello, R., and Bianchi, D. (2015). Oxygen minimum zones in the tropical Pacific across CMIP5 models: Mean state differences and climate change trends. *Biogeosciences*, 12:5429–5454.

Carr, M. E., Friedrichs, M. A., Schmeltz, M., Noguchi Aita, M., Antoine, D., Arrigo, K. R., Asanuma, I., Aumont, O., Barber, R., Behrenfeld, M., Bidigare, R., Buitenhuis, E. T., Campbell, J., Ciotti, A., Dierssen, H., Dowell, M., Dunne, J., Esaias, W., Gentili, B., Gregg, W., Groom, S., Hoepffner, N., Ishizaka, J., Kameda, T., Le Quéré, C., Lohrenz, S., Marra, J., Mélin, F., Moore, K., Morel, A., Reddy, T. E., Ryan, J., Scardi, M., Smyth, T., Turpie, K., Tilstone, G., Waters, K., and Yamanaka, Y. (2006). A comparison of global estimates of marine primary production from ocean color. *Deep. Res. Part II Top. Stud. Oceanogr.*, 53(5-7):741–770.

Cavan, E. L., Henson, S. A., Belcher, A., and Sanders, R. (2017). Role of zooplankton in determining the efficiency of the biological carbon pump. *Biogeosciences*, 14(1):177–186.

Chavez, F. P. and Messié, M. (2009). A comparison of Eastern Boundary Upwelling Ecosystems. *Prog. Oceanogr.*, 83(1-4):80–96.

Cocco, V., Joos, F., Steinacher, M., Frölicher, T. L., Bopp, L., Dunne, J., Gehlen, M., Heinze, C., Orr, J., Oschlies, A., Schneider, B., Segschneider, J., and Tjiputra, J. (2013). Oxygen and indicators of stress for marine life in multi-model global warming projections. *Biogeosciences*, 10(3):1849–1868.

Cooley, S. R. (2012). How human communities could 'feel' changing ocean biogeochemistry. *Curr. Opin. Environ. Sustain.*, 4(3):258–263.

Décima, M., Landry, M. R., and Rykaczewski, R. R. (2011). Broad scale patterns in mesozooplankton biomass and grazing in the eastern equatorial Pacific. *Deep. Res. Part II Top. Stud. Oceanogr.*, 58(3-4):387–399.

Devol, A. H. and Hartnett, H. E. (2001). Role of the oxygen-deficient zone in transfer of organic carbon to the deep ocean. *Limnol. Ocean.*, 46(7):1684–1690.

DeVries, T., Liang, J. H., and Deutsch, C. (2014). A mechanistic particle flux model applied to the oceanic phosphorus cycle. *Biogeosciences*, 11:5381–5398.

Dilling, L. and Alldredge, A. L. (2000). Fragmentation of marine snow by swimming macrozooplankton: A new process impacting carbon cycling in the sea. *Deep. Res. Part I*, 47:1227–1245.

Duteil, O., Böning, C. W., and Oschlies, A. (2014). Variability in subtropical-tropical cells drives oxygen levels in the tropical Pacific Ocean. *Geophys. Res. Lett.*, 41(24):8926–8934.

Engel, A. and Schartau, M. (1999). Influence of transparent exopolymer particles (TEP) on sinking velocity of Nitzschia closterium aggregates. *Mar. Ecol. Prog. Ser.*, 182:69–76.

Fowler, S. W. and Knauer, G. A. (1986). Role of Large Particles in the Transport of Elements and Organic Compounds Through the Oceanic Water Column. *Prog. Oceanogr.*, 16:147–194.

Garcia, H. E., Locarnini, R. a., Boyer, T. P., and Antonov, J. I. (2006). World Ocean Atlas 2005, Volume 3: Dissolved Oxygen, Apparent Oxygen Utilization, and Oxygen Saturation. *S. Levitus, Ed. NOAA Atlas NESDIS 63, U.S. Gov. Print. Off. Washington, D.C.*, 3:342.

Gehlen, M., Bopp, L., Emprin, N., Aumont, O., Heinze, C., and Ragueneau, O. (2006). Reconciling surface ocean productivity, export fluxes and sediment composition in a global biogeochemical ocean model. *Biogeosciences*, 3:521–537.

Gorsky, G., Ohman, M. D., Picheral, M., Gasparini, S., Stemmann, L., Romagnan, J. B., Cawood, A., Pesant, S., García-Comas, C., and Prejger, F. (2010). Digital zooplankton image analysis using the ZooScan integrated system. *J. Plankton Res.*, 32(3):285–303.

Guidi, L., Gorsky, G., Claustre, H., Miquel, J. C., Picheral, M., and Stemmann, L. (2008). Distribution and fluxes of aggregates >100 μm in the upper kilometer of the South-Eastern Pacific. *Biogeosciences*, 5:1361–1372.

Guidi, L., Legendre, L., Reygondeau, G., Uitz, J., Stemmann, L., and Henson, S. A. (2015). A new look at ocean carbon remineralization for estimating deepwater sequestration. *Global Biogeochem. Cycles*, 29:1044–1059.

Henson, S. A., Yool, A., and Sanders, R. (2015). Variability in efficiency of particulate organic carbon export: A model study. *Global Biogeochem. Cycles*, 29:33–45.

Hernández-León, S., Olivar, M. P., Fernández de Puelles, M. L., Bode, A., Castellón, A., López-Pérez, C., Tuset, V. M., and González-Gordillo, J. I. (2019). Zooplankton and Micronekton Active Flux Across the Tropical and Subtropical Atlantic Ocean. *Front. Mar. Sci.*, 6(535):1–20.

Hofmann, M. and Schellnhuber, H. J. (2010). Ocean acidification: a millennial challenge. *Energy Environ. Sci.*, 3:1883–1896.

Holland, H. D. (2006). The oxygenation of the atmosphere and oceans. *Philos. Trans. R. Soc. B Biol. Sci.*, 361:903–915.

Honjo, S., Manganini, S. J., Krishfield, R. A., and Francois, R. (2008). Particulate organic carbon fluxes to the ocean interior and factors controlling the biological pump: A synthesis of global sediment trap programs since 1983. *Prog. Oceanogr.*, 76:217–285.

Hughes, B. B., Levey, M. D., Fountain, M. C., Carlisle, A. B., Chavez, F. P., and Gleason, M. G. (2015). Climate mediates hypoxic stress on fish diversity and nursery function at the land-sea interface. *PNAS*, 112(26):8025–8030.

Ingall, E. and Jahnke, R. (1994). Evidence for enhanced phosphorus regeneration from marine sediments overlain by oxygen depleted waters. *Geochim. Cosmochim. Acta*, 58(11):2571–2575.

Iversen, M. H. and Ploug, H. (2013). Temperature effects on carbon-specific respiration rate and sinking velocity of diatom aggregates - potential implications for deep ocean export processes. *Biogeosciences*, 10(6):4073–4085.

Jackson, G. A. and Burd, A. B. (2015). Simulating aggregate dynamics in ocean biogeochemical models. *Prog. Oceanogr.*, 133:55–65.

Jackson, G. A. and Lochmann, S. E. (1992). Effect of coagulation on nutrient and light limitation of an algal bloom. *Limnol. Ocean.*, 37(1):77–89.

Jokulsdottir, T. (2011). *Sinking biological aggregates - a model study*. PhD thesis.

Karstensen, J., Stramma, L., and Visbeck, M. (2008). Oxygen minimum zones in the eastern tropical Atlantic and Pacific oceans. *Prog. Oceanogr.*, 77:331–350.

Keller, D. P., Oschlies, A., and Eby, M. (2012). A new marine ecosystem model for the University of Victoria earth system climate model. *Geosci. Model Dev.*, 5(5):1195–1220.

Kelly, T. B., Davison, P. C., Goericke, R., Landry, M. R., Ohman, M. D., and Stukel, M. R. (2019). The Importance of Mesozooplankton Diel Vertical Migration for Sustaining a Mesopelagic Food Web. *Front. Mar. Sci.*, 6(508):1–18.

Khatiwala, S. (2007). A computational framework for simulation of biogeochemical tracers in the ocean. *Global Biogeochem. Cycles*, 21.

Khatiwala, S. (2018). Transport Matrix Method software for ocean biogeochemical simulations. Technical report.

Khatiwala, S., Visbeck, M., and Cane, M. A. (2005). Accelerated simulation of passive tracers in ocean circulation models. *Ocean Model.*, 9:51–69.

Kiko, R., Biastoch, A., Brandt, P., Cravatte, S., Hauss, H., Hummels, R., Kriest, I., Marin, F., McDonnell, A. M. P., Oschlies, A., Picheral, M., Schwarzkopf, F. U., Thurnherr, A. M., and Stemmann, L. (2017). Biological and physical influences on marine snowfall at the equator. *Nat. Geosci.*, 10:852–858.

Kiko, R., Brandt, P., Christiansen, S., Faustmann, J., Kriest, I., and Robinson, C. (2020). Zooplankton-Mediated Fluxes in the Eastern Tropical North Atlantic. *Front. Mar. Sci.*, 7:1–21.

Kiko, R. and Hauss, H. (2019). On the Estimation of Zooplankton-Mediated Active Fluxes in Oxygen Minimum Zone Regions. *Front. Mar. Sci.*, 6(741):1–16.

Kiørboe, T. (2003). Marine snow microbial communities: scaling of abundances with aggregate size. *Aquat. Microb. Ecol.*, 33:67–75.

Kriest, I. (2002). Different parameterizations of marine snow in a 1D-model and their influence on representation of marine snow, nitrogen budget and sedimentation. *Deep. Res. Part I*, 49:2133–2162.

Kriest, I. and Evans, G. T. (1999). Representing phytoplankton aggregates in biogeochemical models. *Deep. Res. Part I*, 46:1841–1859.

Kriest, I. and Evans, G. T. (2000). A vertically resolved model for phytoplankton aggregation. *Proc. Indian Acad. Sci. Earth Planet. Sci.*, 109:453–469.

Kriest, I., Khatiwala, S., and Oschlies, A. (2010). Towards an assessment of simple global marine biogeochemical models of different complexity. *Prog. Oceanogr.*, 86:337–360.

Kriest, I. and Oschlies, A. (2008). On the treatment of particulate organic matter sinking in large-scale models of marine biogeochemical cycles. *Biogeosciences*, 5:55–72.

Kriest, I. and Oschlies, A. (2013). Swept under the carpet: Organic matter burial decreases global ocean biogeochemical model sensitivity to remineralization length scale. *Biogeosciences*, 10(12):8401–8422.

Kriest, I. and Oschlies, A. (2015). MOPS-1.0: Towards a model for the regulation of the global oceanic nitrogen budget by marine biogeochemical processes. *Geosci. Model Dev.*, 8:2929–2957.

Kriest, I., Oschlies, A., and Khatiwala, S. (2012). Sensitivity analysis of simple global marine biogeochemical models. *Global Biogeochem. Cycles*, 26:1–15.

Kriest, I., Sauerland, V., Khatiwala, S., Srivastav, A., and Oschlies, A. (2017). Calibrating a global three-dimensional biogeochemical ocean model (MOPS-1.0). *Geosci. Model Dev.*, 10:127–154.

Kwon, E. Y. and Primeau, F. (2006). Optimization and sensitivity study of a biogeochemistry ocean model using an implicit solver and in situ phosphate data. *Global Biogeochem. Cycles*, 20:1–13.

Kwon, E. Y., Primeau, F., and Sarmiento, J. L. (2009). The impact of remineralization depth on the air-sea carbon balance. *Nat. Geosci.*, 2:630–635.

Le Moigne, F. A. C., Henson, S. A., Sanders, R. J., and Madsen, E. (2013). Global database of surface ocean particulate organic carbon export fluxes diagnosed from the Th technique. *Earth Syst. Sci. Data*, 5:295–304.

Lee, C., Peterson, M. L., Wakeham, S. G., Armstrong, R. A., Cochran, J. K., Miquel, J. C., Fowler, S. W., Hirschberg, D., Beck, A., and Xue, J. (2009). Particulate organic matter and ballast fluxes measured using time-series and settling velocity sediment traps in the northwestern Mediterranean Sea. *Deep. Res. II*, 56:1420–1436.

Limburg, K. E., Breitburg, D., Swaney, D. P., and Jacinto, G. (2020). Ocean Deoxygenation: A Primer. *One Earth*, 2(1):24–29.

Longhurst, A. R., Bedo, A. W., Harrison, W. G., Head, E. J., and Sameoto, D. D. (1990). Vertical flux of respiratory carbon by oceanic diel migrant biota. *Deep Sea Res. Part A, Oceanogr. Res. Pap.*, 37(4):685–694.

Lutz, M. J., Caldeira, K., Dunbar, R. B., and Behrenfeld, M. J. (2007). Seasonal rhythms of net primary production and particulate organic carbon flux to depth describe the efficiency of biological pump in the global ocean. *J. Geophys. Res. Ocean.*, 112:1–26.

Maier-Reimer, E. (1993). Geochemical cycles in an ocean general circulation model. Preindustrial tracer distributions. *Glob. Biogeochem. Cycles*, 7(3):645–677.

Maier-Reimer, E., Kriest, I., Segschneider, J., and Wetzel, P. (2005). The HAMburg Ocean Carbon Cycle Model HAMOCC 5.1 - Technical Description Release 1.1. *Berichte zur Erdsystemforsch.*, 14:57pp.

Maier-Reimer, E., Mikolajewicz, U., and Winguth, A. (1996). Future ocean uptake of CO2: Interaction between ocean circulation and biology. *Clim. Dyn.*, 12(10):711–722.

Marsay, C. M., Sanders, R. J., Henson, S. A., Pabortsava, K., Achterberg, E. P., and Lampitt, R. S. (2015). Attenuation of sinking particulate organic carbon flux through the mesopelagic ocean. *PNAS*, 112(4):1089–1094.

Martin, J. H., Knauer, G. A., Karlt, D. M., and Broenkow, W. W. (1987). VERTEX: carbon cycling in the northeast Pacific. *Deep. Res.*, 34(2):267–285.

Matear, R. J. and Hirst, A. C. (2003). Long-term changes in dissolved oxygen concentrations in the ocean caused by protracted global warming. *Global Biogeochem. Cycles*, 17(4).

McCave, I. N. (1975). Vertical flux of particles in the ocean. *Deep. Res.*, 22:491–502.

McCave, I. N. (1984). Size spectra and aggregation of suspended particles in the deep ocean. *Deep Sea Res.*, 31(4):329–352.

McDonnell, A. M. P. (2011). *Marine particle dynamics: sinking velocities, size distributions, fluxes, and microbial degradation rates*. PhD thesis.

Meyer, K. M., Ridgwell, A., and Payne, J. L. (2016). The influence of the biological pump on ocean chemistry: Implications for long-term trends in marine redox chemistry, the global carbon cycle, and marine animal ecosystems. *Geobiology*, 14(3):207–219.

Miller, S. H., Breitburg, D. L., Burrell, R. B., and Keppel, A. G. (2016). Acidification increases sensitivity to hypoxia in important forage fishes. *Mar. Ecol. Prog. Ser.*, 549:1–8.

Moore, J. K. and Doney, S. C. (2007). Iron availability limits the ocean nitrogen inventory stabilizing feedbacks between marine denitrification and nitrogen fixation. *Global Biogeochem. Cycles*, 21(2):1–12.

Moriarty, R., Buitenhuis, E. T., and Le Quéré, C. (2013). Distribution of known macrozooplankton abundance and biomass in the global ocean. *Earth Syst. Sci. Data*, 5:45–55.

Murray, J. W., Stewart, K., Kassakian, S., Krynytzky, M., and Dijulio, D. (2005). Oxic, suboxic, and anoxic conditions in the Black Sea. In A. Gilbert, V. Y.-H. and (eds.), N. P., editors, *Clim. Chang. coastline Migr. as factors Hum. Adapt. to circum-pontic Reg. from past to Forecast*, pages 1–21.

Najjar, R. G., Jin, X., Louanchi, F., Aumont, O., Caldeira, K., Doney, S. C., Dutay, J. C., Follows, M., Gruber, N., Joos, F., Lindsay, K., Maier-Reimer, E., Matear, R. J., Matsumoto, K., Monfray, P., Mouchet, A., Orr, J. C., Plattner, G. K., Sarmiento, J. L., Schlitzer, R., Slater, R. D., Weirig, M. F., Yamanaka, Y., and Yool, A. (2007). Impact of circulation on export production, dissolved organic matter, and dissolved oxygen in

the ocean: Results from Phase II of the Ocean Carbon-cycle Model Intercomparison Project (OCMIP-2). *Global Biogeochem. Cycles*, 21:1–22.

Niemeyer, D., Kriest, I., and Oschlies, A. (2019). The effect of marine aggregate parameterisations on nutrients and oxygen minimum zones in a global biogeochemical model. *Biogeosciences*, 16(15):3095–3111.

Oschlies, A. and Kähler, P. (2004). Biotic contribution to air-sea fluxes of CO2 and O2 and its relation to new production, export production, and net community production. *Glob. Biogeochem. Cycles*, 18:1–17.

Oschlies, A., Schulz, K. G., Riebesell, U., and Schmittner, A. (2008). Simulated 21st century's increase in oceanic suboxia by CO2-enhanced biotic carbon export. *Global Biogeochem. Cycles*, 22:1–10.

Passow, U. and Carlson, C. A. (2012). The biological pump in a high CO2 world. *Mar. Ecol. Prog. Ser.*, 470:249–271.

Paulmier, A. and Ruiz-Pino, D. (2009). Oxygen minimum zones (OMZs) in the modern ocean. *Prog. Oceanogr.*, 80(3-4):113–128.

Picheral, M., Guidi, L., Stemmann, L., Karl, D. M., Iddaoud, G., and Gorsky, G. (2010). The Underwater Vision Profiler 5: An advanced instrument for high spatial resolution studies of particle size spectra and zooplankton. *Limnol. Ocean.*, 8:462–473.

Ploug, H. (2001). Small-scale oxygen fluxes and remineralization in sinking aggregates. *Limnol. Ocean.*, 46(7):1624–1631.

Ploug, H. and Grossart, H.-P. (2000). Bacterial growth and grazing on diatom aggregates: Respiratory carbon turnover as a function of aggregate size and sinking velocity. *Limnol. Ocean.*, 45(7):1467–1475.

Ploug, H., Iversen, M. H., and Fischer, G. (2008). Ballast, sinking velocity, and apparent diffusivity within marine snow and zooplankton fecal pellets: Implications for substrate turnover by attached bacteria. *Limnol. Ocean.*, 53(5):1878–1886.

Rabalais, N. N., Cai, W. J., Carstensen, J., Conley, D. J., Fry, B., Hu, X., Quinones-Rivera, Z., Rosenberg, R., Slomp, C. P., Turner, E., Voss, M., Wissel, B., and Zhang, J. (2014). Eutrophication-Driven Deoxygenation in the Coastal Ocean. *Oceanography*, 27(1):172–183.

Robinson, C. (2019). Microbial respiration, the engine of ocean deoxygenation. *Front. Mar. Sci.*, 5(533):1–13.

Romero, O. E., Baumann, K.-H., Zonneveld, K. A. F., Donner, B., Hefter, J., Hamady, B., and Fischer, G. (2020). Variability of phyto- and zooplankton communities in the Mauritanian coastal upwelling between 2003 and 2008. *Biogeosciences*, 17:187–214.

Ruiz, J. and Izquierdo, A. (1997). A simple model for the break-up of marine aggregates by turbulent shear. *Ocean. Acta*, 20(4):597–605.

Rutherford, S., Hondt, S. D., and Prell, W. (1999). Environmental controls on the geographic distribution of zooplankton diversity. 400:749–753.

Sabine, C. L., Feely Richard, A., Gruber, N., Key Robert, M., Lee, K., Bullister John, L., Wanninkhof, R., Wong, C. S., Wallace Douglas, W. R., Tilbrook, B., Millero Frank, J., Peng Tsung, H., Kozyr, A., Ono, T., and Rios Aida, F. (2004). The oceanic sink for anthropogenic CO2. *Science (80)*, 305(5682):367–371.

Sarmiento, J. L., Hughes, T. M. C., Stouffer, R. J., and Manabe, S. (1998). Simulated response of ocean carbon cycle to climate warming. *Lett. to Nat.*, 393:245–249.

Sarmiento, J. L. and Orr, J. C. (1991). Three-dimensional simulations of the impact of Southern Ocean nutrient depletion on atmospheric CO2 and ocean chemistry. *Limnol. Oceanogr.*, 36(8):1928–1950.

Sarmiento, J. L. and Toggweiler, J. R. (1984). A new model for the role of the oceans in determing atmospheric pCO2. *Nature*, 308:621–624.

Sauerland, V., Kriest, I., Oschlies, A., and Srivastav, A. (2019). Multiobjective Calibration of a Global Biogeochemical Ocean Model Against Nutrients, Oxygen, and Oxygen Minimum Zones. *J. Adv. Model. Earth Syst.*, 11:1–24.

Schartau, M., Wallhead, P., Hemmings, J., Löptien, U., Kriest, I., Krishna, S., Ward, B. A., Slawig, T., and Oschlies, A. (2017). Reviews and syntheses: Parameter identification in marine planktonic ecosystem modelling. *Biogeosciences*, 14:1647–1701.

Schlanger, S. and Jenkyns, H. (1976). Cretaceous Oceanic Anoxic Events: Causes and Consquences. *Geol. en Mijnb.*, 55:179–184.

Schmidtko, S., Stramma, L., and Visbeck, M. (2017). Decline in global oceanic oxygen content during the past five decades. *Res. Lett.*, 542:335–339.

Schmittner, A., Oschlies, A., Giraud, X., Eby, M., and Simmons, H. L. (2005). A global model of the marine ecosystem for long-term simulations: Sensitivity to ocean mixing, buoyancy forcing, particle sinking, and dissolved organic matter cycling. *Global Biogeochem. Cycles*, 19:1–17.

Schmittner, A., Oschlies, A., Matthews, H. D., and Galbraith, E. D. (2008). Future changes in climate, ocean circulation, ecosystems, and biogeochemical cycling simulated for a business-as-usual CO2 emission scenario until year 4000 AD. *Global Biogeochem. Cycles*, 22:1–21.

Schwinger, J., Goris, N., Tjiputra, J. F., Kriest, I., Bentsen, M., Bethke, I., Ilicak, M., Assmann, K. M., and Heinze, C. (2016). Evaluation of NorESM-OC (versions 1 and 1.2), the ocean carbon-cycle stand-alone configuration of the Norwegian Earth System Model (NorESM1). *Geosci. Model Dev.*, 9:2589–2622.

Segschneider, J. and Bendtsen, J. (2013). Temperature-dependent remineralization in a warming ocean increases surface pCO2 through changes in marine ecosystem composition. *Global Biogeochem. Cycles*, 27:1214–1225.

Seibel, B. A. (2011). Critical oxygen levels and metabolic suppression in oceanic oxygen minimum zones. *J. Exp. Biol.*, 214(2):326–336.

Solomon, S., Qin, D., Manning, M., Chen, Z., Marquis, M., Averyt, K., Tignor, M., and (eds.), H. M. (2007). *IPCC, 2007: Climate Change 2007: The Physical Science Basis. Contribution of Working Group I to the Fourth Assessment Report of the Intergovernmental Panel on Climate Change*. Cambridge University Press.

Steinberg, D. K., Cope, J. S., Wilson, S. E., and Kobari, T. (2008). A comparison of mesopelagic mesozooplankton community structure in the subtropical and subarctic North Pacific Ocean. *Deep. Res. Part II Top. Stud. Oceanogr.*, 55(14-15):1615–1635.

Steinberg, D. K., Goldthwait, S. A., and Hansell, D. A. (2002). Zooplankton vertical migration and the active transport of dissolved organic and inorganic nitrogen in the Sargasso Sea. *Deep. Res. I*, 49:1445–1461.

Stemmann, L., Jackson, G. A., and Ianson, D. (2004). A vertical model of particle size distributions and fluxes in the midwater column that includes biological and physical processes - Part I: Model formulation.

Stramma, L., Oschlies, A., and Schmidtko, S. (2012). Mismatch between observed and modeled trends in dissolved upper-ocean oxygen over the last 50 yr. *Biogeosciences*, 9(10):4045–4057.

Stramma, L., Prince, E. D., Schmidtko, S., Luo, J., Hoolihan, J. P., Visbeck, M., Wallace, D. W. R., Brandt, P., and Körtzinger, A. (2011). Expansion of oxygen minimum zones may reduce available habitat for tropical pelagic fishes. *Nat. Clim. Chang.*, 2:33–37.

Stukel, M. R., Ohman, M. D., Kelly, T. B., and Biard, T. (2019). The roles of suspension-feeding and flux-feeding zooplankton as gatekeepers of particle flux into the mesopelagic ocean in the Northeast Pacific. *Front. Mar. Sci.*, 6(397):1–16.

Tiano, L., Garcia-Robledo, E., Dalsgaard, T., Devol, A. H., Ward, B. B., Ulloa, O., Canfield, D. E., and Peter Revsbech, N. (2014). Oxygen distribution and aerobic respiration in the north and south eastern tropical Pacific oxygen minimum zones. *Deep. Res. Part I Oceanogr. Res. Pap.*, 94:173–183.

Tsandev, I. and Slomp, C. P. (2009). Modeling phosphorus cycling and carbon burial during Cretaceous Oceanic Anoxic Events. *Earth Planet. Sci. Lett.*, 286(1-2):71–79.

Turner, J. T. (2015). Zooplankton fecal pellets, marine snow, phytodetritus and the ocean's biological pump. *Prog. Oceanogr.*, 130:205–248.

U.S. Department of Energy Office of Science (2008). Carbon Cycling and Biosequestration Integrating Biology and Climate Through Systems Science: Report from the March 2008 Workshop. Technical report.

Volk, T. and Hoffert, M. I. (1985). Ocean carbon pump: Analysis of relative stregths and efficiencies in ocean-driven atmospheric CO2 changes. *Geophys. Monogr.*, 32:99–110.

Wallmann, K. (2010). Phosphorus imbalance in the global ocean? *Global Biogeochem. Cycles*, 24(4):1–12.

Wells, M. L. and Goldberg, E. D. (1992). Marine submicron particles. *Mar. Chem.*, 40:5–18.

Wilson, S. E., Steinberg, D. K., and Buesseler, K. O. (2008). Changes in fecal pellet characteristics with depth as indicators of zooplankton repackaging of particles in the mesopelagic zone of the subtropical and subarctic North Pacific Ocean. *Deep. Res. Part II Top. Stud. Oceanogr.*, 55:1636–1647.

Wishner, K. F., Seibel, B. A., Roman, C., Deutsch, C., Outram, D., Shaw, C. T., Birk, M. A., Mislan, K. A. S., Adams, T. J., Moore, D., and Riley, S. (2018). Ocean deoxygenation and zooplankton : Very small oxygen differences matter. *Sci. Adv.*, 4:1–8.

Yool, A., Popova, E. E., and Anderson, T. R. (2011). MEDUSA-1.0: A new intermediate complexity plankton ecosystem model for the global domain. *Geosci. Model Dev.*, 4:381–417.

Thanks to ...

... **Andreas** for giving me the opportunity and the trust of writing my doctoral thesis, for support and helpful discussions and for giving me the freedom (and the financial resources) of travelling to Villefranche-sur-Mer and Corsica and moreover joining M138 to see the overall picture.

... **Iris** for always taking time, for the motivation at the right time and in the perfect dose, for helpful discussions, for answering countless questions, ... for perfect supervision throughout my doctoral thesis. Thank you for your excellent mentoring!

... **Iris Kriest, Birgit Schneider, Andreas Oschlies** and **Martin Frank** for taking the time for being my examiners.

... **Tronje** for introducing me into the mysteries of biogeochemical modelling and Matlab. Thanks for never being annoyed by my never-ending questions!

... **Leni** for giving me the chance to join M138 and for helpful discussions about zooplankton egestion.

... **Rainer** for the support and helpful advices regarding the UVP5-dataset.

... **Katrin Meissner** for never getting sick of sending very detailed and helpful manuscript corrections again and again and again....and again.

... **Angela**, **Britta**, **Fabian**, **Fi**, **Henning**, **Julia**, **Karin**, **Leni**, **Madeleine**, **Ulrike**, **Volkmar** and **Wolfgang** for many very helpful advices and proofreading my thesis and to all the others who contributed to this thesis in many ways.

... **all BM group members** for a kind welcome in a collegial environment and the great support throughout my doctoral thesis.

... **the SFB 754** for providing the financial support of this project and **the members of the SFB 754**, who broadened my horizon during several retreats and colloquia regarding the world of oxygen minimum zones.

... **Nadine, Madeleine, Marie, Kristin** and **Clarissa** for companionship, encouragement and relaxed lunchtimes.

Erklärung

Hiermit erkläre ich, dass die vorliegende Arbeit mit dem Titel: 'Modelling features of the biological pump and its impact on marine oxygen distribution' von mir selbstständig angefertigt wurde. Bis auf zitierte Referenzen und Beratung meiner Betreuer wurden keine weiteren Quellen verwendet. Diese Arbeit ist unter Einhaltung der Regeln guter wissenschaftlicher Praxis der Deutschen Forschungsgemeinschaft entstanden. Sie wurde weder im Rahmen eines Prüfungsverfahrens an anderer Stelle vorgelegt noch veröffentlicht. Es wurde kein akademischer Grad entzogen. Ich erkläre mich einverstanden, dass diese Arbeit an die Bibliothek des GEOMAR und die Universitätsbibliothek der CAU weitergeleitet wird.

Kiel, Juni 2020

_____

(Daniela Niemeyer)